A Dissertation for the Degree of Doctor of Philosophy

Enhancement of Polymer-mediated Gene Expression by Hyperosmotic Polymannitol and Polyxylitol based Gene Transporters

February 2015

Pankaj Garg

Department of Biosystems & Biomaterials Science and Engineering

Seoul National University

Dedicated to my Parents, my beloved wife
&
Hemant Garg

ABSTRACT

Successful treatment of genetic diseases by gene therapy requires efficient delivery of therapeutic DNA into specific cells, followed by safe and long-term expression of the encoded gene product at physiologically relevant levels. Efficient translocation of transgene faces physical and metabolic barriers throughout its voyage to the nucleus of targeted cells. Crossing the biological barriers such as cell membrane, tumor mass and blood brain barrier (BBB) are challenging for effective and efficient gene therapy. Novel strategies and rational designing of polymeric vector can lead to the evolution of highly efficient and safe gene delivery carrier. This study uncovers the implications and applications of polyhydroxyl containing hyperosmotic polymers in crossing biological barriers for enhanced gene delivery. This dissertation aims to:

(i) The synthesis of polymannitol- and polydixylitol-based vectors to utilize the osmotic activity due to hydroxyl groups for accelerated cellular uptake and enhanced gene transfection. Various endocytosis

inhibition studies verify the stimulation of caveolae and cyclooxygenase-2 (COX-2) - dependent endocytosis to be the main route of cellular internalization to account for enhanced transgene expression.

(ii) The research introduces the application of polydixylitol based hyperosmotic polymer (PdXYP) in transmigrating BBB by intra-arterial infusion of osmotic polyol by triggering cellular uptake via selective stimulation of caveolae-mediated endocytosis. *In vitro* BBB model and *in vivo* transfection results showed higher transfection efficiency in brain astrocytes. *In vivo* bioimaging and mechanistic investigation proved the potential of the system reaching deeper in to the tumor mass.

(iii) A combination treatment that uses hyperosmotic non-viral vectors and nanopatterned matrix to promote gene delivery into cells indicates the importance of synergistic cues in designing non-viral gene delivery platforms and strategies for gene therapy.

(iv) The delivery of therapeutic siRNA in cancer cells using

polymannitol-based vector (PMGT) exemplifies the vector as a strategy to inhibit tumor progression. c-Jun N-terminal kinase 2 (JNK2) is primarily responsible for the oncogenic transformation of the transcription factor c-Jun. Expression of the proto-oncogene c-Jun progresses the cell cycle from G1 to S phase, but when its expression becomes awry it leads to uncontrolled proliferation and angiogenesis. Delivering a JNK2 siRNA in tumor tissue was anticipated to reverse the condition with subsequent onset of apoptosis which predominantly requires an efficient delivering system capable of penetrating through the compact tumor mass. In the present study, it was demonstrated that PMGT with inherent hyperosmotic properties was able to penetrate through and deliver the siJNK2 in the subcutaneous tumor of xenograft mice. Hyperosmotic activity of polymannitol was shown to account for the enhanced therapeutic delivery both *in vitro* and *in vivo* because of the induction of COX-2 which firstly stimulates caveolin-1 for caveolae-mediated endocytosis of the polyplexes and secondly activates caspase-9 to induce apoptosis in cancer cells. Further suppression of JNK2 and hence c-Jun expression led to the inhibition of tumor growth in xenograft mice model.

Thus, the synthesis and application of hyperosmotic polymers demonstrated their facilitation in crossing the biological barriers by elevating the osmolarity of the extracellular matrix.

Keywords: Hyperosmotic, Mannitol, Xylitol, siRNA, COX-2, Caveolae, Blood Brain Barrier

Student number: 2010-31334

CONTENTS

LIST OF TABLES

LIST OF FIGURES

LIST OF ABBREVIATIONS

AAV	Adeno-associated virus
ATP	Adenosine triphosphate
BBB	Blood brain barrier
COX-2	Cyclooxygenase-2
DLS	Dynamic light scattering microscope
DNA	Deoxyribonucleic acid
DMSO	Dimethyl sulphoxide
EDTA	Ethylenediaminetetraacetic acid
EMSA	Electrophoretic mobility shift assay
GFP	Green fluorescent protein
GPC	Gel permeation chromatography
HMW	High molecular weight
JNK	c-Jun N-terminal kinase
LMW	Low molecular weight
miRNA	micro RNA

MTT	3-(4, 5-Dimethyl thioazol-2-yl)-2, 5-diphenyl tetrazolium bromide
NMR	Nuclear magnetic resonance
NLS	Nuclear localization sequence
NPCs	Nuclear pore complexes
PEI	Polyethyleneimine
pDNA	plasmid DNA
PLL	Poly L lysine
PEG	Poly ethylene glycol
RNA	Ribonucleic acid
SDS-PAGE	Sodium dodecyl sulfate polyacrylamide gel electrophoresis
siRNA	Small interfering ribonucleic acid
siScr	Scrambled small interfering ribonucleic acid
TRITC	Tetramethylrhodamine isothiocyanate
TEM	Transmission electron microscope
TEER	Trans endothelial electrical resistance

CHAPTER 1

Gene Therapy: Introduction

1.1 Description of gene therapy

Gene-based therapy is the intentional modulation of gene expression in specific cells to treat pathological conditions. It is a set of strategies and experimental techniques to treat or prevent diseases at genetic level by introducing exogenous nucleic acids in to the host cells. Introducing a foreign gene in to the host cell can produce desired changes at the genetic level leading to exactly similar progeny forever. A variety of nucleic acids such as DNA, small interfering RNA (siRNA) and oligonucleotides have been delivered to activate or inactivate or knockdown the improperly functioning mutated genes at nuclear or cytoplasmic level. Gene therapy covers a broad spectrum of applications, from gene replacement for genetic or acquired diseases such as cancer, to vaccination, each with different requirements for gene delivery. For instance, addition of gene responsible for apoptosis in to cancer cells can cause programmed death of cancer cells. Genes that express differentiation related signaling molecules have potential to

initiate differentiation of stem cells into required lineages by osteogenesis, neurogenesis and angiogenesis etc. More recently the addition of Yamanaka factors (Oct4, Sox2, Klf4, c-myc) in to somatic cells produced induced pluripotent cells that made revolutionary development in the field of tissue engineering. Therefore, due to enormous number of therapeutic possibilities the potential of nucleic acid (DNA, siRNA) drugs in treating life threatening ailments has been realized and the gene therapy research has gained momentum. As therapeutic DNA cannot penetrate biological membranes it necessitates the formulation of gene delivery vector systems to deliver the gene that can express encoded proteins into target cells. Following are the governing steps that determine the potential of any gene delivery system.

1) Nucleic acid binding and endurance against nuclease degradation

2) Circumvent immune system of the body and overcome biological barriers

3) Cellular uptake of vector and escape from endosomal degradation

4) Unpacking of DNA from vector inside cytoplasm & nuclear translocation.

Thus, knowledge of the aforementioned transport barriers of gene delivery (Fig. 1.1) is important in developing and identifying therapeutically effective gene delivery vectors.

1.2 Gene delivery vectors

Modulation of gene expression is accomplished by introducing exogenous nucleic acids such as DNA, mRNA, siRNA, microRNA (miRNA) or antisense oligonucleotides [1]. To deliver exogenous genes at the desired location, a fundamental engineering challenge of gene-based therapy is the development of safe and effective delivery vectors. Both viral [2, 3] and non-viral vectors are used for systemic delivery in clinical trials. Viral vectors have been widely investigated as vehicles for transgene delivery. Majority of clinical trials carried out so far have used adeno-associated virus (AAV), and vaccinia virus. However, they are plagued by the issues of recognition by the host's immune defense mechanism and limited capacity of carrying genetic materials [4-7]. After the death of 18 year old patient Jesse Gelsinger in 1991 during gene therapy clinical trial of adenoviral vector, research progressed towards the less immunogenic non-viral vector systems [8, 9]. Other important reasons for switching towards non-viral vectors are the capacity of carrying low transgene size, relatively expensive production

of viral vectors and difficulty in scaling up.

Non-viral gene therapy has the potential to address many of these limitations, particularly with respect to safety. Non-viral vectors such as cationic polymers have attracted more attention than viral vectors because of their immense chemical diversity and potential for functionalization. A diverse collection of synthetic vectors has been developed to bring therapeutic nucleic acids to their sites of action. Cationic molecules such as poly (L-lysine) (PLL) and polyethylenimine (PEI) have shown great ability to condense DNA and has been massively studied. Numerous modified variants of PLL with enhanced gene delivery properties have been reported [10, 11]. One example includes PLL covered with the hydrophilic polymer PEG, which is designed to minimize nonspecific interaction with serum components and thereby increase circulation time [12].

PEI and its derivatives are among the most studied polymeric materials for gene delivery [13, 14]. Amine groups present in PEI are responsible for its high charge density that aid in DNA condensation and buffering tendency during endosomal escape. The advancement in the study of PEI based vectors have shown that the transfection efficiency and cytotoxicity of PEI strongly depend on its structural properties such as

molecular weight and the linear versus the branched PEI [15]. Since, PEI has been known for its cytotoxicity, a series of modifications to PEI has been investigated.

Many altered forms of PEI has been synthesized which includes its copolymerization with PEG for improved stability and biocompatibility, with polyols for biodegradability and accelerated uptake, degradable disulphide-crosslinked PEIs for reduced toxicity and alkylated PEI for increased potency [16-19]. Due to the major issue of cytotoxicity associated with PLL and PEI numerous other cationic polymers such as lipids [20], polymethacrylates [21, 22] polypeptides, celluloses [23], chitosan [24-26], dendrimers including polyamidoamine or PAMAM dendrimers [27], poly (vinyl pyrrolidone) and polyamine polymers [14] are under preclinical investigations.

In brief, although a variety of effective polymeric non-viral vectors have been designed over past three decades, and much has been learned about their structure–function relationships [28], DNA-based drugs inherently pose greater delivery challenges including the difficulty of crossing the biological barrier and lower transfection efficiency. Investigations of the cellular itinerary of DNA vectorised by synthetic molecules have provided insight into the nature of potential barriers to

gene transfer [29]. The following sections describe some of the biological barriers towards the uptake of genes for their effective expression in the target cell.

1.3 Biological barriers to gene delivery

Successful gene therapy requires efficient delivery of therapeutic nucleic acids in to the targeted organs and cells, followed by the stable expression of delivered gene product at physiologically relevant level. The journey of the foreign genes requires overcoming numerous obstacles before they reach to the cell nucleus. These biological barriers can be broadly classified in to the extracellular barriers and intracellular barriers (Fig. 1.1).

1.3.1 Extracellular barrier

In vitro delivery

Determination of *in vitro* gene delivery efficiency is the primary step towards the elimination of non-effective vectors amongst the probable lead vectors. Before coming in contact with the cellular environment, vector must have the propensity to bind with nucleic acids to form stable complexes [30].

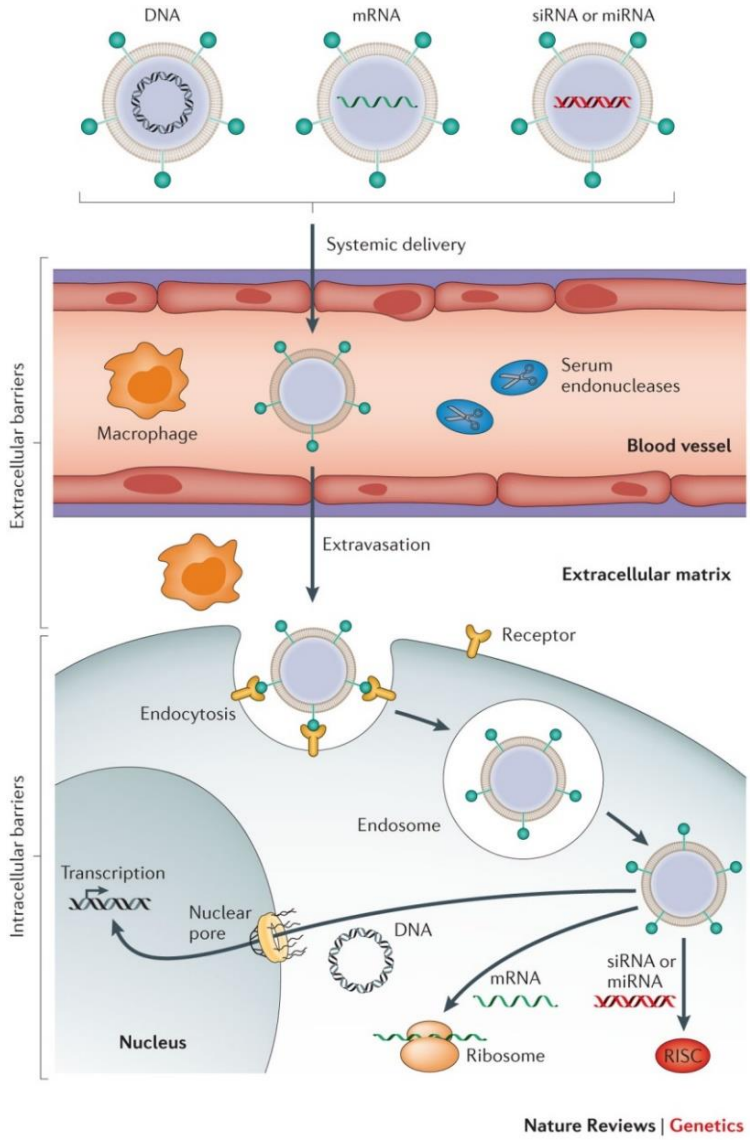

Fig. 1.1 A schematic overview of barriers to successful gene delivery of nucleic acids using non-viral vectors.

A loosely bound complex when added to the cell supplement medium, may get dismantled even before it reaches to the nucleus, as certain serum proteins can interfere with or prevent stable complex formation [31, 32]. The aggregation of the complexes in the cell nourishing medium is another hurdle that can diminish the efficiency of gene transporters [33]. Because aggregated complexes become larger and thus unsuitable for cellular internalization, the polyplex aggregation is one of the root causes for lower transfection efficiencies by non-viral gene delivery vectors. In case of cationic non-viral vectors which interact with negatively charged cell membrane due to their positive zeta potential may lead to higher cytotoxicity as a result of particle aggregation. Aggregated polyplexes due to very high cumulative positive charge may rupture the cell membrane ending up in high cytotoxic effect [34]. In some cases, aggregation of vector/DNA polyplexes may produce false positive results that will lead to the contradictory outcomes *in vivo.* During *in vitro* experiments the aggregated/sedimented vectors can interact with adherent cells, and thus may exhibit gene delivery. However, when the vector is applied *in vivo,* the polyplex aggregation results in poor transfection by means of sedimentation and clearance in systemic circulation. Therefore, in case

of cationic polymers, non-aggregation and the optimal zeta potential is the key factor for high cell viability and efficient delivery.

Along with the proper vector design, optimal cell density, cell type and cell exposure time to vector are other important factors for *in vitro* gene delivery. The aforementioned hurdles can be easily manipulated and overcome with the proper vector design.

In vivo delivery

The biggest challenge in gene therapy is to overcome the *in vivo* gene delivery barriers. Regardless of the method by which a non-viral vector is administered *in vivo* (e.g., by inhalation, intramuscular injection, intravascular injection, etc.), it will unavoidably come in contact with the extracellular environment. Before reaching to the target organ it must cross several barriers that can result in rapid clearance and/or degradation of the vector [35]. Intravenously delivered naked DNA has been shown to have a very short half-life within serum, in the range of 1.2 to 21 minutes due to its degradation by the endo- and exonuclease activity [36]. While neutral polyplexes undergoes self-aggregation, the cationic complexes form aggregates with serum proteins and subsequently gets cleared from the systemic circulation [37].

Immediately after intravenous injection, delivery vehicles come in contact with the negatively charged blood components (erythrocytes, leukocytes, macrophages, and platelets), allowing for electrostatic interactions between cells and cationic vectors [38]. This electrostatic interaction leads to aggregation resulting in a large accumulation of polyplexes in the fine capillaries, where they eventually undergo clearance [39]. Furthermore, the systemic clearance of polyplexes is also dependent on their particle size [40]. However, the particle size restrictions have been dependent on the type of targeting tissue, in most of the cases optical mean particle size has been identified as 100 nm. Studies have shown that while the larger particles (~400 nm) cannot pass through the capillary gaps, the smaller particles (~70 nm) are more prone to renal excretion through glomeruli in the kidney [40]. Besides the above mentioned extracellular barriers which are common for most of the gene delivery vectors, problems that still remains are the organ and tissue specific biological barriers. For example in the lung, alveolar macrophage is regarded as a major barrier to both viral and non-viral delivery since this professional phagocytic cell "eats" up delivery agents before they can transfect any other cell type [41]. Blood brain barrier (BBB) and compact tumor masses are the typical examples of

the tissues that offer major extracellular impediment during *in vivo* gene delivery. The architecture of BBB, which is formed primarily of tight junctions between the cerebral capillary endothelium and surrounding perivascular elements, restricts the influx of molecules from blood stream into the brain [42] and makes it impermeable to most therapeutic molecules, including nucleic acids [43]. Similarly, a compact mass of tumor cells composed of approximately 50% tumor and stromal cells hinders the delivery of cancer therapeutics to deep-seated cancer cells. Since gene needs to be delivered in to the deep seated cancer cells, it becomes necessary to overcome the compactness of tumor tissues.

1.3.2 Intracellular barrier

As soon as the gene loaded vector reaches in the proximity of cells, the challenges to cross various intracellular barriers begins. These barriers include binding to the cell surface, traversing the plasma membrane, escaping lysosomal degradation, and overcoming the nuclear envelope [44]. The appropriate design of a non-viral gene vector requires a complete understanding of the mechanisms by which they interact with the targeted cells, uptake pathways used for the internalization (Fig. 1.2)

and subsequent intracellular events before nuclear translocation [45, 46].

Cellular uptake pathways

Due to the large size and hydrophilic nature majority of non-viral vectors cannot cross the cell membrane barrier. It has been proved that endocytosis is the main machinery of cellular internalization for most of the non-viral vectors [36]. Endocytosis refers to the cellular uptake of macromolecules and solutes into membrane-bound vesicles derived by the cell membrane invagination and pinching off of the plasma membrane [47]. However, there are multiple mechanisms which govern endocytosis (Fig. 1.3).

Vesicle fate and endosomal degradation

Only a small fraction of internalized plasmid DNA penetrates in to the cytoplasm. Plasmid DNA encounters the diffusional and metabolic barriers of the cytoplasm, further decreasing the number of intact plasmid molecules reaching the nuclear pore complex (NPC) [49]. Irrespective of the mode of cellular uptake, vector/DNA complex will be localized within the endocytic vesicles which carries enzymes responsible for nucleic acid degradation [50].

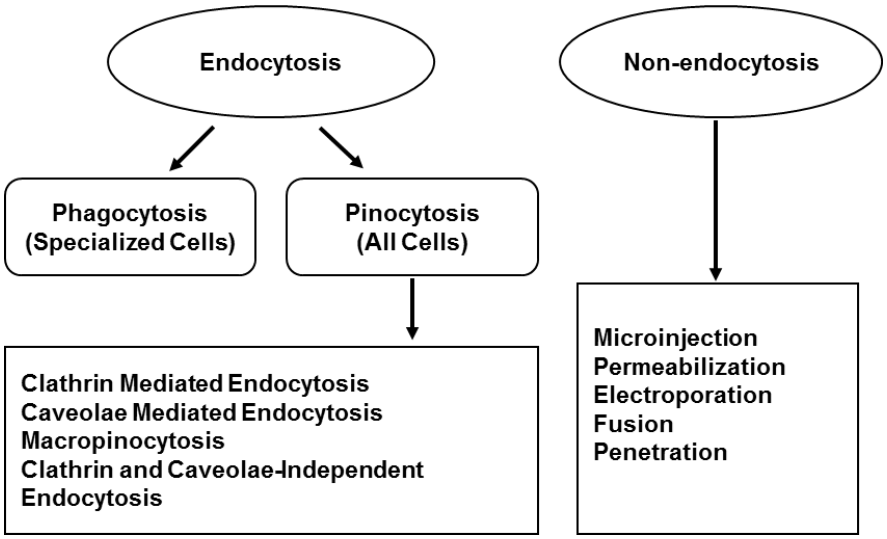

Fig. 1.2 Different uptake pathways in non-viral gene delivery.

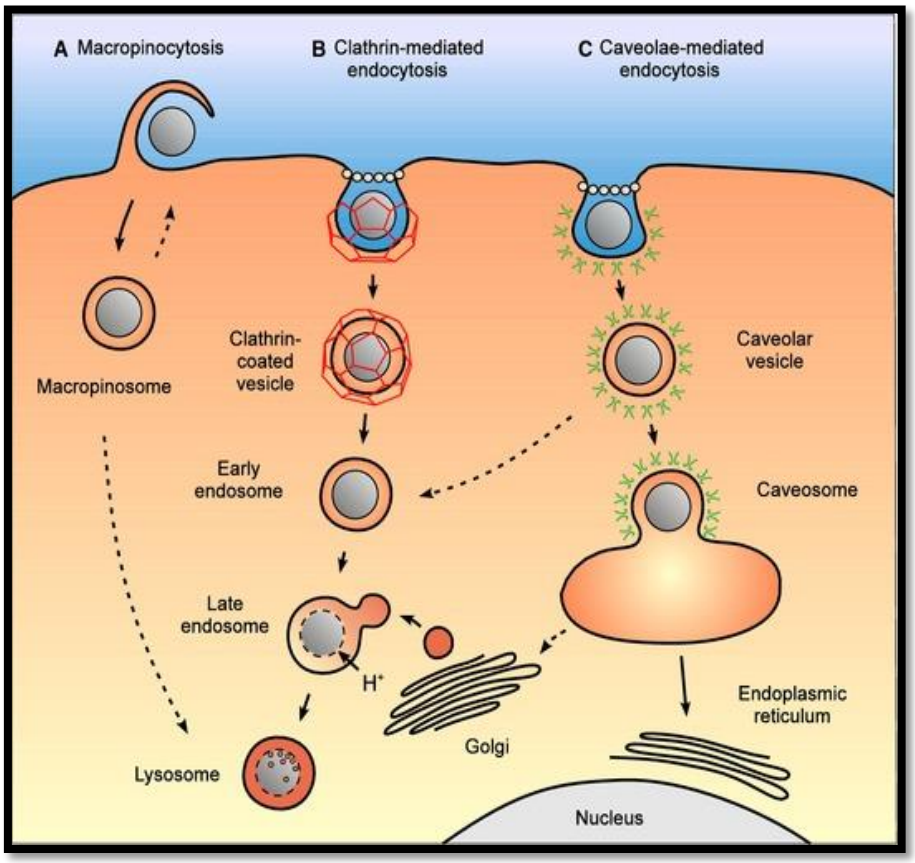

Fig. 1.3 Intracellular nanocarrier trafficking following macropinocytosis, clathrin-mediated endocytosis and caveolae-mediated endocytosis. (**A)** Macropinocytosis leads to the formation of a macropinosome, which is thought to eventually fuse with lysosomes or recycle its content to the surface. (**B)** Clathrin-mediated endocytosis of a nanocarrier leads to the formation of an early endosome, which is acidified and fuses with pre-lysosomal vesicles containing enzymes (in red) to give rise to a late endosome and finally a lysosome, an acidic

and enzyme-rich environment prone to nanocarrier and drug degradation. Unless a lysosomal delivery is desired, strategies for a cytosolic drug delivery by this route will focus on the drug escape from the endosome as early as possible. (**C)** Caveolae-mediated endocytosis of a nanocarrier gives rise to a caveolar vesicle that can be delivered to caveosome, avoiding a degradative acidic and enzyme-rich environment. Adopted from the reference [48].

After endosome formation it undergoes rapid acidification (pH ~4.5) by ATPase proton pump enzymes and leads to the activation of degradative enzymes [51-54]. The trapped nanoplexes inside these endosomes must escape out in to the cytoplasm before they get degraded by the enzymes. Every non-viral gene delivery vehicle requires overcoming these derivative bags which is a most common limiting factor in the overall transfection efficiencies of designed vectors.

Unpacking of DNA & nuclear translocation

After releasing from the endosome, unloading of DNA from the vector is a prerequisite before its nuclear translocation. However, premature release of the DNA from the vector may expose the DNA to enzymatic degradation before expression can occur. The size of polyplex is much larger than the nuclear pore (~40 nm) therefore it cannot enter the nucleus. Moreover, if the non-viral vector enters the nucleus, it could potentially interfere with cellular transcription machinery thereby can reduce or prevent transgene expression. Therefore, it is suggested that the unpacking of DNA from the vector in cytoplasm is as important as its packing while developing a non-viral gene delivery vector.

Nuclear translocation of nucleic acid is the last step in the delivery of cargo. After the release of nanoplex in to the cytoplasm, nucleic acid must reach to its target nuclear compartment. The nuclear envelope that encapsulates the nucleus is an effective barrier to gene delivery [55-57] allowing only 1~10 % of the transfected plasmid to reach to the nucleus. In case of naked DNA, smaller fragments (<300 bp) can passively diffuse in to the nucleus. In most of the cases the nuclear translocation happens during cell division when nuclear envelope is temporarily disassembled and vector/DNA complexes can be sequestered within the daughter cell nuclei [58]. This is the basis of the ease with which conventional non-viral vectors transfect rapidly dividing immortalized cancer cell lines, but show only poor transfection rates in non-dividing cells. Since efficient transfection of slow dividing or terminally differentiated cells is required for *in vivo* human gene therapy of genetic diseases, there is considerable interest in improving the nuclear import efficiency of non-viral vectors. Overcoming nuclear translocation is poorly studied and requires more extensive research to investigate potential solutions (Table 1.1).

1.4 Overcoming biological barriers

An ingenious gene transporter that can overcome above discussed barriers could be a major invention in the field of gene therapy. Over the decades, many successful strategies and techniques has been developed which helps to overcome these barriers [59]. A plethora of non-viral vectors (liposomes, cationic polymers, dendrimers etc.) have been synthesized and tried in animal models which claims to be unobstructed by at least some of these biological barriers. Recent research has focused on improving the efficiency of non-viral vectors through structural modifications and inclusion of specific functional groups to the carrier molecule. Current reports showcase the application of hyperosmotic polymers for traversing the compact blood brain barriers and tumor mass [60, 61]. In these studies, tissues were pretreated with hyperosmotic mannitol solution, which loosens tight junctions between cells of the BBB, and were then treated with various gene/drug delivery vehicles [62]. Therefore in recent studies the osmotically active compounds (glycerol, mannitol, sorbitol and xylitol) has been incorporated in to the vector backbone, making hyperosmoticity an integral part of vector for transmigration of nucleic acids through BBB and compact tumor mass [63-65].

Table 1.1 Biological Barriers, challenges and opportunities [88-95]

Site	**Type of barrier**	**Challenges**	**Prospects**
Blood Circulation	Blood nucleases Particle instability Clearance by microphages Capillary blockade	Protection of nucleic acids from nucleases Prevention of unwanted opsonization	Systemic delivery after I.V. injection Selectivity mediated by tissue specific promoters
Capillary endothelium	Tissue specific characteristics: Continuous (skin, muscle), compact (BBB)	Extravasation Particularly in organs with continuous endothelia	Delivery to hepatocytes Delivery to tumors, or at the site of angiogenesis Selective receptor mediated extravasation
Tissue interstitium	Extracellular nucleases Poor distribution within tissue High hydrostatic pressure in tumors	Protection of DNA from nucleases and unwanted binding	Direct intramuscular injection Direct injection in to tumors BBB opening by hyperosmotic polymers
Cell membrane	Poor cellular internalization	Optimized physical properties for uptake	Receptor mediated endocytosis Modulation of cellular uptake
Endosome	Trafficking to lysosomes and consequent degradation	Incorporate endosomolytic agent	Buffering capacity Viral peptide for endosome escape
Cytoplasm	Inefficient cytoplasmic transport Poor unloading of DNA and carrier	Optimize site of escape from vesicular system	Use of microtubule transport system for nuclear translocation
Nucleus	Inefficient uptake in to the nucleus	Designing DNA suitable for nuclear translocation	Use of active transport through nuclear pore complex

To prevent non-specific interactions with blood and serum components, the vector can be shielded from the extracellular matrix by coupling of hydrophilic molecules such as polyethylene glycol (PEG) [66, 67]. Different types of targeting ligands such as peptides [68, 69] and vitamins [70-72] has been used for targeting specific tissue or organ. Two or more ligands including monoclonal antibodies and small molecules can also be used for highly specific targeting, particularly in case of cancer gene therapy [73, 74]. Some of the physical methods such as electroporation, particle bombardment and microbubble bursting by ultrasound can also be possible for direct cellular delivery [75-79]. As soon as the vector/DNA complex undergoes endocytosis it must escape endosomal degradation. Commonly used strategy for endosomal escape is the endosomal bursting before its maturation by endosomotropic agents that cause buffering of acidic environment inside the vesicles resulting in endosome bursting and release of vector [53, 80]. Polyethyleneimine based polymers are such examples which contain many titrable amine groups that become protonated in the low pH of endosomes, creating a passive chloride influx, in turn causing osmotic swelling and rupture of the endosome [81]. After endosomal escape it is necessary for the vector to release DNA, as vector itself

may prevent transgene expression. In general it is believed that the separation of DNA from the vector occurs as a result of competing electrostatic interaction/exchange between the DNA and various intracellular cations, anions, and DNA-binding proteins present inside the cell. Some researchers have shown the effect of degree of polymerization on the release of the DNA, with smaller polycations releasing DNA faster compared to the longer chains [82-84]. A number of other methods for enhancing nuclear import have been studied using cell's nuclear import machinery. These approaches include complexing plasmid DNA with nuclear localizing signal (NLS) peptides, nuclear proteins or small molecule ligands. Due to the varied success of NLS peptides at promotion of nuclear import, it is still unclear if this will be a promising approach for gene therapy [85-87].

1.5 Scope of the dissertation

Desired gene delivery vector should be capable of making stable complex with DNA, increase cellular uptake, overcome endosomal escape and help polyplex in nuclear translocation. An enormous amount of research has been conducted to develop highly efficient polymer based non-viral gene delivery vehicles. However, the cationic polymers are still having lower efficacy due to their incompetence to

cross biological barriers effectively. Other bottlenecks in gene delivery are vector cytotoxicity, cellular targeting and non-biodegradability of polymer after delivery of cargo.

In conjunction with current efforts in the field of gene delivery, first objective of this dissertation is to develop the novel polymers which have low cytotoxicity and high transfection efficiency. The second objective is to modulate the cellular internalization pathways to accelerate polyplex uptake and endosomal escape. The final goal is to overcome the multiple barriers (extracellular and intracellular) of gene delivery by combining designed strategies.

Chapter 2 of the dissertation describes the synthesis of osmotically active polymannitol based gene transporter that accelerates the cellular uptake process by caveolae and COX-2 mediated endocytosis. The study explains how the extracellular disturbances due to osmotic pressure can affect endocytosis mechanism and lead to increased uptake of polyplexes.

Chapter 3 is the development of highly hyperosmotic polyxylitol based polymer that strengthens the concept of osmolarity driven enhancement in transfection efficiency of cationic polymers. This chapter also

suggests application of hyperosmotic polymers in crossing the blood brain barrier and compact tumor mass.

Chapter 4 highlights the application of non-viral gene delivery in the field of tissue engineering. The study emphasizes on the synergistically enhanced gene transfection on nanopatterned matrix for osteogenic differentiation of alveolar bone mesenchymal stem cells.

Chapter 5 discusses the applicability of polymannitol based polymer to deliver therapeutic JNK2 siRNA in cancer cells. A new probable mechanism of cellular uptake by hyperosmotic polymers has been proposed.

CHAPTER 2

Efficient Transfection by Hyperosmotic Polymannitol-Based Gene Transporter through Regulation of Caveolae and COX-2 Induced Endocytosis

2.1 Introduction

It is widely accepted that non-viral vectors have become an important gene delivery tool primarily due to their safety concerns compared to the viral vectors which have immunological and potentially mutational disadvantages [28, 29]. Non-viral vectors with large DNA carrying capacity can be easily tailored to specific therapeutic needs, at the same time being cost effective for large scale production. Their major disadvantage of low transfection efficiency have been improved upon, however it should be noted that we are still far away from a system that could be considered as satisfactory [96, 97]. Since the inefficiency of these vectors in gene delivery can be attributed to specific hurdles or barriers on a systemic as well as sub cellular level, strategies to surmount these barriers will be of major interest [97, 98]. The success

of non-viral gene delivery system requires a rational strategy for overcoming the barriers such as crossing cell membrane and escaping from endosomes before lysosomal degradation [99]. Therefore the regulation of cellular uptake to cross cell membrane is one of the key strategies important for efficient gene transfection. Several strategies such as usage of cell penetrating peptides [100, 101] and exercising target specific ligands [102] are the common examples to overcome the cell membrane barrier. Besides these techniques the researchers are keen to discover innovative methods to manipulate and regulate the cellular uptake mechanism for better cellular delivery.

In our recent studies we have tried to establish the concept of regulation of cellular uptake using hyperosmotically active polymers. Polymers containing multiple hydroxyl groups draw water molecules and create a hyperosmotic environment around the cell membrane which might play a role in regulation of cellular internalization mechanism. Our recent studies have shown the application of glycerol, sorbitol and mannitol-based hyperosmotic polymers help in increasing the cellular uptake and enhanced transfection efficiency [63, 103, 104]. Although these previous studies draw attention to the application of osmotically active compounds in gene delivery systems, the actual mechanism and

regulation of cellular uptake is still obscure.

Recently some papers have suggested that hydrophobic modifications have proven to effect the cellular uptake of polyplexes by their interactions with the lipid constituent of the cell membrane. Hydrophobic modifications have also been shown to improve the transfection efficiency of PEI by allowing effective interactions with the hydrophobic lipids in cellular membranes that facilitate the uptake and internalization of polyplexes. Hydrophobic modifications have also been known to bring an element of insolubility, which restricts the incorporation of a higher degree of hydrophobicity in the molecules. The inquisitiveness motivated us to synthesize a hyperosmotically active gene carrier using mannitol dimethacrylate (MDM) as a monomer having hydrophobic methyl groups, which was then cross linked with LMW bPEI (1.2 kDa) by Michael addition reaction to obtain polymannitol based gene transporter (PMGT). Since the route of endocytosis plays a pivotal role in determining intracellular fate of polyplexes, the various components of gene delivery vector modulating these routes could underscore the efficiency of their gene transportation. Accordingly, the various components of PMGT will be conceptually anticipated to contribute for efficient gene transportation. Free hydroxyl

groups in polymannitol backbone may serve for better DNA complexation and bring stability to the polyplexes due to intracellular hydrogen bonding. PMGT may also have impact on accelerating transfection process by initiating osmotically induced cellular internalization through stimulation of various signaling cascade. LMW bPEI cross linked with degradable ester linkages may reduce cytotoxicity by getting discharged into smaller fragments upon degradation. Moreover, the methyl groups of the mannitol dimethacrylate monomer would supposedly bring hydrophobicity to the polymer which led to the higher expectation for PMGT to increase transfection efficiency in comparison to polymannitol based gene transporter obtained by mannitol diacrylate (PMT) and LMW bPEI [103]. Hydrophobicity of the polyplexes enhanced its compatibility with plasma membrane through hydrophobic interactions and allows its smooth and unobstructed entry to improve gene transfection efficiency [105, 106]. Therefore, the hydrophobic property might help PMGT to interact with phospholipid bilayer of cell membrane and facilitate its cellular uptake. Hence, it was envisaged that PMGT might enjoy osmotic activity of mannitol in combination with hydrophobicity of methyl groups and high buffering capacity of bPEI to breach through

cell membrane and compact tumor cell mass for the delivery of therapeutic gene. Moreover, in the present study mechanistic investigations explored the effect of hyperosmotic stress and hydrophobic group on cellular machinery and how it may regulate the caveolae and COX-2 induced endocytosis leading to enhanced cellular uptake.

2.2 Materials and Methods

Materials

bPEI (Mn: 1.2 kDa and 25 kDa), dimethyl sulfoxide (DMSO), methacryloyl chloride (MAC), D-mannitol, genistein, wortmannin, chlorpromazine, methyl-β-cyclodextrin, bafilomycin A1 and 3-(4, 5-dimethyl thioazol-2-yl)-2, 5-diphenyl tetrazolium bromide (MTT) reagent were purchased from Sigma (St. Louis, Mo, USA). Luciferase reporter, pGL3- vector with SV-40 promoter and enhancer encoding firefly (Photonus pyralis) luciferase were obtained from Promega (Madison, WI, USA). Enhanced green fluorescent protein (EGFP) gene, was obtained from Clontech (Palo Alto, CA, USA). Tetramethylrhodamine isothiocyanate (TRITC) and YOYO-1 iodide fluorescent dyes were purchased from Molecular Probes, Invitrogen

(Oregon, USA) and plasmid purification kit was obtained from Qiagen, France. The concentration of purified DNA was determined at 260 nm UV absorbance. Non-specific scrambled siRNA (siScr), luciferase siRNA (siLuc) (Table 2.1) were purchased from Genolution Pharmacuticals, Inc. (Seoul, South Korea). All other chemicals used in this study were of analytical reagent grade.

Cell culture and animal

Human hepatocellular liver carcinoma cells (HepG2) and human cervix epithelial carcinoma cells (HeLa) were maintained in low glucose Dulbecco's Modified Eagle's Culture Medium (DMEM) (Sigma, USA) with 10% FBS. Adenocarcinoma human alveolar basal epithelial cells (A549) were maintained in Roswell Park Memorial Institute (RPMI)-1640 culture medium supplemented with 10% heat-inactivated fetal bovine serum (FBS) Hyclone Laboratories, USA) and 1% antibiotic cocktail of streptomycin and penicillin. All cells were maintained under standard culture conditions of 37℃ and 5% CO_2.

C57BL/6 mice were obtained from the breeding colony of Human Cancer Consortium National Cancer Institute (Frederick, MD, USA)

Table 2.1 siRNA sequences

siRNA	**Sense (5'→3')**	**Anti-sense (5'→3')**
siRNA	CGUACGCGGAAUACU	UCGAAGUAUUCCGCGU
scrambled	UCGAUU	ACGUU
siRNA	CUUACGCUGAGUACU	UCGAAGUACUCAGCGU
Luciferase	UCGAUU	AAGUU

and kept in a laboratory animal facility maintained at 23 ± 2°C and 50 ± 20% relative humidity under a 12 h light/dark cycle. All experimental protocols were reviewed and approved by Animal Care and Use Committee at Seoul National University (SNU-111216-4).

Synthesis of polymannitol based gene transporter (PMGT)

PMGT was synthesized in a two-step reaction in which mannitol was first esterified with methacryloyl chloride to form mannitol dimethacrylate (MDM) monomer, and then copolymerized with bPEI (1.2 kDa) by a Michael addition reaction to obtain PMGT. PMT was prepared by same method previously reported [103].

Synthesis of MDM

Mannitol dimethacrylate (MDM) monomer was synthesized by reaction of mannitol with 2 equivalents of methacryloyl chloride. An emulsion was prepared by dissolving mannitol (1 g) in DMF (20 mL) and pyridine (10 mL) followed by drop wise addition of methacryloyl chloride solution (1.2 mL dissolved in 5mL DMF) at 4℃with constant stirring overnight. After reaction completion, HCl.pyridine salts were filtered and filtrate was dropped to diethylether. The product was precipitated in a syrupy liquid form and dried over vacuum.

Synthesis of PMGT

PMGT was prepared by Michael addition reaction [107] between LMW bPEI and MDM. Briefly, the synthesized MDM (0.38 g) dissolved in DMSO (5 mL) was added drop wise to 1 equivalent of bPEI (1.2 kDa, dissolved in 10 mL DMSO) and reacted at 60℃ with constant stirring for 24 h. After reaction completion, mixture was dialyzed using a Spectra/Por membrane (MWCO: 3500Da; Spectrum Medical Industries, Inc., Los Angeles, CA, USA) for 36 h at 4^{o}C against distilled water. Finally, the synthesized polymer was lyophilized and stored at -70^{o}C.

Characterization of PMGT

^{1}H NMR spectra of MDM and PMGT in D_2O were recorded using an Advanced 600 spectrometer (Bruker, Germany). The absolute molecular weight of PMGT was measured by gel permeation chromatography coupled with multiangle laser light scattering (GPC-MALLS) using a Sodex OH pack SB-803 HQ (Phenomenex, Torrells, CA, USA) column (column temperature 25℃; flow rate 0.5 mL/min).

Gel retardation assay

PMGT was complexed with DNA (0.1µg pGL3) at various N/P ratios (2, 3, 5, and 10) for 30 min at RT with the total volume adjusted to 20 µL. 1X loading dye (Biosesang, Korea) was added, and the samples were resolved on a 0.8% agarose gel in 1X TAE buffer containing ethidium bromide (EtBr, 0.1 µg/mL). Gel electrophoresis was conducted at 100 V for 40 min in 1X TAE running buffer, and images were captured under ultraviolet illumination to assess DNA complexation ability of PMGT.

Protection and release assay

Ability of PMGT to protect condensed DNA against cytoplasmic nucleases was examined by treating PMGT/DNA complexes (N/P 20) with DNase I. PMGT/DNA complexes and free DNA were incubated separately with DNase I (1 µL, 50 units) in DNase/Mg2+ digestion buffer containing Tris-Cl (50 mM, pH 7.6) and $MgCl_2$ (10 mM) at 37℃ for 30 min. The nucleases were inactivated by adding 5 µL EDTA (100 mM) followed by incubation at 70ºC for 10 min and incubated for another 30 min at RT. Finally, protected DNA was released from the complexes with the addition of 5 µL 1wt% sodium dodecyl sulfate (SDS) in distilled water for 2 h. Released DNA was

detected by resolving on a 0.8% agarose gel (with 0.1 μg/mL EtBr) in 1X TAE running buffer at 100 V for 40 min.

Measurement of particle size and zeta potential

A dynamic light scattering spectrophotometer (DLS 8000, Otsuka Electronics, Osaka, Japan) was used to measure the size and zeta potential of the PMGT/DNA complexes in comparison to the PEI25kDa/DNA complexes with 90° and 20° scattering angles at 25℃, respectively. The samples were incubated for 30 min in distilled water at N/P ratios of 10, 15, 20, and 25 with 40 μg/mL of final DNA concentration in a total volume of 1 mL. In order to investigate the effects of serum proteins on the stability of PMGT/DNA complexes (N/P 20) compared to PEI25kDa/DNA complexes (N/P 10), serum concentrations of 0%, 10%, 20%, and 30% were added to the prepared complexes and their sizes were then measured.

Observation of PMGT/DNA nanoplexes

The morphology and size of the PMGT/DNA (N/P 20) and PEI25kDa/DNA complexes (N/P 10) were confirmed by EF-TEM (LIBRA 120, Carl Zeiss, Germany). Polyplexes were loaded on a carbon grid, dried for 2 h, stained with 1% uranyl acetate for 10 s,

washed with distilled water, and dried for an additional 10 min. Samples were then analyzed under an electron microscope. Similarly, lyophilized PMGT/DNA and PEI 25kDa/DNA samples were resuspended in PBS and analyzed under electron microscope.

Osmolarity of PMGT

Osmolarity of aqueous solutions of mannitol, MDM and PMGT at various concentrations (2%, 3%, 5%, and 10%) were measured as mOsm using cryoscopic osmometer 030 (Ganatec, USA) and calculated as the depression in freezing point of solutions.

Degradation study of PMGT polyplexes

TRITC (25 μL, 1 mg/100 μL in DMF) was added to PMGT (1 mL, 10 mg/mL in H2O) to block ~1% of its total amines and stirred overnight. Unreacted TRITC was removed by washing with ethyl acetate (3 × 2mL) which was then lyophilized and resuspended in water. A549 cells were transfected with TRITC-PMGT/DNA complexes (N/P 20). A Carl Zeiss LSM 710 inverted laser scanning confocal microscope was used to monitor its intracellular degradation after 3 h, 2 days, 5 days and 7 days. Cell viability was also observed after 3 h, 2, 5, and 7 days of transfection by MTT assay as described in the following section.

Cytotoxicity of PMGT/DNA and PMT/DNA complexes

PMGT *in vitro* cytotoxicity was evaluated by MTT assay in three cell lines (A549, HeLa, and HepG2) and compared with that of PMT and PEI25kDa. At monolayer confluency, cells were trypsinized and seeded in a 24-well plate at 10 x 10^4 initial cell density in 1 mL growth media and allowed to grow to 80% confluency prior to polyplex treatment. Cells were treated at various N/P ratios (10, 15, 20, and 25) in serum-free medium that was changed with serum-containing medium after 3 h. Thirty-six hours later, 500 µL of MTT solution in 1X PBS (0.5 mg/mL) was added to each well and incubated for an additional 3 h. The medium was carefully aspirated, and left behind purple formazan crystals were dissolved in DMSO (500 µL). Dissolved formazan (100 µL) from each well were transferred to 96-well plate and absorbance was measured at 540 nm using a VERSAmax tunable microplate reader (Sunnyvale, CA, USA). All experiments were conducted in triplicate.

In vitro transfection in the absence and presence of serum

Transfection studies were performed in A549, HeLa and HepG2 cells at an initial cell density of 10 x 10^4 in 24-well plate. At 80% cell confluency, PMGT/pGL3 (1 µg), and PEI25kDa/pGL3 polyplexes were

treated at various N/P ratios (10, 15, 20 and 25) in serum-free medium, which was exchanged with fresh medium containing serum (10% FBS) after 3 h. After 24 h of standard incubation conditions, luciferase assay was performed according to the manufacturer's protocol. A chemiluminometer (Autolumat, LB953; EG&G Berthold, Germany) was used to measure relative light units (RLUs) normalized with protein concentration in the cell extract estimated using a BCA protein assay kit (Pierce Biotechnology, Rockford, IL, USA). The effect of serum on polyplex stability for its possible use in biological systems was investigated in the A549 cell line. At N/P 20, cells were transfected with 0%, 10%, 20%, and 30% serum concentrations in 24-well plate, and luciferase assay was performed as described above. Transfection activity was measured in triplicate as RLUs/mg protein.

Flow cytometry measurement

The percent transfection efficiency of PMGT/tGFP (1 µg) polyplexes in comparison with PEI25kDa/tGFP polyplexes was estimated by flow cytometry in A549 cells. Transfected cells were harvested with 0.25% trypsin/EDTA and washed twice with 1X PBS. Cells expressing GFP acquired from a total of 10,000 cells were scored through a FACS calibrator system (Becton-Dickinson, San Jose, CA, USA) to determine

the percent transfection. To demonstrate stable transfection by PMGT for *in vivo* suitability, A549 cells were incubated for 2, 3, and 5 days post-transfection and percentage transfection was quantified using FACS.

Silencing efficiency of PMGT

A549 cell were transfected with Lipofectamine^{TM}/pGL3 (1 µg) complexes in serum-free medium. After 3 h, the medium was aspirated and PMGT/siLuc or siScr (N/P 20) and PEI25k/siLuc or siScr complexes (N/P 10) were added containing 50, 75, 100 and 150 pM siRNA concentrations. Cells were incubated for additional 3 h, after which medium was replaced with complete medium containing 10% serum. Finally, 48 h later luciferase expression was measured by luciferase assay and normalized with the protein concentration in the cell extract. The luciferase silencing efficiency was calculated as the relative percentage of luciferase activity to the control cells without siRNA treatment.

MTT assay was also performed to show no toxic effects of PMGT/siRNA complexes. The cytotoxicity of PMGT/siRNA (N/P 20) and PEI25k/siRNA complexes (N/P 10) was evaluated in A549 cells at

various siRNA concentrations of 50, 100, 150 pM. After 36 h MTT assay was performed as described in the following section.

In vivo gene expression and bio-distribution of PMGT/DNA complexes

Animal study was performed in wild type male C57BL/6 mice lungs (4 mice /group) to analyze *in vivo* gene expression by aerosol delivery of polyplexes. Aerosol was prepared by complexing PMGT (N/P 20) with 1 mg of turboGFP (tGFP) (Origene, Rockville, USA) and delivered to 6-week old mice lungs by placing the mice inside a nose-only exposure chamber (NOEC; Dusturbo, Seoul, Korea) for 40 min. After 48 h, mice were sacrificed and lungs were perfused with phosphate-buffered-saline through trachea. Lungs were fixed in 4% paraformaldehyde for 12 h and then preserved in 30% sucrose for 48 h at 4^{o}C. Lungs were embedded in a Tissue-TekOCT compound (Sakura, Torrance, CA, USA) at < 20℃. Cryostat was used to prepare 20 µm thick lung sections, mounted on slides and observed for tGFP expression using a ZeissLSM510 confocal microscope (Carl Zeiss, Inc.).

For *in vivo* biodistribution analysis, PMGT (N/P 20) and PEI25kDa (N/P 10) were complexed with pGL3 (30 µg) in normal saline (final

volume 100 µL). Similarly, naked DNA in normal saline was used as a control. Complexes were delivered to 6-week old C57BL/6 mice intravenously (i.v.) through the tail vein using a 40 U insulin syringe (1 mL with a needle size 0.30 x 8 mm). After four days of gene delivery, animals were sacrificed by cervical dislocation and all vital organs were dissected. Organs were washed with chilled normal saline, weighed, chopped, and suspended to 25% w/v homogenate in 2.5X cell lysis buffer (Promega, USA) and centrifuged (10,000 rpm, 10 min, 4°C). Cell lysate (100 µL) from each sample was assayed for luciferase activity using a chemiluminometer.

Mechanistic studies for high transfection efficiency by PMGT:

Packed cell volume (PCV) test

Osmotic activity of polymannitol in the PMGT backbone was measured by PCV test. Briefly, 2, 3, and 5 wt% mannitol in the PMGT were mixed with 10 $x10^5$ A549 cells in mini-PCV tubes, incubated for 10 min and centrifuged at 4500 rpm for 1 min. Similar experiments were performed with same amount of pure mannitol as a control. A decrease in volume in PCV tube was calculated as percentage decrease in cell volume.

Effect of COX-2 inhibition on hyperosmotically driven transfection

SC58236, a potent inhibitor of COX-2, was used to verify the relationship between PMGT hyperosmotic effect and COX-2 release. Different concentrations of SC58236 (0, 5, 10 and 20 µM/L) were prepared in serum free medium from the stock solution in DMSO. A549 cells were treated with SC58236 prior to transfection for 1, 2 and 4 h, after which PMGT/DNA (N/P 20) and PEI25kDa/DNA (N/P 10) polyplexes were added and transfection efficiency was measured 24 h later as RLUs/mg of protein by luciferase assay using above stated protocols.

ELISA assay for determining COX-2 expression under hyperosmotic stress

8.8 cm^2 culture dishes were seeded at 40 x 10^4 initial cell density and treated with PMGT/tGFP (N/P 20) and PEI 25k/tGFP (N/P 10) polyplexes. Cells were harvested at different time intervals (1h, 3h and 6h) to obtain cell lysate. COX-2 sandwich ELISA (Pathscan, cell signaling technology, USA) was performed for the quantification of hyperosmotically induced COX-2 in cell lysates according to the manufacturer's protocol and absorbance was measured at 450 nm.

COX-2 inhibition study by confocal microscopy

A Carl Zeiss LSM 710 inverted laser scanning confocal microscope was used to monitor intracellular trafficking of TRITC-labeled PMGT and YOYO-1 labeled pDNA in A549 cells in the presence and absence of SC58236. pDNA (1 µg) was labeled with YOYO-1 iodide (2 µL, 1 mM solution in DMSO) by stirring for 2h at 25 ± 1 ℃ in dark, and then stored at -20 ℃. A549 cells seeded in 6 well plate at 20 x 10^4 cells/well were transfected with dual labeled PMGT/DNA complexes with and without SC58236. After 120 min of incubation, cells were washed with 1× PBS (3×500 µL) and fixed with 4% paraformaldehyde for 10 min at 4 ℃. DAPI was used to counter-stain the nuclear DNA of fixed cells, and images were procured from confocal microscopy and quantified using custom designed MATLAB program.

Endocytosis inhibition study

The route of PMGT uptake was analyzed by inhibiting various endocytosis pathways and their subsequent effect on transfection was observed.

Inhibition of caveolae-mediated endocytosis

Caveolae dependent endocytosis was investigated using the inhibitors β-methyl cyclodextrin (BMC) (2.5, 6.5 and 10 mg/mL) and genistein (100, 200 and 300 µM). After 1 h of incubation at 37℃ with inhibitors A549 cells were transfected with PMGT/DNA complexes (N/P 20) in serum free medium. Luciferase activity was measured 24 h later as RLUs/mg of protein.

Inhibition of clathrin and macropinocytosis-mediated endocytosis

Chlorpromazine and wortmannin were used to investigate clathrin and macropinocytosis dependent endocytosis respectively. A549 cells were pre-treated with varying concentrations of chlorpromazine (1, 2 and 3µg/mL) and wortmannin (50, 100 and 200 nM) in serum free medium and incubated for 1 h at 37℃ before the addition of PMGT/DNA complexes (N/P 20).

Proton sponge effect by PEI in PMGT

A549 cells in 24-well plates (10×10^4cells/well initial cell density) at 80% confluency were incubated with endosome proton pump inhibitor, bafilomycin A1 (a specific inhibitor of vacuolar type H+ - ATPase) (200 nm in DMSO) for 10 min just before transfection to ensure endosomal escape of PMGT. Inhibitor was aspirated followed by

PMGT/DNA (N/P 20) and PEI25kDa/DNA (N/P 10) complexes addition. Cells without bafilomycin A1 treatment were taken as control. The cells were measured for their luciferase activity in triplicate.

2.3 Results

Physicochemical characterization of synthesized PMGT

Newly synthesized gene delivery carrier PMGT incorporates osmolyte properties of hydroxyl groups and hydrophobic methyl groups in the carrier. The primary hydroxyl groups of mannitol when reacted with methacryloyl chloride primarily led to the formation of 1, 6 disubstituted mannitol dimethacrylate (MDM) due to higher reactivity of primary alcohols than secondary alcohols (Fig. 2.1). To avoid isomer formation and polysubstitution mannitol and methacryloyl chloride were reacted at 1:2 molar ratio. ^{1}H NMR spectra of MDM showed intense peaks at 5.6-6.2 ppm representing protons in the vinyl group (Fig. 2.2A). Thereafter, MDM was cross-linked with LMW bPEI by Michael addition reaction to synthesize PMGT (Fig. 2.1) evidenced by ^{1}H NMR that showed disappearance of MDM vinyl proton peaks (Fig. 2.2B).

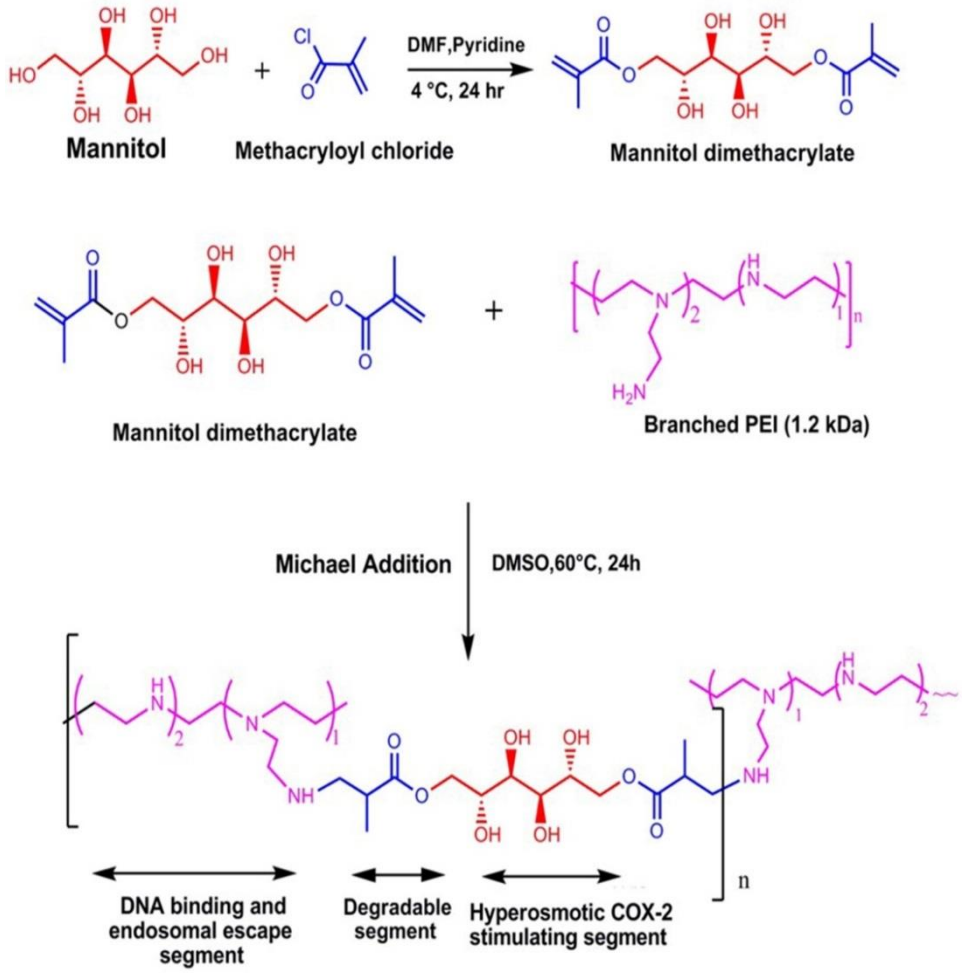

Fig. 2.1 Reaction scheme for PMGT synthesis

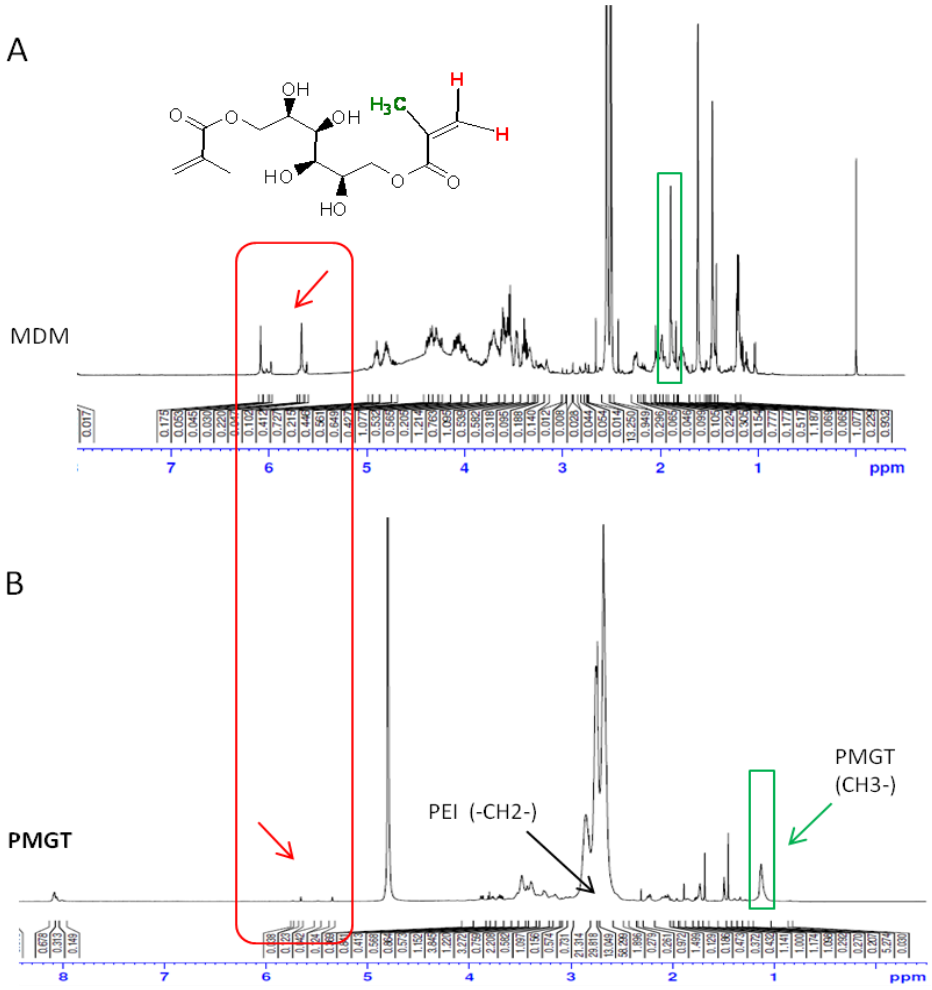

Fig. 2.2 Characterization of PMGT copolymer: ^{1}H-NMR spectra of (A) MDM in DMSO and (B) PMGT in D_2O

The synthesized PMGT was characterized as a gene carrier; DNA condensation and protection ability; size, zeta potential and morphology of polyplexes; and osmolarity. The composition of mannitol in PMGT estimated by NMR was about 36.7 mol-% and the MW measured by GPC was 8500~8800 Da, which suggests appropriate size of the polymer necessary for effective binding with nucleic acids. Gel retardation assay further demonstrated the ability of PMGT to condense DNA by completely retarding its migration in the agarose gel at a lower N/P ratio of 3 (Fig. 2.3B), suggesting a high PMGT complexation capacity. Further, through DNA protection & release assay, PMGT showed to protect the complexed DNA as visible in lane 4 of Fig. 2.3A, suggestion of its protection against intracellular DNase degradation contrary to the complete degradation of naked DNA (lane 2, Fig. 2.3A).

Electrostatic condensation of DNA with PMGT resulted in nanosized cationic particles suitable for cellular uptake when confirmed by dynamic light scattering spectrophotometer (DLS) and EF-TEM. DLS revealed a decreasing trend in PMGT/DNA nanoplex sizes from 200 to 110 nm with increasing N/P ratios (Fig. 2.3C) due to stronger complexation with DNA. Zeta potential measurements also showed a

similar decreasing pattern with an increase in N/P ratios of the polyplexes (Fig. 2.3E). However, it is noteworthy that PMGT showed an initial decrease and then stable zeta potential at around +15 to +20 mV, suggesting the role of polymannitol hydroxyl groups in shielding the surface charge of complexes probably due to the formation of hydrogen bonds between polymannitol and DNA leading to stable zeta potential contrary to increasing zeta potential of PEI25kDa/DNA complexes. A harmonized and stable charge density on PMGT polyplexes, achieved by LMW PEI and hydroxyl groups ensures interaction with anionic membrane proteins to initiate polyplex internalization. In addition, it also reduces cytotoxicity caused by high charge density leading to cell membrane rupture. The polyplex sizes estimated with increasing serum concentrations showed a continuous increase in the hydrodynamic diameter of PEI25kDa/DNA complexes due to aggregation with the negatively charged serum proteins making the polyplex sizes unsuitable for cellular uptake.

Contrarily, PMGT/DNA complexes showed no significant increase in polyplex sizes, suggesting minimal interaction with serum proteins and favorable transfection (Fig. 2.3D). This stable behavior of polyplexes can be attributed to the hydroxyl groups of polymannitol backbone

which first shields the polyplexes by making intermolecular hydrogen bonds with DNA and secondly, its partial negative charges prevent their interaction with serum proteins by generating repulsion in an anionic environment. Therefore polyplexes maintain uniform size distribution throughout its voyage to the nucleus which is also apparent from the lower polydispersity index (PDI) of < 0.2 and EF-TEM images. Around 120 nm sizes of PMGT/DNA complexes taken before and after lyophilization showed well-defined spherical morphologies and no aggregation in comparison to PEI25kDa/DNA complexes (Fig. 2.3F). Contrary to PEI25kDa/DNA complexes that underwent aggregation after lyophilization, the intact morphologies of PMGT/DNA complexes demonstrate their robustness and suitability for powder formulations in aerosol administration.

Moreover, the intrinsic hyperosmotic property of PMGT was elucidated by measuring its osmolarity that tend to increase with the increase in its concentration (Table 2.2) due to polymannitol backbone. This reflects its tendency to induce hyperosmotic stress on the cells to accelerate the cellular uptake process.

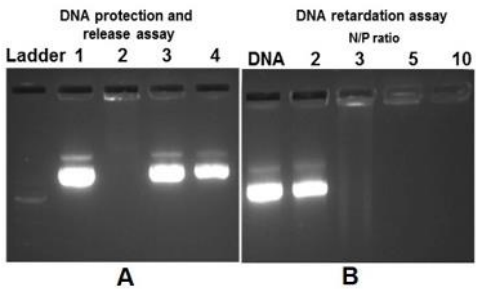
DNA protection and release assay
Ladder 1 2 3 4
DNA retardation assay
N/P ratio
DNA 2 3 5 10
A
B

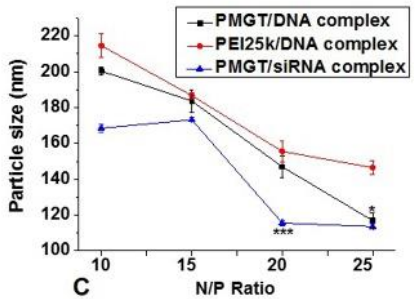
PMGT/DNA complex
PEI25k/DNA complex
PMGT/siRNA complex
Particle size (nm)
N/P Ratio
C

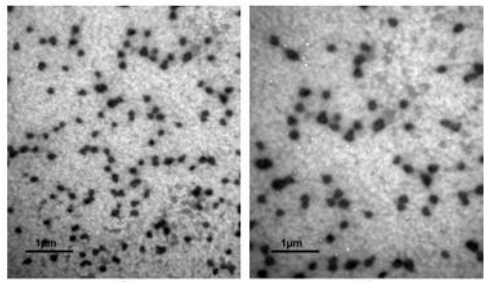
i
ii

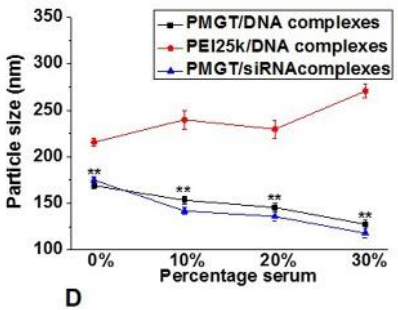
PMGT/DNA complexes
PEI25k/DNA complexes
PMGT/siRNAcomplexes
Particle size (nm)
Percentage serum
D

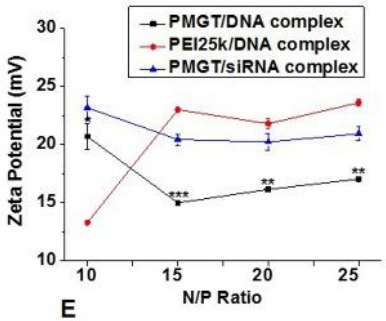
PMGT/DNA complex
PEI25k/DNA complex
PMGT/siRNA complex
Zeta Potential (mV)
N/P Ratio
E

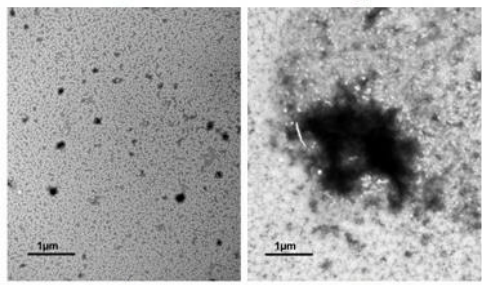
iii
iv
F

Fig. 2.3 Physico-chemical characterization of PMGT copolymer. (A) DNA protection and release assay: DNA was released by adding 1% SDS to PMGT/pGL3 complexes at an N/P ratio of 20; (Lane 1) pGL3 without DNase I, (Lane 2) pGL3 with DNase I, (Lane 3) PMGT/pGL3 complexes without DNase I, and (Lane 4) PMGT/pGL3 complexes with DNase I. (B) Gel electrophoresis of PMGT/pGL3 (0.1 μg) complexes at various N/P ratios ranging from 2 to 10. Characterization of PMGT/DNA complexes: (C) particle sizes without serum, (D) particle sizes in various serum percentages, and (E) zeta potential (F) EF-TEM images of (i) PMGT/pGL3, (ii) lyophilized PMGT/pGL3, (iii) PEI 25k/pGL3, and (iv) lyophilized PEI 25k/pGL3 complexes at N/P ratio of 20.(n = 3, error bar represents SD) (*$p < 0.05$; **$p < 0.01$; ***$p < 0.001$, one-way ANOVA).

Table 2.2 Osmolarity of aqueous solutions of pure mannitol, sorbitol, dixylitol and their corresponding diacrylates at various concentrations measured as mOsm, calculated from the depression in freezing point of solutions.

Conc.	**Osmolarity [mOsm]**					
	Mannitol	**MDM**	**PMGT**	**PEI 1.2 kDa**	**PMGT/DNA polyplex (N/P 20)**	**PEI/DNA polyplex (N/P 20)**
2%	144	61	69	0	70	8
3%	267	104	111	14	101	26
5%	391	142	151	25	139	33
10%	788	299	332	56	273	65

In vitro cell viability and transfection efficiency of PMGT polyplexes

Cell viability of PMGT/DNA complexes was estimated by MTT assay that showed about 95% cell viability in A549, HeLa, and HepG2 mammalian carcinoma cell lines at various N/P ratios in comparison to PMT/DNA (~ 94%), PEI25k/DNA (~ 60%) and Lipofectamine/DNA (~ 70%) indicating that cell viability of the PMGT/DNA complexes was not much different from PMT/DNA complexes regardless of the hydrophobic methyl groups in the PMGT (Fig. 2.4). Fate of PMGT/DNA complexes was also observed under confocal microscopy after 3 h, 2, 5, and 7 days post-transfection which showed gradual disappearance of PMGT (Fig. 2.5A) to demonstrate its degradation tendency that accounts for higher cell viability (Fig. 2.5B) and biocompatibility. Issue of biodegradability is answered by the presence of degradable ester linkages (Fig. 2.1) between polymannitol and bPEI. Cleavage of these bonds inside the biological system leaves polymer into smaller fragments which can be easily exocytosed.

In vitro PMGT/pGL3 transfection in A549, HeLa, and HepG2 cell lines showed higher transfection efficiency, particularly at N/P 15 & 20 due to its hyperosmotic behavior and hydrophobic methyl groups present in

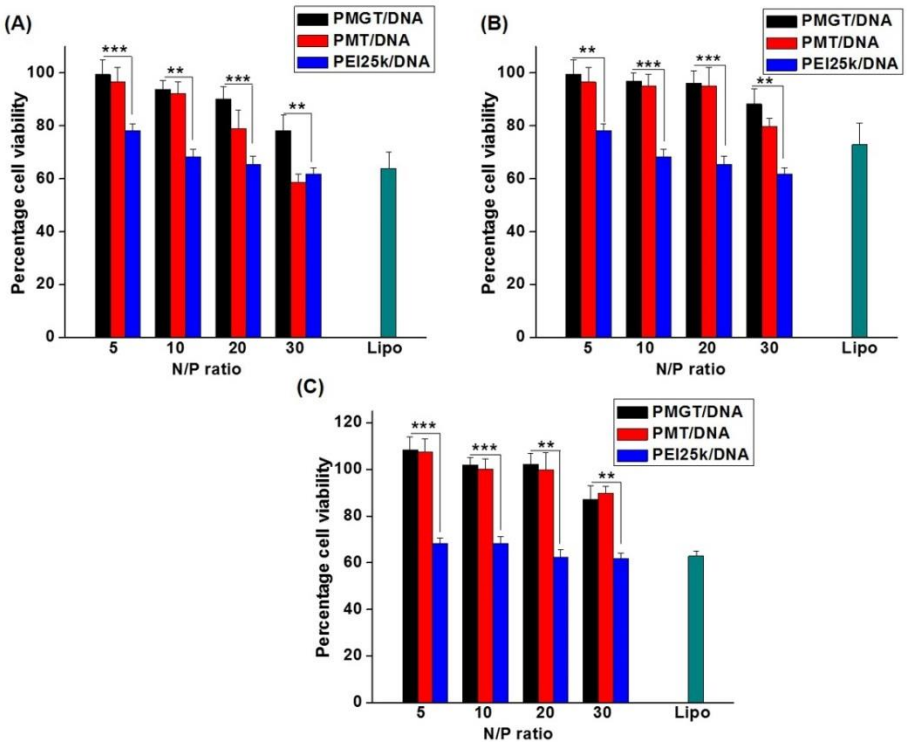

Fig. 2.4 Cytotoxicity of PMGT/ pGL3 complexes compared to PMT/pGL3 and PEI25K /DNA complexes at various N/P ratios in different cell lines: (A) A549; (B) HeLa; and (C) HepG2 (n= 3, error bar represents SD) (*p < 0.05;**p < 0.01; ***p < 0.001, one-way ANOVA).

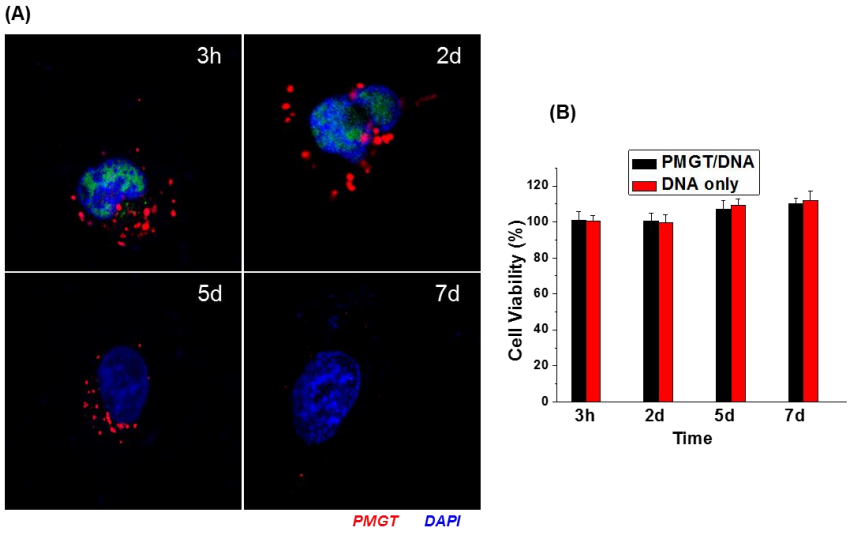

Fig. 2.5 *In vitro* degradation study of PMGT. (A) Confocal images showing PMGT (red) decreasing significantly after 2 days and drastically after 5 days (magnification:100X). (B) Cell viability after 3 h, 2, 5, and 7 days in A549 cells (n = 3).

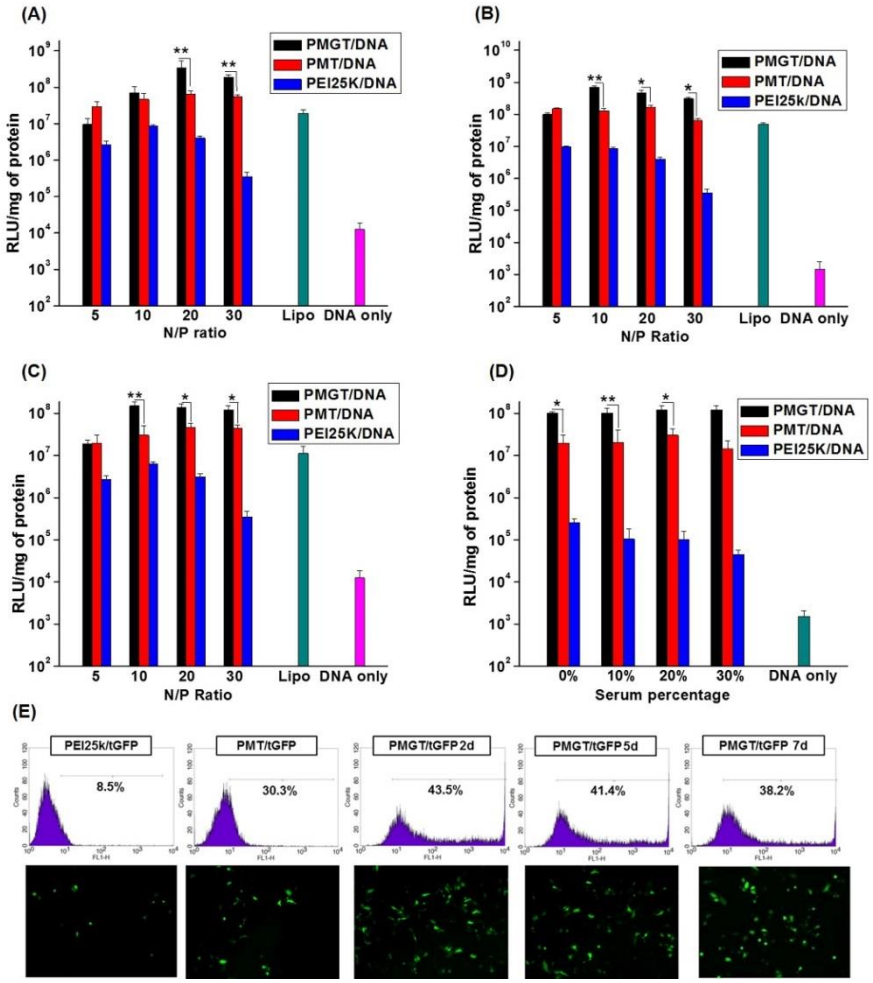

Fig. 2.6 Luciferase activity of PMGT/ pGL3 complexes without serum at various N/P ratios in different cell lines: (A) A549; (B) HeLa; and (C) HepG2 (D) Luciferase activity of PMGT/pGL3 complexes in various serum percentages in A549 cells (n= 3, error bar represents SD) (*$p < 0.05$; **$p < 0.01$, ***$p < 0.001$, one-way ANOVA). (E) Transfection efficiency of PEI, PMT and PMGT by FACS analysis.

the PMGT rendering better cellular uptake. PMGT (N/P 20) resulted in a 15-20 fold increase in luciferase expression over PEI25kDa (N/P 10) and 5-6 fold increase over PMT (N/P 20) (Fig. 2.6A, B, C). Flow cytometry also recorded this crucial result of increased transfection efficiency of PMGT (35 - 40 %) over 8 – 10 % efficiency of PEI25kDa and 25-30% efficiency of PMT (Fig. 2.6E) which indicated the probable role of hydrophobic properties of PMGT in cellular uptake process. Moreover, transfection efficiency after 7 days dropped by only 3-5 %, suggestion of stable transfection by PMGT (Fig. 2.6E). The crucial result is the increase in the transfection efficiency of PMGT over PMT. It is noteworthy that even at the same N/P ratios luciferase activity was higher for PMGT over PMT, clearly suggesting the advantageous role of hydrophobic methyl groups of PMGT assisting in cellular entry of PMGT though cell viability does not resulted in much differences.

Transfection efficiency of PMGT in terms of siRNA delivery was also estimated by silencing luciferase expression using luciferase siRNA (siLuc). PMGT/siLuc showed an increased silencing efficiency reaching up to 90% in comparison to PEI25k/siLuc. The silencing activity becomes stable after 100 pM of siRNA concentration. As

expected non-specific scrambled siRNA (siScr) and naked siLuc exhibited negligible silencing (Fig.2.7). Cell viability assay of PMGT/siLuc verifies that the improved PMGT-mediated gene silencing was not affected by cytotoxicity (Fig. 2.8).

Serum affects the transfection efficiency firstly by exhibiting an intrinsic DNase activity to degrade the loosely bound DNA and secondly, by interacting with cationic polymer to cause polyplex aggregation [108]. The transfection results in the presence of serum demonstrated the effectiveness of PMGT in restraining the complexes from binding with serum proteins primarily due to the shielding effect of its hydroxyl groups, ensuring unaffected transfection up to 20% serum concentration (Fig. 2.6D). The results are in accordance with the aforementioned particle size measurements at various percent serum concentrations. Therefore, stable transfection over 7 days and unaffected gene expression in the presence of serum suggests possibility of its *in vivo* application.

In vivo gene expression and biodistribution of PMGT/DNA complexes

Non-invasive aerosol delivery was chosen over intravenous delivery for

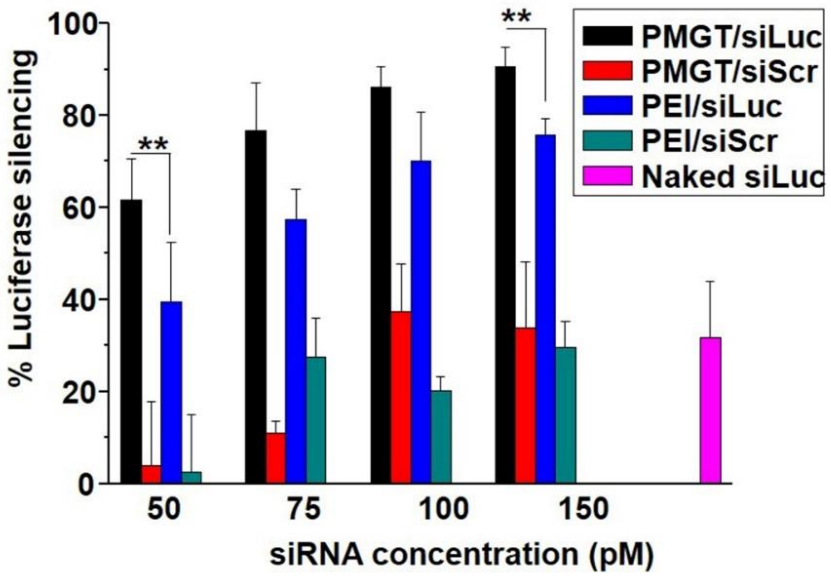

Fig. 2.7 Silencing efficiency of PMGT/siLuc and PEI25k/siLuc complexes in A549 cells compared to the respective scrambled siRNA (siScr) group (n = 3, error bar represents SD), (*p < 0.05; **p < 0.01, ***p < 0.001, one-way ANOVA).

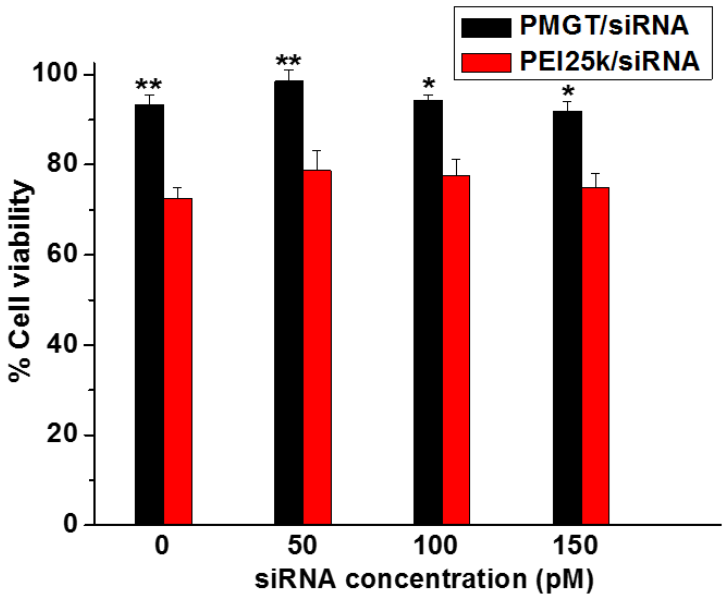

Fig. 2.8 Cytotoxicity of PMGT/siRNA and PEI25k/siRNA complexes at various siRNA concentrations in A549 cells. (*n* = 3, error bar represents SD) (*p < 0.05, one-way ANOVA).

expression of the target gene in respiratory system as it allows DNA deposition in the lungs at pulmonary region and prolongs DNA retention time, whereas intravenous gene delivery causes quick systemic distribution with a shorter half-life in the lungs [109]. Moreover, stability of PMGT/DNA nanoplexes even after lyophilization makes it suitable for aerosol application (Fig. 2.3F ii, iv). Aerosol administration of PMGT/tGFP complexes (N/P 20) in C57BL/6 mice lungs (n=4) showed enhanced tGFP expression in contrast to PEI25kDa/tGFP administered mice (Fig. 2.9A).

Biodistribution of PMGT/pGL3 complexes in 6-week old C57BL/6 mice showed the highest luciferase expression in spleen, followed by lung, brain and kidney, with negligible expression in liver and heart (Fig. 2.9B). Hyperosmoticity offered by polymannitol backbone enhanced cellular uptake, especially in the lung and brain, which typically allow restricted entry for therapeutics [110]. Immediately after i.v. injection, polyplexes tend to aggregate with blood cells and plasma components, resulting in accumulation of polyplexes in the fine capillaries of the lung [24, 97] where they extravasate into the lung tissues due to the hyperosmotic environment created by the polymer.

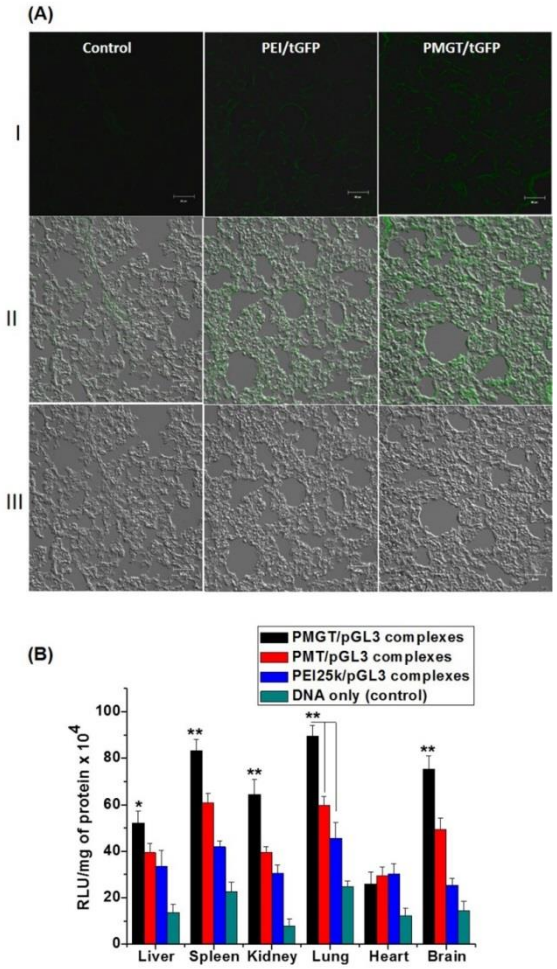

Fig. 2.9 *In vivo* biodistribution of PMGT. (A) Fluorescent microscopic images of *in vivo* tGFP expression after aerosol administration to mice (C57BL/6) lungs (n=4). Quadrants of control, PEI25k/tGFP and PMGT/tGFP showing (I) fluorescent, (II) merged and (III) phase contrast images respectively. (B) Graph showing biodistribution by luciferase expression in various organs after 3 days of intravenous injection in mice (C57BL/6).

Therefore, luciferase delivered by PMGT was much expressed in the mouse lung and brain in comparison to PEI25kDa.

Hyperosmotic tendency of PMGT induces COX-2 expression

Since mannitol's hyperosmotic behavior is vastly used clinically in crossing the biological barriers [111], it necessitated to determine its retained hyperosmotic tendency in PMGT to deliver osmotic shocks to the cells [112]. A549 cells ($10x10^5$ cells/ PCV tube) treated with increasing concentrations of PMGT (2, 3, and 5 wt%) showed 7, 9, and 14% decrease in cell volume, similar to the trend when treated with the same amount of pure mannitol to show 10, 15, and 22% decrease in cell volume (Fig. 2.10A). These results, in accordance with the osmometer measurements (Table 2.2) demonstrated that like pure mannitol, the incorporated polymannitol in PMGT has ability to squeeze out water from the cells owing to its hyperosmotic behavior, thereby assisting PMGT/DNA complexes to penetrate through the biological barriers.

Elegant early findings reveal that under hypertonic conditions, osmotic equilibrium is regained by an intracellular accumulation of organic osmolytes via COX-2 induction [113].

In order to confirm whether COX-2 expression under PMGT induced

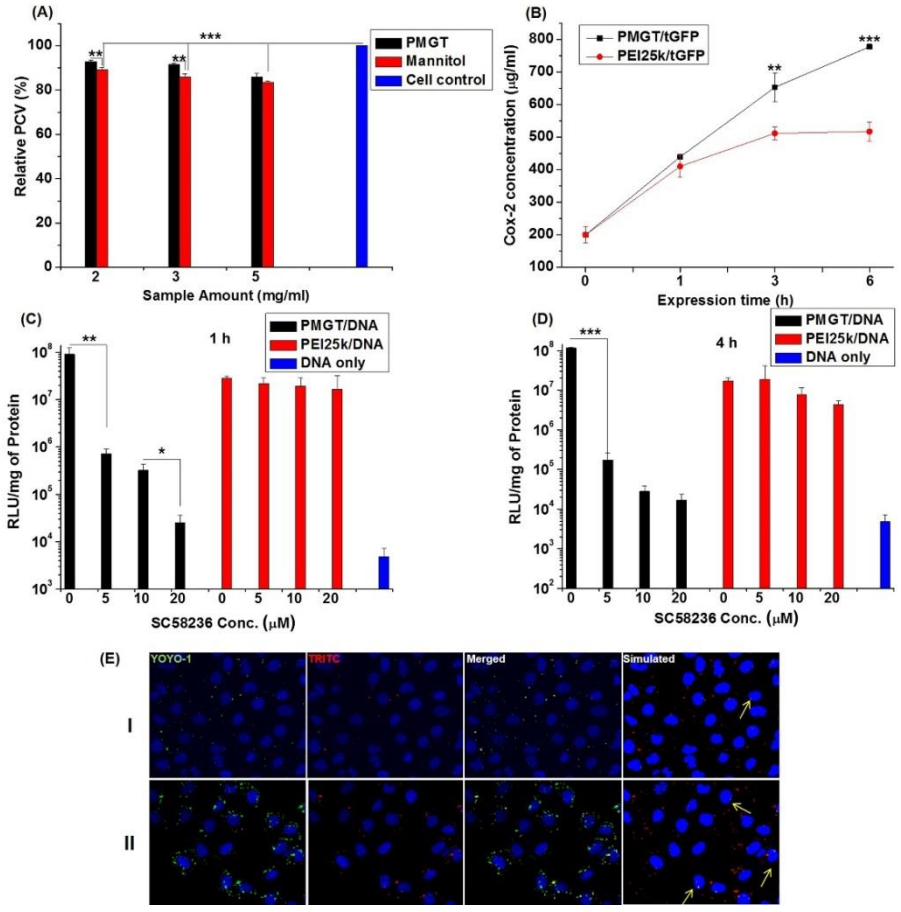

Fig. 2.10 Mechanistic investigations for enhanced transfection of PMGT: (A) Effect of polymannitol's hyperosmotic activity on packed cell volume (A) Bafilomycin A1 study, (C and D) Effect of COX-2 inhibitions (at 1 and 4 h) by SC58236 on PMGT-mediated gene transfection. (n = 3, error bar represents SD) (*$p < 0.05$, **$p < 0.01$; ***$p < 0.001$, one-way ANOVA). (E) Confocal microscopic images of PMGT/DNA polyplexes showing uptake of nanoparticles. (I) In the

presence of COX-2 inhibitor SC58236; (II) In the absence of COX-2 inhibitor SC58236. MATALB simulation tool is used to estimate the particles present inside the nucleus (blue). Quadrants showing pDNA labeled with YOYO-1(green) and nucleus (blue) and PMGT labeled with TRITC (red), overlaid pictures showing yellow color polyplex (green and red). MATLAB simulated pictures showing particles inside the nucleus as white.

hyperosmotic stress, COX-2 ELISA assay was performed. The results showed an increased concentration of COX-2 with time in cell lysates treated with PMGT polyplexes in comparison to PEI25kDa treated cell lysates, suggesting the role of hyperosmotic effect of hydroxyl groups in polymannitol backbone in encouraging the release of osmoprotectant COX-2 (Fig. 2.10B). A weak COX-2 expression induced by PEI25kDa might be a toxicity related inflammatory response. Hence the enhancement in transfection efficiency was probably due to the disturbed osmotic environment on the cell surface that increased cellular uptake of PMGT polyplexes via COX-2 induction.

COX-2 induction enhances cellular uptake of PMGT/DNA complexes

From the ELISA assay it was clear that COX-2 was induced due to hyperosmotic property of PMGT, but to elucidate the effect of COX-2 induction on cellular uptake resulting in high transfection efficiency, COX-2 expression was inhibited by SC58236 as a COX-2 inhibitor and change in transfection activity was observed. A549 cells transfected with PMGT/DNA and PEI25k/DNA complexes in the presence of SC58236 showed a sudden decrease (~20 fold) in PMGT-mediated transfection at an inhibitor concentration of 5 μM which gradually decreased further in a dose dependent manner (Fig. 2.10C, D).

On the other hand, no significant inhibitor effect (even at 20 µM concentration) on PEI25kDa-mediated transfection activity was observed, suggesting that SC58236 only inhibits the COX-2-mediated PMGT accumulation and decelerates polyplex uptake mitigating the effect of polymannitol backbone. A slight decrease in PEI25kDa transfection after 4 h was probably due to stress induced cell death. The results clearly state a determining role of polymannitol backbone and induced COX-2 protein for enhanced transfection.

Moreover, confocal images also confirmed that the internalization of PMGT/DNA polyplexes was decreased in the presence of SC58236 from 15% to 3% due to inhibition of COX-2 showing its incapability to restore osmotic balance by polyplex internalization (Fig. 2.10E).

COX-2 expression elicit caveolae-mediated endocytosis

The mode of endocytosis to accumulate polyplexes was investigated using various inhibitors of caveolae (β-methyl cyclodextrin and genistein), clathrin (chlorpromazine), and macropinocytosis (wortmannin) and their effect on transfection efficiency of PMGT was carefully observed in A549 cells.

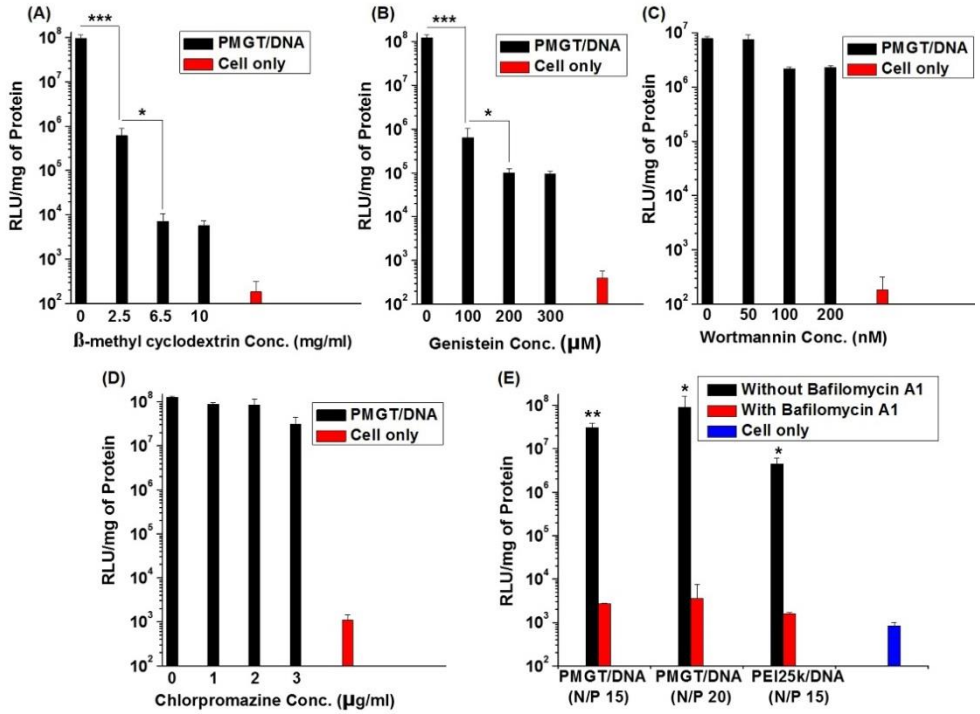

Fig. 2.11 Effect of inhibitors on transfection. (A) β-methyl cyclodextrin, (B) genistein, (C) chlorpromazine and (D) wortmannin. (n = 3, error bar represents SD) (E) Bafilomycin A1 (*p < 0.05, **p < 0.01; ***p < 0.001, one-way ANOVA).

While inhibition of macropinocytosis and clathrin-mediated endocytosis demonstrated no decrease in the transfection efficiency of PMGT, depletion of cholesterol rafts in caveolae by genistein and β-methyl cyclodextrin (BMC) caused a significant decrease in transfection, suggesting the role of caveolae-mediated endocytosis in the cellular uptake of PMGT/DNA complexes (Fig. 2.11), although the hydrophobic methyl groups in the PMGT did not affect the endocytosis pathway compared to the PMT ones [10]. The caveolae pathway is likely to be initiated by PMGT due to the hyperosmotically induced COX-2 for intracellular accumulation of PMGT polyplexes to restore osmotic equilibrium.

Furthermore, PEI part in PMGT backbone are responsible for H^+ absorption which leads to an influx of Cl^- ions and water that causes the endosomes to swell and burst, a mechanism called proton sponge effect. Inhibition of vacuolar type H^+ ATPases by bafilomycin A1 showed 1000-folds decrease (N/P 20, Fig. 2.11E) in the transfection of PMGT, suggesting the ability of PMGT to escape endosomal degradation. The inhibitor prevented endosomal acidification and hence ceased its bursting to release the transporter.

2.4 Discussion

Our findings show that, the inherent hyperosmotic properties of gene transporter can modify the internalization pathway by initiating cell signaling cascade. Therefore, interest aroused towards PMGT due to its combined hyperosmotic and hydrophobic properties. We sought that hyperosmotic polymannitol part with hydrophobic methyl groups in the PMGT could trail the gene transporter through membrane barrier. MDM utilizes the formation of ester linkage between its allyl group and amines of the LMW bPEI by Michael addition reaction to polymerize into PMGT. The robustness of PMGT was demonstrated by its ability to protect nucleic acids against DNase degradation and its biocompatibility was assured by higher cell viability and degradation study. The nanosized structure (~150 nm) and stable surface charge of PMGT/DNA complexes make it suitable for trouble free cellular uptake. In addition, 20 folds higher luciferase expression of PMGT than PEI25kDa shows the importance of hydroxyl groups in inducing osmotic stress and other signaling molecules to accelerate uptake process. And, 5-6 folds higher luciferase expression of PMGT compared to PMT demonstrated the significance of hydrophobic methyl groups for smooth trans-membrane delivery of polyplexes

although the hydrophobic methyl groups in the PMGT did not affect cell viability. The methyl groups help in enhancing delivery by forming hydrophobic interactions with the lipid constituent of plasma membrane. The hydrophobic interactions of PMGT with plasma membrane in addition to electrostatic interactions smoothens the cellular internalization process. The enhancement in transfection efficiency compared to PMT and PEI25kDa is its most striking feature to suggest the combined role of hydrophobicity and hyperosmoticity in cellular uptake.

Extracellular disturbances may have significant effect on cellular functions, transmembrane transport and endocytosis [114]. Depending upon the required cellular function, different endocytic routes regulate the fate of endosomes in co-operation with other signaling molecules. These routes include clathrin-mediated endocytosis, caveolae-mediated endocytosis, macropinocytosis and phagocytosis. An understanding of internalization through these multifaceted routes in response to a stimulus is essential since the internalization mode of polyplexes will have a direct impact on transfection efficiency [115]. Though polymers enter via both clathrin- and caveolae-mediated endocytosis [116, 117], inhibition studies revealed that hyperosmotic stimulus by PMGT

predominantly induced caveolae-mediated endocytosis. Since hyperosmotically active compounds selectively stimulate caveolae formation [104], we found that this stimulation is related with the up-regulation of COX-2 inflammatory molecules. As caveolae are enriched with membranous enzymes and co-localized signaling molecules such as COX-2 [118], we speculate that depletion of caveolae lipid raft by inhibitor destroys its integrity and disrupts the co-localized COX-2, resulting in complete gene expression failure (Fig. 2.11). Membrane impermeable agents such as mannitol and NaCl increase intracellular COX-2 protein levels by exerting hypertonic effect. In a similar way, the hyperosmotic effect of PMGT induces COX–2 expression as an inflammatory response to regain equilibrium across the cell membrane. This leads to fast cellular uptake of hyperosmotic polyplexes via caveolae- mediated endocytosis resulting in enhanced transfection. A decrease in transfection activity of PMGT by COX-2 specific inhibitor (SC58236) suggests a close link between hyperosmotic effect and COX-2 induction. ELISA results also showed increased COX-2 expression with increase in polymannitol content.

In addition, confocal studies in the presence of COX-2 inhibitor showed a reduction in the internalization of polyplexes compared to

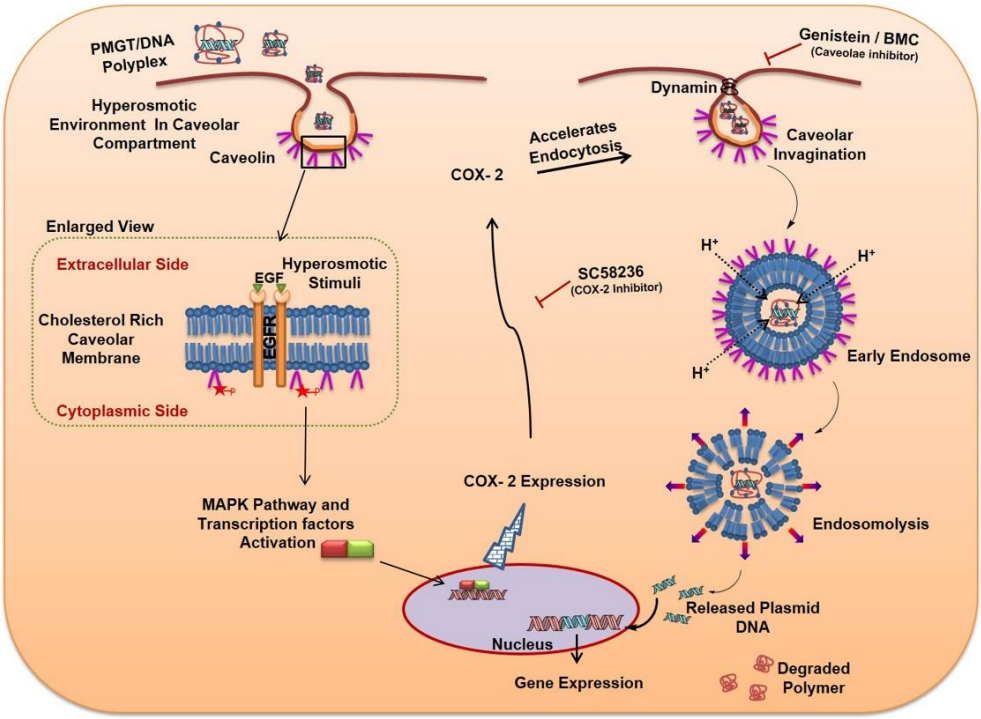

Fig. 2.12 Diagrammatic representation of the proposed mechanism of PMGT internalization through co-localized COX-2 and caveolae-mediated endocytosis

that in the absence of inhibitor. These results collectively illustrate that the PMGT's hyperosmotic stimuli upregulates COX-2 expression and helps in increasing cellular uptake. As a general mechanism, COX-2 enzyme generates an inflammatory response against hyperosmotic stimuli [119]. This response helps cells to escape apoptosis by regulating fast osmolyte internalization [120] for subduing cellular stress. Recent studies have reported that osmotic stimuli activate cell surface EGFR receptors that commence activation of downstream MAPKs. This ultimately signals an osmoprotectant (transcription factor) which induces cytoprotective COX-2 expression to ensure cell survival by enhancing cellular uptake [113, 119, 121-125].

A pictorial representation of the PMGT uptake mechanism, illustrated in figure 2.12, articulates the cellular machinery involved in delivering a gene.

2.5 Conclusion

In conclusion, polymannitol-based gene transporter (PMGT) avails the hyperosmotic properties of polymannitol and hydrophobic effects of methyl groups as an integral part of the vector for better plasma membrane crossover leading to enhanced nucleic acid delivery. The

methyl groups help in improving delivery by hydrophobic interactions with the lipid component of plasma membrane. The polymannitol backbone through its hydroxyl groups corresponds to better DNA complexation and polyplex stability by forming hydrogen bonds that results in particle size of ~150 nm appropriate for cellular uptake. The robustness of PMGT was demonstrated by its ability to protect nucleic acids against DNase degradation and its biocompatibility was assured by higher cell viability. Mechanistic investigations revealed that cationic PMGT binds to the cell surface and generates a hyperosmotic environment at the extracellular side. This hyperosmotic stimulus was found to stimulate COX-2 induction which was responsible for enhancement in cellular uptake, as suggested by COX-2 inhibition, ELISA and confocal studies. In order to restore osmotic equilibrium across the cell membrane, COX-2 enhanced polyplex accumulation by activating caveolae-mediated endocytosis. The study illustrates increased cellular uptake and thus higher transfection efficiency by modulating the mode of internalization route through combined effect of hydrophobic and hyperosmotic properties of PMGT. Therefore, the attributes of PMGT demonstrated in the present study show its

potential applications in developing more profound gene and drug delivery systems.

CHAPTER 3

Hyperosmotic Polydixylitol for Crossing Blood Brain Barrier and Nucleic Acid Delivery

3.1 Introduction

Brain represents a particularly inaccessible organ for the delivery of therapeutic molecules due to the presence of compact blood-brain-barrier (BBB), which excludes the brain-specific delivery of 100% of large molecules and more than 98% of small therapeutic molecules [126, 127]. The architecture of BBB, which is formed primarily of tight junctions between the cerebral capillary endothelium and surrounding perivascular elements, restricts the influx of molecules from blood s tream into the brain [42] and makes it impermeable to most therapeutic molecules, including nucleic acids [43]. Similarly, a compact mass of tumor cells composed of approximately 50% tumor and stromal cells hinders the delivery of cancer therapeutics to deep-seated cancer cells [128, 129]. This compactness of biological tissues precludes pharmacotherapy or requires the use of invasive procedures to bypass the barrier [130]. Therefore, clinical translation of various

competent drugs and nucleic acid therapeutics has been obstructed by these biological barriers [131-134]. For instance, to deliver genes to neurons, viral vectors have been directly injected into selected regions of the brain because BBB impedes their entrance into the brain when delivered systemically [135]. However, using this invasive technique, transduction is limited to the injection site only [135]. Therefore, the search for ways to overcome these biological barriers to reach the specific site of action has been the major driving force for the significant development of delivery vectors [136] that will not only protect the therapeutic molecules from degradation in the biological milieu but also steer their cellular entry [127].

Biological barriers can be globally disrupted by the intra-arterial infusion of osmotic agents, such as mannitol solution, to increase their permeability [135, 137]. A customarily applied method for penetration across biological barriers is the use of these hyperosmotic solutions, which elevates the blood plasma osmolality, resulting in an enhanced flow of water from tissues and thereby loosening the highly compact cell mass and facilitating the vector to cross the barriers and deliver the therapeutic molecules to cells, previously difficult to transfect [60]. Hence, the concept of combining osmotic BBB-opening with vectors to

achieve CNS gene-expression was proposed [61]. In these studies, tissues were pretreated with hyperosmotic mannitol solution, which loosens tight junctions between cells of BBB, and were then treated with various gene/drug delivery vehicles [62, 138]. However, the effect of mannitol solution is often temporary, vanishing after ~ 30 min, sometimes even before the drug or DNA crosses the barrier [139]. Moreover, even after overcoming the BBB, cell membrane barrier and endosomal trapping of the vector still remains challenging towards the successful delivery in brain cells.

The development of an ingenious delivery vehicle may provide an important solution to overcome multiple barriers of cellular delivery. Our group recently proposed the use of mannitol and sorbitol -based gene transporters for enhanced transfection efficiency in cancer cells due to the presence of osmotically active hydroxyl groups [63-65]. The number and stereochemistry of the hydroxyl groups affects the hyperosmotic activity and intracellular behavior of gene transporters [140]. Therefore, it is expected that increasing the number of hydroxyl groups in the polymer backbone of gene transporter, would increase its hyperosmotic properties that could then facilitate their application in crossing the highly compact BBB. Because sugar alcohols possessing

eight hydroxyl groups are not commercially available, here we synthesized the highly hyperosmotic xylitol dimer as an analog of an octamer using the method presented in scheme 3.1. The current report showcases polydixylitol-based polymer (PdXYP), containing polyol groups as an integral part of the gene delivery vector capable of intra-arterial infusion of osmotically active nanoplexes across the blood-brain-barrier. Moreover, the mechanistic observation indicated directed cellular uptake by cells due to the stimulation of specific endocytosis pathways, resulting in a higher level of gene transfection efficiency.

3.2 Materials and Methods

Synthesis of Polydixylitol based gene transporter (PdXYP)

(a) Synthesis of dXY: Xylitol was first converted into crystalline diacetone xylitol by the method used by Raymond and Hudson for the condensation of xylitol and acetone [141]. The terminal hydroxyl group of xylitol diacetone was reacted with trifluoromethane sulphonyl chloride to make TMSXD. TMSDX was reacted with Xy-Ac (1.2 eq) in presence of dry THF to form dXy-Ac in dry THF [142] and the product was finally converted in to dXY by acidic ring opening as described in a previous reported method [143].

Synthesis of XYdAc: Mixture of 10.0 g. of crystalline Xylitol, 200mL of acetone, 20 g of anhydrous copper sulfate and 200ul of concentrated sulfuric acid was stirred for 48 hours at 35^{o}C. Copper sulfate was separated by filtration and the filtrate was stirred with 10 g. of powdery calcium hydroxide for one hour to neutralize the acid; the solids were removed by filtration and the solvent by distillation in vacuum. The syrupy residue, weighing 7g was obtained and crystallized by dissolving in hexane and cooling at -70^{o}C .

Synthesis of TMSXD: 2mL Trifluoromethanesulfonic anhydride (dissolved in 3mL DCM) was added drop wise to a solution of Xy-dAc (3g) and pyridine (2mL) in DCM (10 mL) at -30 ℃. The reaction was stirred at -30 to -10 ℃ for 3 h after which time TLC (ethyl acetate/DCM, 1:1) showed the complete consumption of the starting material and the formation of one major product . The reaction was diluted with DCM (30 mL) and washed with HCl (2M, 20 mL), and the aqueous layer was extracted with DCM (3 x 20 mL). The combined organic layers washed with brine (30 mL), dried (magnesium sulfate) and concentrated under reduced pressure**,** compound is used without further purification for next step.

Synthesis of dXYdAc: Xy-dAc (2.0 g) and sodium hydride (65%

suspension in oil, 0.6 g) were dissolved in dry tetrahydrofuran (THF, 50 mL) at room temperature and then a solution of TMSXD (1.2 eq) in dry THF (25 mL) was added slowly. The mixture was stirred for 12 h at room temperature. The solution was diluted with EtOAc and washed with brine. After evaporating the solvent, the crude compound was purified through column chromatography (SiO2; CH2Cl2/EtOAc, 4:1) to yield a transparent liquid.

Synthesis of dXY: dXYdAc was suspended in 2 M HCl (50 mL) and then MeOH was added to form a homogenous solution. The mixture was stirred at 90 ^{o}C for 6 h and then the solvent was evaporated under vacuum to yield the product.

(b) Synthesis of dXYdA: Dixylitol diacrylate (dXYA) monomer was synthesized by esterification of dixylitol with 2 equivalents of acryloyl chloride. An emulsion was prepared by dissolving dixylitol (1 g) in DMF (20 mL) and pyridine (10 mL) followed by dropwise addition of acryloyl chloride solution (1.2 mL dissolved in 5 mL DMF) at 4 ^{o}C with constant stirring [64]. After reaction completion, HCl–pyridine salts were filtered and the filtrate was dropped into diethyl ether. The product was precipitated in as a syrupy liquid and dried under vacuum.

(c) Synthesis of PdXYP: PdXYP was prepared by Michael addition

reaction between LMW bPEI (1.2 kDa) and dXYA. Briefly, the synthesized dXYdA (0.38 g in 5mL DMSO) was added dropwise to 1 equivalent of bPEI (1.2 kDa, dissolved in 10 mL DMSO) and reacted at 60 ^{o}C with constant stirring for 24 h. After reaction completion, mixture was dialyzed using a Spectra/Por membrane (MWCO: 3500 Da; Spectrum Medical Industries, Inc., Los Angeles, CA, USA) for 36 h at 4 ^{o}C against distilled water. Finally, the synthesized polymer was lyophilized and stored at -70 ^{o}C.

Characterization of PdXYP and PdXYP/DNA polyplexes

^{1}H NMR spectra dXY and PdXYP in D_2O were recorded using Advanced 600 spectrometer (Bruker, Germany). The mass spectrum of the polymer was measured by Matrix-Assisted Laser Desorption Ionization Mass Spectrometer Voyager-DETM STR Biospectrometry Workstation, MALDI TOF-TOF 5800 System. The elemental composition (C, H, N and O) of the monomer and polymer was measured by Thermo Flash EA1112 Elemental Analyser. The absolute molecular weight of PdXYP polymer was measured by gel permeation chromatography coupled with multiangle laser light scattering (GPC-MALLS) using a Sodex OH pack SB-803 HQ (Phenomenex, Torrells, CA, USA) column (column temperature 25℃; flow rate 0.5 mL/min).

PdXYP polymer was then complexed with DNA (0.1µg) at various N/P ratios (0.1, 0.5, 1, 2, 3, and 5) for 30 min at RT and resolved on a 0.8% agarose gel (with 0.1 µg/mL EtBr) casted in 1X TAE buffer at 100 V for 40 min in 0.5X TAE running buffer. Images were captured under ultraviolet illumination. For DNase protection assay, PdXYP/DNA (N/P 20) polyplexes and free DNA were incubated with DNase I (1 µL, 50 units) in DNase/Mg^{2+} digestion buffer at 37℃. After 30 min, DNase was inactivated by adding 5 µL EDTA (100 mM) at 70℃ for 10 min and incubated for another 30 min at RT. Finally, the protected DNA was released from the complexes with the addition of 5 µL 1% sodium dodecyl sulfate (SDS) for 2 h and resolved on a 0.8% agarose gel (with 0.1 µg/mL EtBr) in 0.5X TAE running buffer at 100 V for 40 min.

PdXYP/DNA polyplexes were characterized using a transmission electron microscope (EF-TEM) (LIBRA 120, Carl Zeiss, Germany) and a dynamic light scattering spectrophotometer (DLS 8000, Otsuka Electronics, Osaka, Japan). The specimens for TEM were prepared by drop-coating the PdXYP/DNA (N/P 20) and PEI25k/DNA (N/P 10) polyplex dispersion onto a carbon grid and then dried for 2 h, after which it was stained with 1% uranyl acetate (10 s) and observed for its morphology. DLS samples were prepared at various N/P ratios (5, 10,

15, 20, 25, and 30) of PdXYP/DNA polyplexes with 40 µg/mL DNA and then measured for their hydrodynamic size and zeta potential with 90° and 20° scattering angles at 25℃.

Osmolarity measurement

Osmolarity of aqueous solutions of sorbitol, mannitol, dixylitol, sorbitol diacrylate, mannitol diacrylate, dixylitol diacrylate and PdXYP/DNA polyplexes at various concentrations (2%, 3%, 5%, 10%) were measured as mOsm using a cryoscopic osmometer 030 (GANAte, USA) and calculated as depression in freezing point of solutions.

Cell culture and animal studies

Low passage human hepatocellular liver carcinoma (HepG2) cells, human cervix epithelial carcinoma (HeLa) cells and adenocarcinoma human alveolar basal epithelial (A549) cells were cultured in T-75 culture flasks (Nunc, Thermo Scientific) in 15 mL complete medium containing low glucose Dulbecco's Modified Eagle's culture medium (DMEM) (Sigma, USA) for HepG2 and HeLa cells and Roswell Park Memorial Institute (RPMI)-1640 culture medium for A549 supplemented with 10% heat-inactivated FBS (Hyclone Laboratories, USA) and 1% antibiotic cocktail of streptomycin and penicillin.

Primary rat astrocytes were maintained in DMEM F-12 medium supplemented with fetal bovine plasma derived serum (10%), heparin (1850 U/mL), bFGF (1.5 ng/mL), insulin (5 μg/mL)-transferrin (5 μg/mL)-sodium selenite (5 ng/mL), hydrocortisone (500 nM) and gentamicin (50 μg/mL). Cells were maintained under standard culture conditions of 37°C and 5% CO_2 for 4 or 5 days, with the culture duration selected to maintain cells under exponential growth and reach ~80% confluency. Cells were then trypsinized, centrifuged at 1200 RPM for 5 min to pellet cells and counted using hemocytometer to seed the cells for experimental assays. For animal study four weeks old nude Balb/c mice were obtained from Orient Bio Inc. (Republic of Korea) and kept in a laboratory animal facility maintained at 23 ± 2℃ and 50 ± 20% relative humidity under a 12 h light/dark cycle. All experimental protocols were reviewed and approved by the Animal Care and Use Committee at Seoul National University (SNU-120409-3).

In vitro transfection and cytotoxicity of PdXYP/DNA polyplexes

Cytotoxicity of PdXYP/DNA and PEI25k/DNA polyplexes at various N/P ratios (5, 10, 15, 20, and 30) were measured in three cancer cell lines (A549, HeLa, and HepG2) and primary rat astrocytes by the reduction of a tetrazolium component (3-(4, 5-dimethylthiazol-2-yl)-2,

5-diphenyltetrazolium bromide, or MTT) (Sigma, St. Louis, Mo, USA) into insoluble purple colored formazan crystals by the mitochondria of the viable cells. Polyplex transfected cells that had been incubated in a 24-well plate (10 x 10^4 initial cell density/well) for 36 h were then incubated with MTT reagent (0.5 mg/mL in 1X PBS) for 3 h, followed by the addition of DMSO (500 µL) to solubilize the colored crystals, and absorbance was measured at 540 nm using a Sunrise^{TM} TECAN ELISA reader (Grödig, Austria).

A549, HeLa, HepG2 cells and primary rat astrocytes at 80% confluency (10 x 10^4 initial cell density/well) in a 24-well plate were transfected with PdXYP/pGL3 (1 µg) and PEI25k/pGL3 polyplexes at various N/P ratios (5, 10, 15, 20 and 30) in serum-free medium, which 3 h later was exchanged with 10% serum containing medium . After 24 h, luciferase assay was performed according to the manufacturer's protocol. A chemiluminometer (Autolumat, LB953; EG&G Berthold, Germany) was used to measure relative light units (RLUs) and normalized with protein concentration in the cell extract estimated using a BCA protein assay kit (Pierce Biotechnology, Rockford, IL, USA). Transfection activity was measured in triplicate as RLUs per mg protein. The % transfection efficiency of PdXYP/tGFP (1 µg) (N/P 20)

was measured and compared with PEI25k/tGFP (N/P 10) in A549 cells 36 h post-transfection using flow cytometry (BD Biosciences, San Jose, CA, USA). Cell expressing GFP acquired from a total of 10000 cells were scored through a FACS calibrator.

Degradation study

TRITC (Molecular Probes, Invitrogen, Oregon, USA) (25μL, 1 mg/100 μL in DMF) was added to PdXYP (1 mL, 10 mg/mL in H_2O) to block ~1% of its total amines, and the mixture was then stirred overnight ($PdXYP^T$). Unreacted TRITC was removed by washing with ethyl acetate (3 x 2 mL), which was then lyophilized and resuspended in water. A549 cells (3 x 10^5 initial cell density/well) after 24 h of incubation in a cover glass bottom dish (SPL Lifesciences, Korea) were transfected with $PdXYP^T$/DNA polyplexes and further incubated for 3 h, 2 d, 3 d, 5 d, and 7 d to study the degradation profile of $PdXYP^T$ polyplexes. The transfected cells were washed 3 times with 1X PBS and then fixed with 4% paraformaldehyde for 10 min at 4℃. DAPI was used to counter-stain the nuclear DNA of fixed cells, and images were procured using a Carl Zeiss LSM 710 inverted laser scanning confocal microscope with ZEN software to monitor fluorescently labeled $PdXYP^T$/DNA polyplexes inside the treated A549 cells. Cell viability

was also observed after 3 h, 2 d, 5 d, and 7 d of transfection by MTT assay.

BBB transmigration assay

Transmigration experiments were conducted on day 5 after the complete activation of BBB kit (Pharmacocell, Japan) when TEER values in each well were > 150 $\Omega x cm^2$. DNA was fluorescently labeled ($tGFP^F$) with bisBenzimide H33258 (Sigma, USA). 1.2 mL media was added to the lower chamber and 0.3 mL media containing free $tGFP^F$ or PdXYP/$tGFP^F$ or PEI25k/$tGFP^F$ polyplexes were added to the upper chamber of the *in vitro* BBB kit and incubated at 37 ℃ for 3 h. 1 mL media was aspirated from the lower chamber and analyzed spectrofluorometrically to determine polyplex BBB-permeability assay. Inserts without cells on the transwell membrane were used as blanks. In other experiments upper chamber of BBB were added with free tGFP and PdXYP/tGFP polyplexes for 3 h. After 48 h the primary rat astrocytes in the lower chamber were analyzed for transfection efficiency using FACS and their lysates for western blot.

Western blot analysis

After transfection, cells were harvested and lysed with 1X RIPA lysis

buffer (Millipore, MA, USA). A BCA protein assay kit (Thermo scientific, MA, USA) was used to measure the protein concentrations. Equal amounts of the protein (25 µg) from each sample were separated by a Novex NuPAGE 4-12% SDS-PAGE gel (Life technologies, CA, USA), transferred to nitrocellulose membrane using iBlot (Invitrogen, USA) and then non-specific binding sites were pre-blocked with 5% skim milk for 1 h at RT. The membrane was washed and probed with anti-caveolin1 (Abcam, ab17052), anti-GFP (Santa Cruz, CA, USA) and anti-β-actin (Abfrontier, Seoul, Korea) antibodies (1:500 dilution) overnight at 4℃. Then, the membrane was incubated with secondary antibody (1:1000 dilution) conjugated with HRP (Invitrogen, CA, USA). Bands were captured using a ChemiDocTM XRS+ (Biorad, CA, USA) imaging system. The band intensities were analyzed quantitatively using ImageJ software (NIH, USA) and plotted as the mean pixel value.

Tumor implantation, in vivo bioimaging and biodistribution

Five weeks old nude Balb/c mice (male, 4 mice/group) were subcutaneously injected with 100 µL of a single cell suspension containing 3 x 10^6 A549 cells. When the tumor size reached 800-1000 mm^3, 100 µL of PdXYP/pGL3 (30 µg) complexes (N/P 20) in normal

saline was locally injected into the tumor. PEI25k/pGL3 (N/P 10) complexes prepared under identical conditions were used as vector control, while naked pGL3 was used as a negative control and the mice were bioimaged after 7 days. The IVIS Imaging system 100 (Xenogen) with Living Image software was used for *in vivo* bioimaging to analyze the luciferase expression. The mice were anaesthetized by intraperitoneal (IP) injection of a Zoletil (40 mg/kg): Rompun (10 mg/kg) (4:1) mixture diluted 8 times in sterile 1X PBS. 200 µL of D-luciferin (15 mg/mL stock solution in DPBS) for a 20 g mouse (3 mg/mouse) was injected intraperitoneally and was quickly distributed throughout the body. Luciferase expressed in cells reacts with luciferin to emit luminescence, which was captured by the IVIS system to show images with intensity proportional to luciferase expression. Images were captured in the plateau phase which usually occurs after 15 min and lasts for 15-20 min.

For *in vivo* biodistribution, 6 week old nude Balb/c mice (male, 4 mice/group) were intravenously injected with 100 µL of PdXYP (N/P 20) and PEI25k (N/P 10) polyplexes in normal saline. Naked pGL3 (30 µg) was used as control. After 5 d, luciferase expression was monitored in various organs of mice using IVIS Imaging system. For luciferase

quantification different organs of mice were dissected out, weighed, homogenized, suspended to 25% w/v homogenate in 2.5X lysis buffer (Promega, USA) and protein concentration in cell lysates were estimated using chemiluminometer.

Lipid raft co-localization study

DNA (1 μg) was labeled with YOYO-1 iodide (2 μL, 1 mM in DMSO) by stirring for 2 h at 25℃ in dark and stored at -20℃ (DNA^F). A549 cells (3 x 10^5 initial cell density/well) after 24 h of incubation in a cover glass bottom dish (SPL Lifesciences, Korea) were transfected with PdXYP/DNA^F and PEI25k/DNA^F polyplexes and further incubated for 15, 30 min. Cells were rinsed with 1X PBS, fixed with 4% paraformaldehyde at 37℃ for 10 min, washed twice with ice cold PBS and then permeabilized with ice-cold 0.2% Tween 20 (in PBS) for 10 min. Non-specific binding was blocked using 10% BSA in 1X PBS for 5 min at RT and then at 4℃ for 1 h because cooling prevents endocytosis of antibodies. Lipid rafts of the fixed cells were then labeled using the orange-fluorescent Alexa Fluor 555 lipid raft labeling kit (Invitrogen) according to the recommended protocol. Nuclei were stained with DAPI (0.1 μg/mL) for 10 min and mounted with Aqua poly/mount (Polysciences, PA, USA). The images were procured from

confocal microscopy at 555/565 Abs/Em.

Endocytosis inhibition study

A549 cells were incubated with caveolae endocytosis inhibitor, β-methyl cyclodextrin (BMC) (0, 2.5, 6.5, 10 mg/mL) for 1 h at 37℃ and then transfected with PdXYP/DNA polyplexes. Similarly, A549 cells were incubated with endosome proton pump inhibitor, bafilomycin A1 (200 nM) for 10 min and transfected with PdXYP/DNA and PEI25k/DNA polyplexes. Luciferase activities were measured as RLUs per mg protein.

3.3 Results and Discussion

We designed a novel gene delivery vector using a combination of appropriate polymer components that not only allows overcoming biological barriers but also enhances the cellular uptake for high transfection efficiency. We propose that (i) the polyol backbone of PdXYP can overcome BBB without affecting transendothelial electrical resistance (TEER) between blood and the brain, (ii) extracellular disturbances caused due to hyperosmotic polydixylitol can modulate the cellular uptake process overcoming the cell membrane barrier, and finally (iii) the LMW PEI component can synergistically overcome the

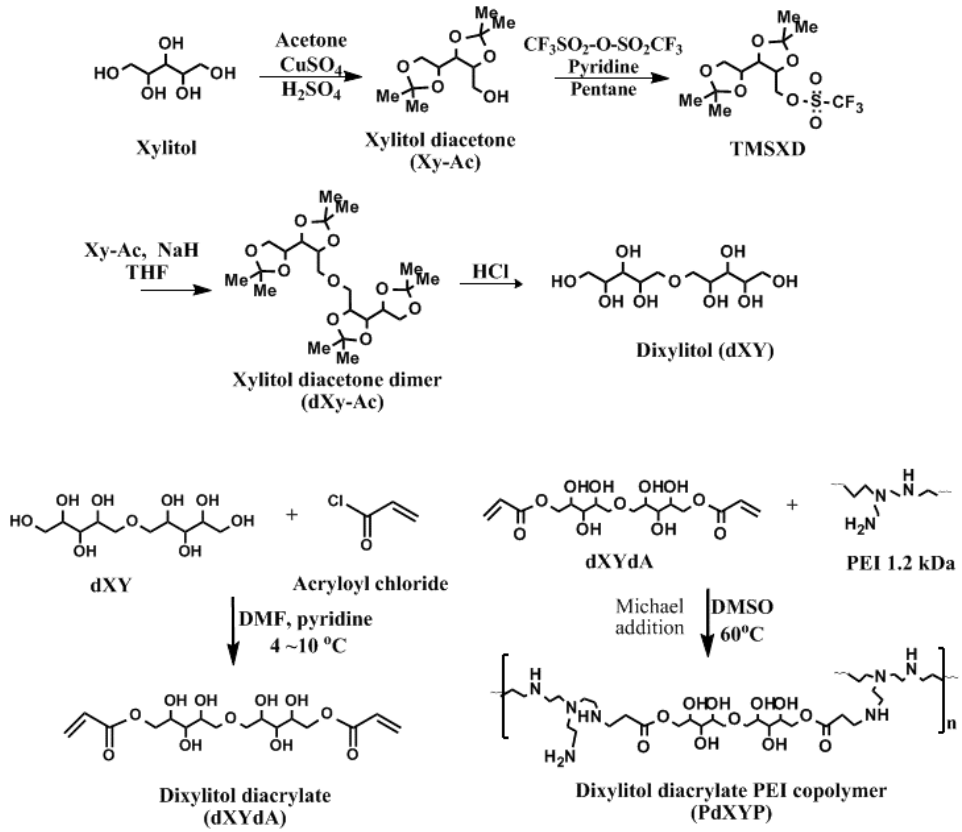

Scheme 3.1 Schematic representation for synthesis of dXY, dXYdA and PdXYP

endosomal barrier due to high buffering tendency, leading to the endosomal escape of PdXYP/DNA nanoplexes and enhancing their cellular bioavailability.

Highly hyperosmotic gene delivery vector, PdXYP was synthesized in three steps. (i) Dixylitol (dXY) containing eight hydroxyl group was synthesized by xylitol dimerization for which xylitol and acetone were condensed into crystalline xylitol diacetone (Xy-dAc). The terminal hydroxyl group of Xy-dAc was then reacted with trifluoromethyl suphonyl chloride to make trifluoromethylsulphonyl xylitol diacetone (TMSXD). TMSXD was reacted with equal molar ratio of Xy-dAc in presence of dry THF to form xylitol diacetone dimer (dXy-dAc) [26]. dXy-dAc was finally converted into dXY by opening the rings in HCl/MeOH solution. ^{1}H NMR of dXY showed peaks at 3.6-4.2 ppm representing –OH groups (Fig. 3.1). (ii) Thereafter, primary –OH groups of dXY were reacted with acryloyl chloride to form 1,8-disubstituted dixylitol diacrylate (dXYdA) monomer (iii) In the last step dXYdA-PEI diblock copolymer, PdXYP was synthesized through the copolymerization of dXYdA and low-molecular-weight (LMW) PEI (1.2 kDa) via the Michael addition reaction [64, 70] (Scheme 3.1). ^{1}H NMR spectra of the final product showed the disappearance of allyl

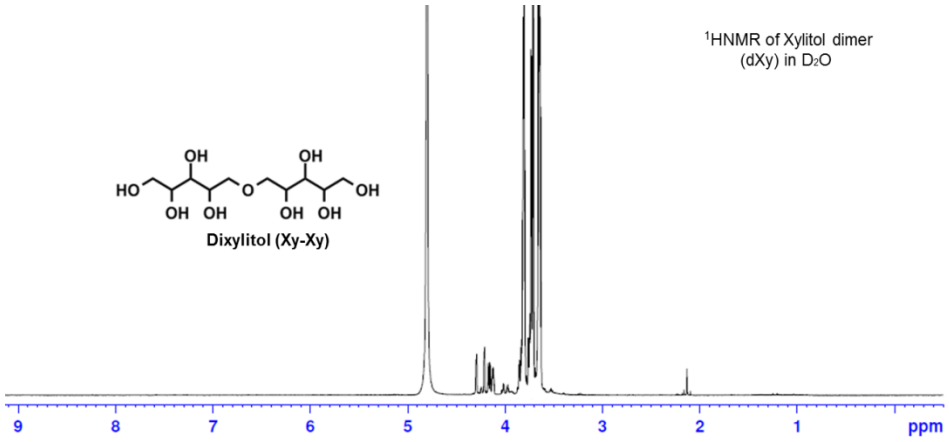

Fig. 3.1 ^{1}HNMR of Xylitol dimer (dXY) in D_2O

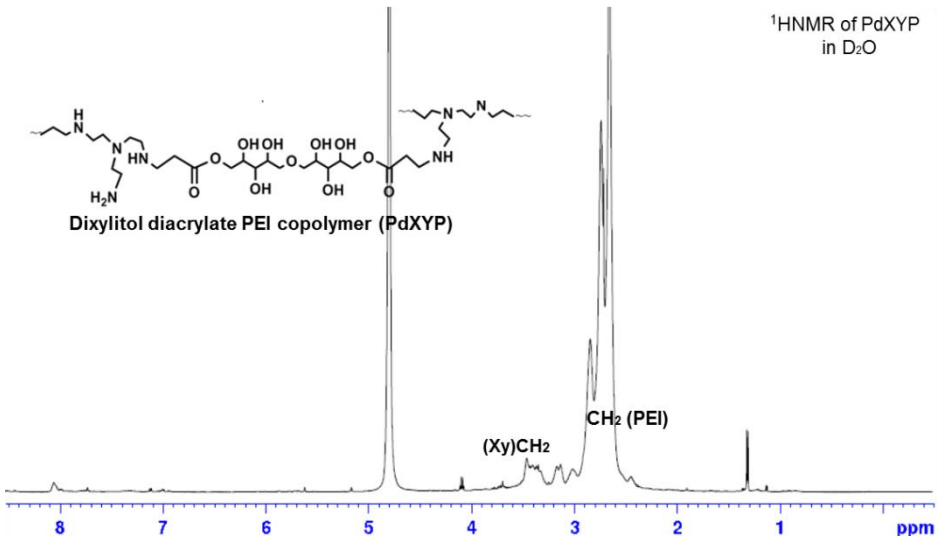

Fig. 3.2 ^{1}HNMR of PdXYP in D_2O

proton peaks confirming the successful synthesis of PdXYP (Fig. 3.2). MALDI-TOF-MS: m/z for dXYDA [M+] = 394.2 and PdXYP [M+] = 11516.89 (Fig. 3.3, 3.4). The composition of dixylitol in PdXYP estimated by NMR was about 42 mol% and the MW measured by GPC was 12-13 kDa, which suggests appropriate size of the polymer for effective binding with DNA (Fig. 3.5A) and forming uniform, stable polyplexes (Fig. 3.6A). PdXYP was also shown to protect the complexed DNA, suggestive of therapeutic DNA protection against intracellular DNase degradation (Fig. 3.5 B).

Particle size measurements of polyplexes using TEM and DLS indicated that PEI25k/DNA formed loose polyplexes with an average size of 250 nm. On the contrary, PdXYP/DNA formed compact and spherical polyplexes with a relatively homogeneous diameter of approximately 100 nm (Fig. 3.6A, B, and 3.7), an optimal size for cellular internalization. Moreover, PdXYP/DNA resulted in ~95% cell viability compared with the high toxicity of PEI25k/DNA and lipofectamine® /DNA polyplexes (Fig. 3.6C, 3.8). The lower cytotoxicity of PdXYP is due to the biodegradable ester linkages between polydixylitol and LMW PEI (Scheme 3.1) and its lower charge density (Fig. 3.6B) because of the formation of intra-molecular

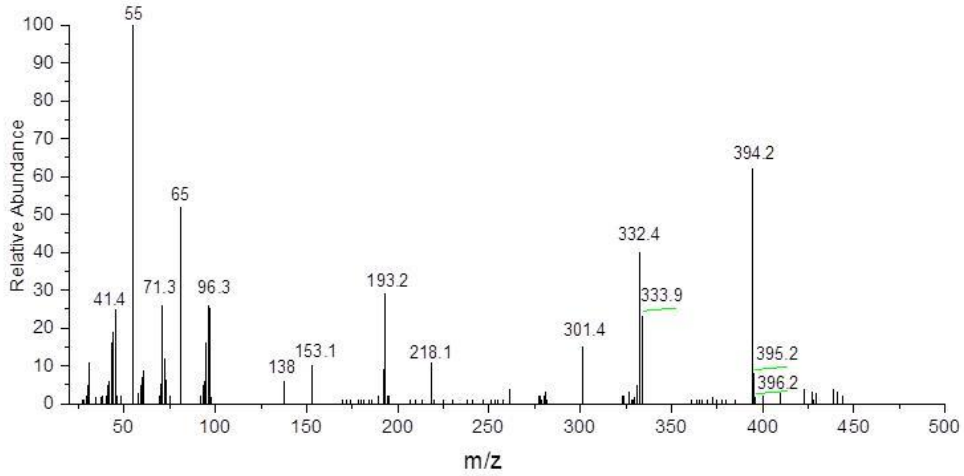

Fig. 3.3 MS spectra of dXYdA

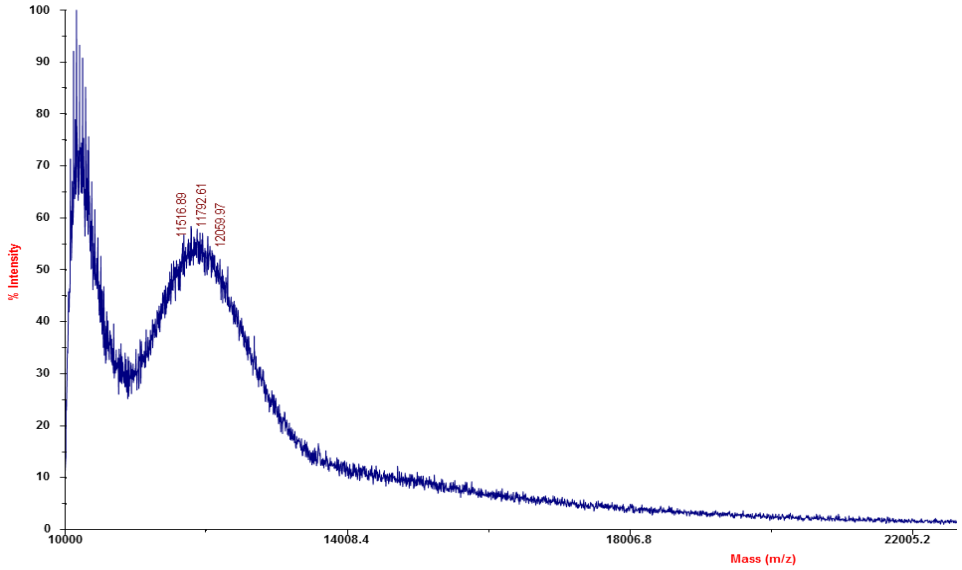

Fig. 3.4 MALDI-TOF-MS of PdXYP

Elemental analysis PdXYP and dXYdA. Elemental analysis of PdXYP found: C, 53.43; H, 11.03; N, 26.88; O, 8.66. Calcd. for C90H214N38O11: C, 53.92; H, 10.76; N, 26.55, O, 8.78 %. For dXYdA Elemental analysis found: C, 48.66; H, 6.81; O, 44.49. Calcd. for C16H26O11: C, 48.73; H, 6.65; O, 44.63%

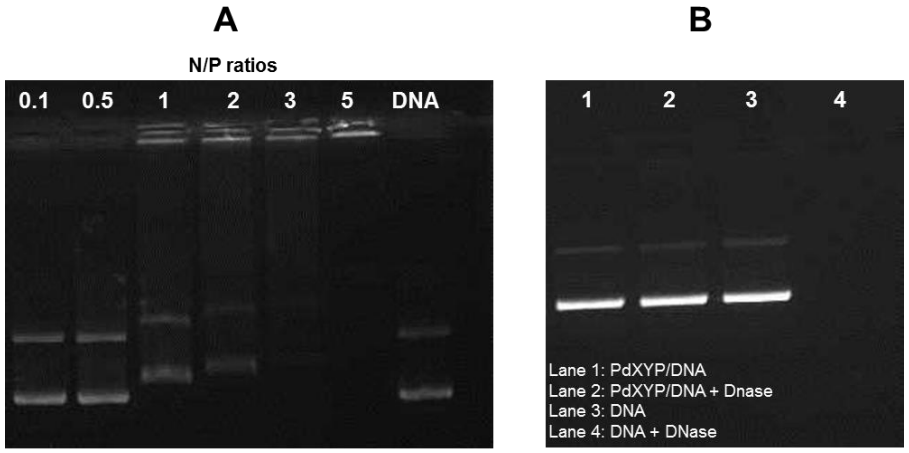

Fig. 3.5 Electrophoretic mobility shift assay. (A) Gel electrophoresis of PdXYP/DNA (0.1ug) complexes at various N/P ratios shows complete retardation at an N/P ratio of 3. (B) DNase protection and release assay. Complexed DNA with PdXYP (N/P 20) was released using 1% SDS. Lane 2 demonstrates protection of the complexed DNA, while Lane 4 shows its complete degradation in the absence of PdXYP.

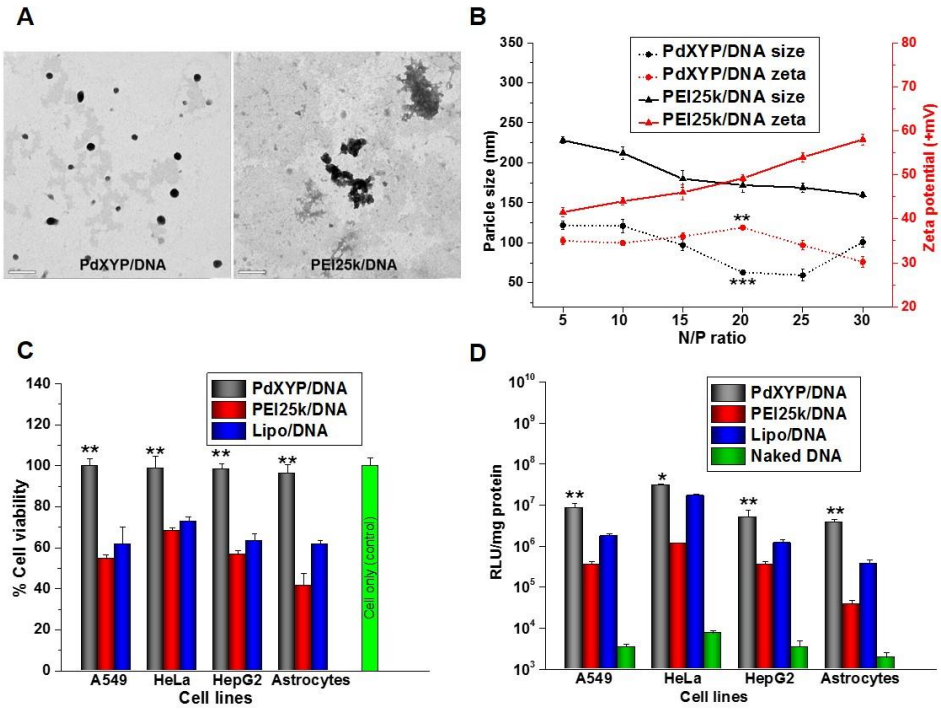

Fig. 3.6 Characterization of PdXYP/DNA polyplexes. (A) EF-TEM images of PdXYP/DNA (N/P 20) and PEI25k/DNA (N/P 10) polyplexes (scale bar: 200 nm). (B) DLS measurements of particle size and zeta potential of PdXYP/DNA and PEI25k/DNA polyplexes at various N/P ratios. (C) Cytotoxicity of PdXYP/DNA polyplexes (N/P 20) in various cell lines (A549, HeLa, HepG2 and rat brain astrocytes) shows no cytotoxicity. (D) Luciferase activity of PdXYP/DNA (N/P 20) polyplexes in various cell lines shows 25-50 fold increase in transfection activity (n = 3, error bar represents SD) (*P < 0.05; **P < 0.01, one-way ANOVA).

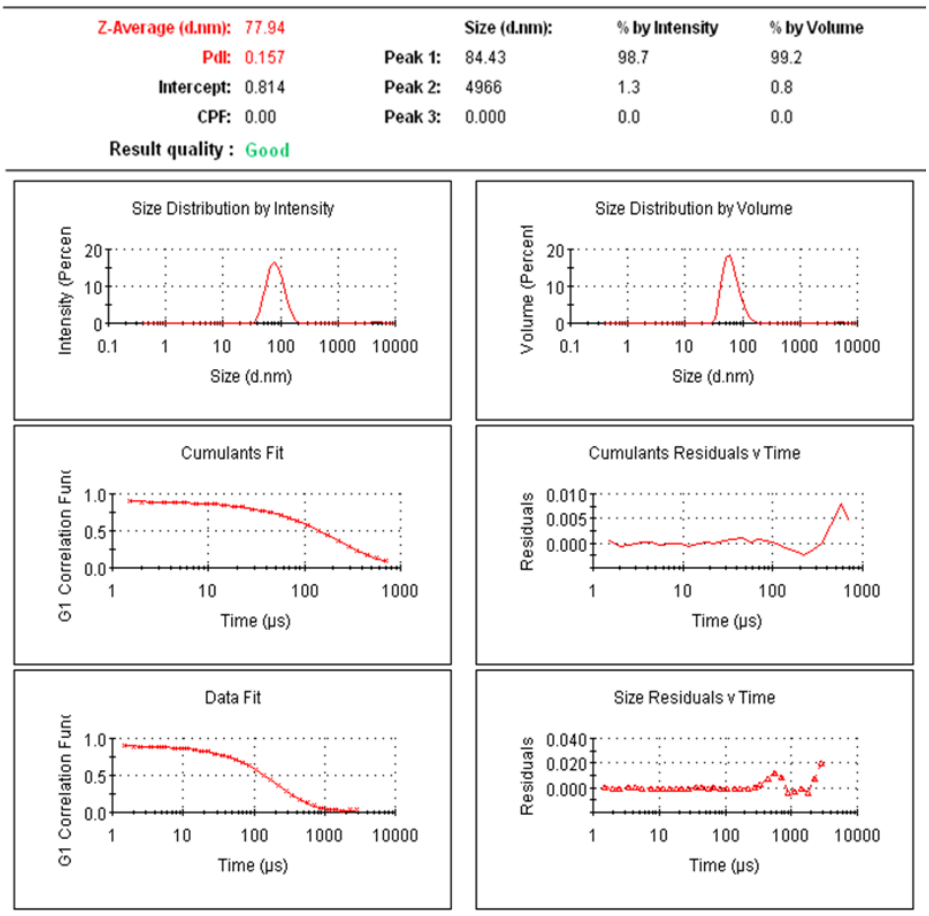

Fig. 3.7 Particle size and distribution measurement by Dynamic Light Scattering (DLS)

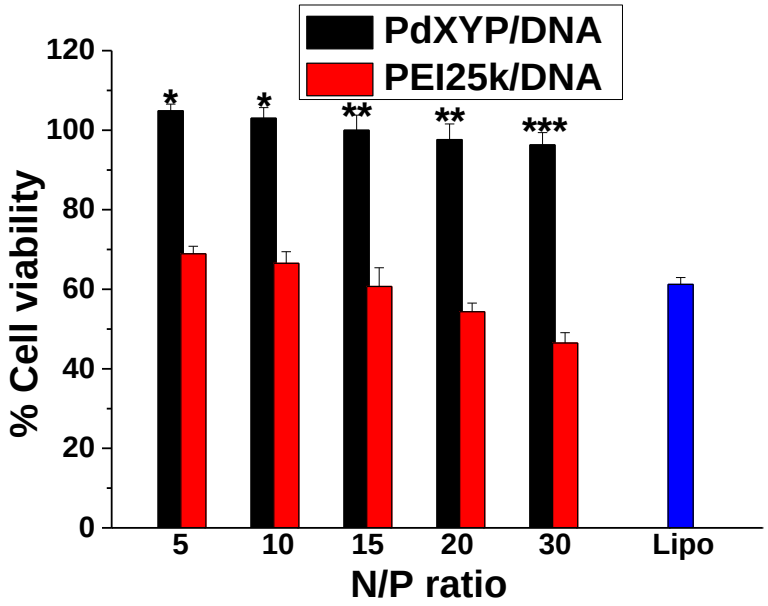

Fig. 3.8 Cytotoxicity of PdXYP/DNA complexes compared to PEI/DNA complexes at various N/P ratios in A549 cells (n=3, error bar represents SD) (*$p < 0.05$, **$p < 0.01$, ***$p < 0.001$, one-way ANOVA)

hydrogen bonds by hydroxyl groups that shield the high surface charge of complexes [64].

In addition, the degradable ester linkages in PdXYP backbone ensured a gradual disappearance of PdXYP after 3h, 2, 3, 5, and 7 days of transfection (Fig. 3.9) by hydrolyzing into smaller degradation products that can be exocytosed. Therefore, the occurrence of vesicles was observed to increase with time (maximum on day 5). This further increases the cell viability of PdXYP complexes (Fig.3.9) making the vector innocuous for nucleic acid delivery.

Further, the transfection efficiency of PdXYP/DNA, as measured in three cancer cell lines (HeLa, HepG2 and A549 cells) and primary rat astrocytes, was markedly higher (25-50 fold) than those of PEI25k/DNA and lipofectamine® /DNA (Fig. 3.6D, 3.10B). FACS also recorded 47% transfection efficiency of PdXYP over 14% of PEI25k (Fig. 3.10A).

Because the biological barriers are major impediment toward the non-invasive delivery of therapeutic agents, we used an *in vitro* BBB model to determine the ability of hyperosmotic PdXYP/DNA polyplexes to transmigrate the blood-brain-barrier (Fig. 3.11A).

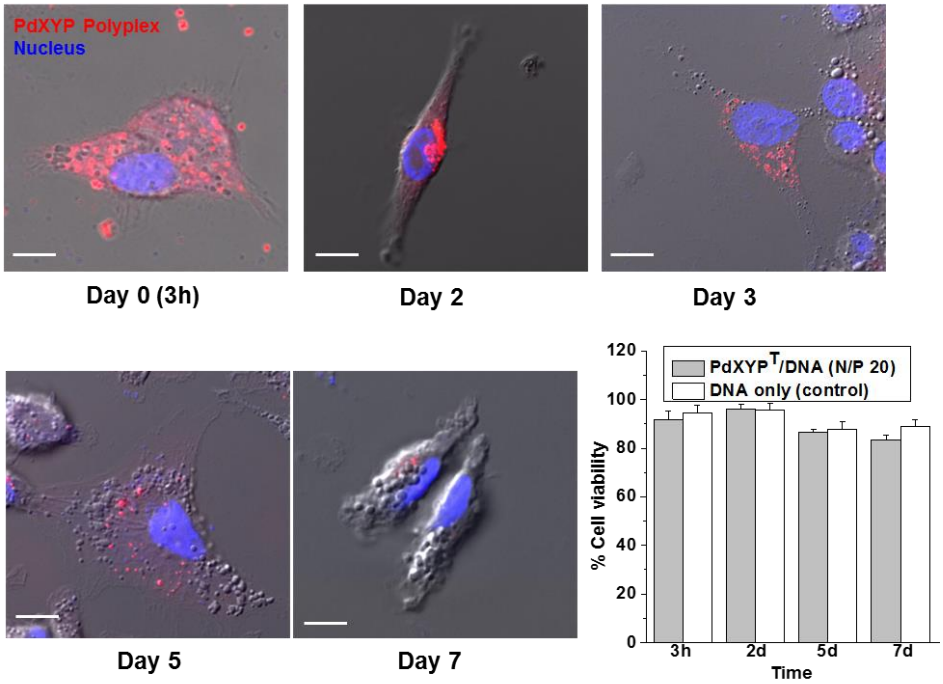

Fig. 3.9 Uptake and degradation of PdXYP^T complexes in A549 cells. Confocal microscopic images of A549 cells with DAPI nuclear staining (blue), observed up to 7 days following transfection with TRITC-labeled PdXYP^T (red). PdXYP^T after cellular uptake (3h) (scale bar: 10 µm) is gradually degraded up to day 7, and the occurrence of vesicular structure represents the increased exocytosis of fragmented PdXYP^T. Cytotoxicity measurements of PdXYP^T/DNA (N/P 20) complexes by MTT assay after 3h, 2d, 5d and 7d of transfection in A549 cells show no cytotoxic effects. Statistical significance was determined using one-way ANOVA (n=3, error bar represents SD).

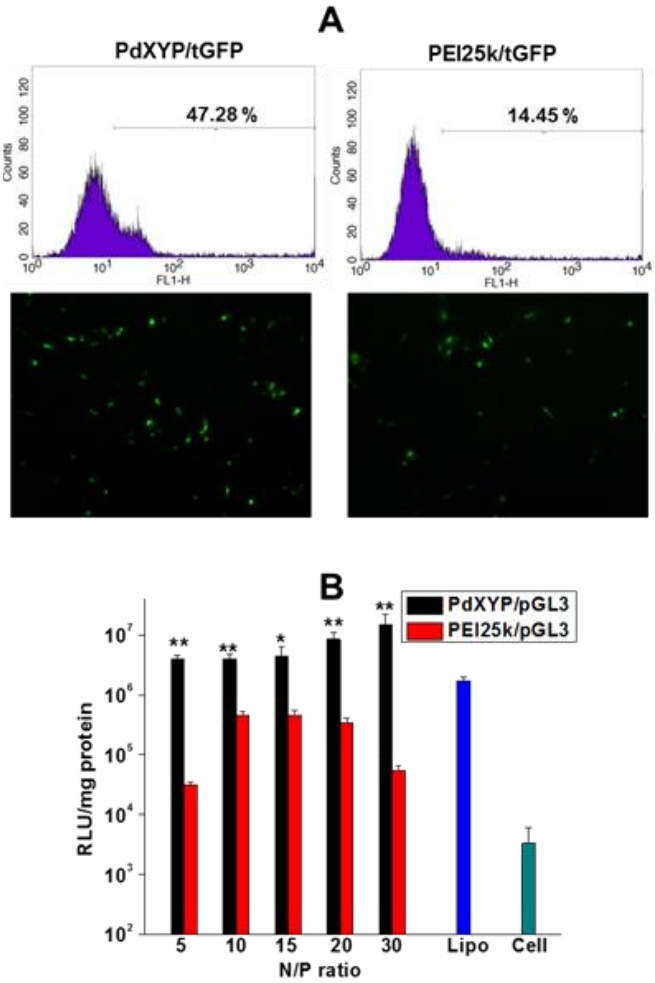

Fig. 3.10 Transfection efficiency of PdXYP/DNA in A549 cells. (A) FACS studies showing 47% transfection efficiency of PdXYP/tGFP (N/P 20) over 14% of PEI/tGFP (N/P 10) complexes with corresponding transfection images. (B) Luciferase activity of PdXYP/pGL3 complexes at various N/P ratios (n=3, error bar represents SD) (**$p < 0.01$, one-way ANOVA).

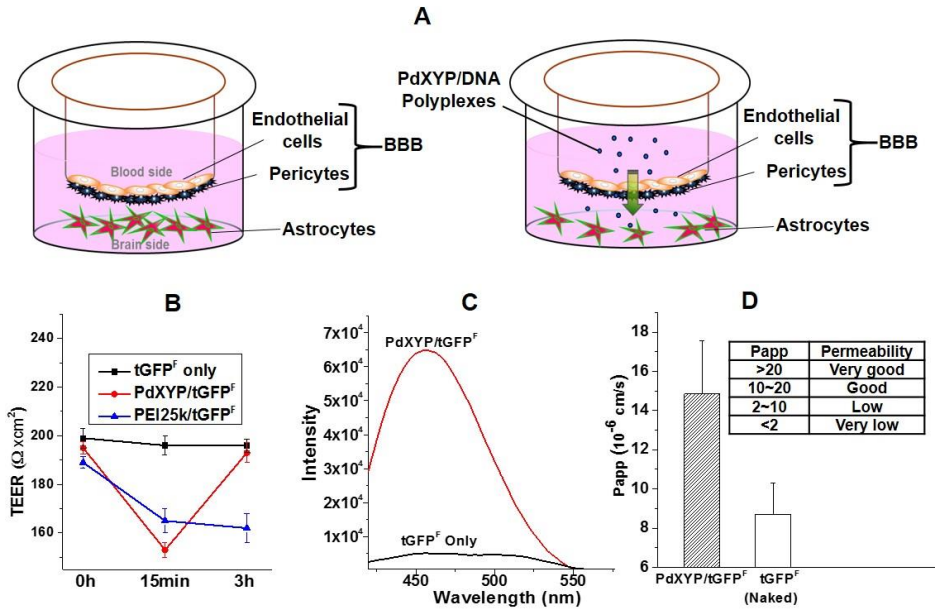

Fig. 3.11 Transmigration of PdXYP/tGFP^F polyplexes across the BBB model. (A) *In vitro* BBB model representing the transmigration of PdXYP/DNA polyplexes in blood-to-brain direction. (B) Fluorescence signal distribution of transmigrated tGFP^F recovered on the brain side (lower chamber) following 3 h of treatment with PdXYP polyplexes and naked tGFP^F show enhanced transmigration efficiency of PdXYP. (C) Transendothelial electrical resistance across BBB membrane before and after treatment with polyplexes show no functional damage of BBB with PdXYP (D) Permeability assay shows good BBB penetration ability of PdXYP/tGFP^F polyplexes measured in terms of apparent permeability coefficient (Papp) (10^{-6} cm/s) (n = 3, error bar represents SD).

Our results show that after 3 h of incubation of PdXYP/tGFP^{F} polyplexes in the upper chamber (blood side) of the BBB model, nearly 73% of the original fluorescence was recovered in the lower chamber (brain side). Using similar conditions with naked tGFP^{F}, only 13% of the original fluorescence was recovered (Fig. 3.11C). This result shows that the transmigration efficiency of DNA across the BBB increases significantly following its complexation with PdXYP. Furthermore, an immediate depression in TEER values within 15 min of PdXYP polyplexes addition indicates the loosening of BBB due to hyperosmotic stress allowing the polyplexes to pass through the barrier. However, 3 h later the original TEER was resumed to indicate the functional integrity of BBB and that no damage was caused by PdXYP polyplexes while traversing through this barrier (Fig. 3.11B). PEI25k polyplexes, on the other hand showed very low TEER measurements since their addition which was never resumed to indicate heavy functional damage to BBB due to cytotoxicity and therefore, was excluded in subsequent experiments to avoid false results. The penetration of PdXYP/DNA polyplexes through the brain endothelial and pericytes layer of BBB in a blood-to-brain direction was calculated as the apparent permeability coefficient Papp (10^{-6} cm/s) based on

Fick's law using the equation:

P_{app} (10^{-6} cm/s) = V_A/A x $[C]_{luminal}$ x $\Delta[C]_{abluminal}/\Delta t$

where V_A: volume of abluminal chamber (cm^3), A: membrane surface area (0.33 cm^2), $[C]_L$: initial luminal tracer concentration (ng/mL), $[C]_A$: abluminal tracer concentration (ng/mL), Δt: time of experiment (s).

PdXYP showed a good permeability (Papp: 17) through the BBB as compared to low permeability of free DNA (Papp: 8) (Fig. 3.11D). In subsequent experiments, we evaluated the efficiency of PdXYP/tGFP polyplexes, added in upper chamber of BBB kit, to transfect astrocytes cells present in the lower chamber across the BBB. After 48 h, FACS and western blot analysis indicated that PdXYP polyplexes retains its function after BBB transmigration and showed 18.5% transfection activity in brain astrocytes (Fig. 3.12). *In vivo* bio-distribution analysis of PdXYP/pGL3 polyplexes after intravenous injection in six week old mice showed gene (luciferase) expression in various organs, including prominent expression in the brain, compared with that of PEI25k/DNA polyplexes (Fig. 3.13A, 3.14), indicating the effectiveness of hyperosmotic behavior of PdXYP in crossing BBB.

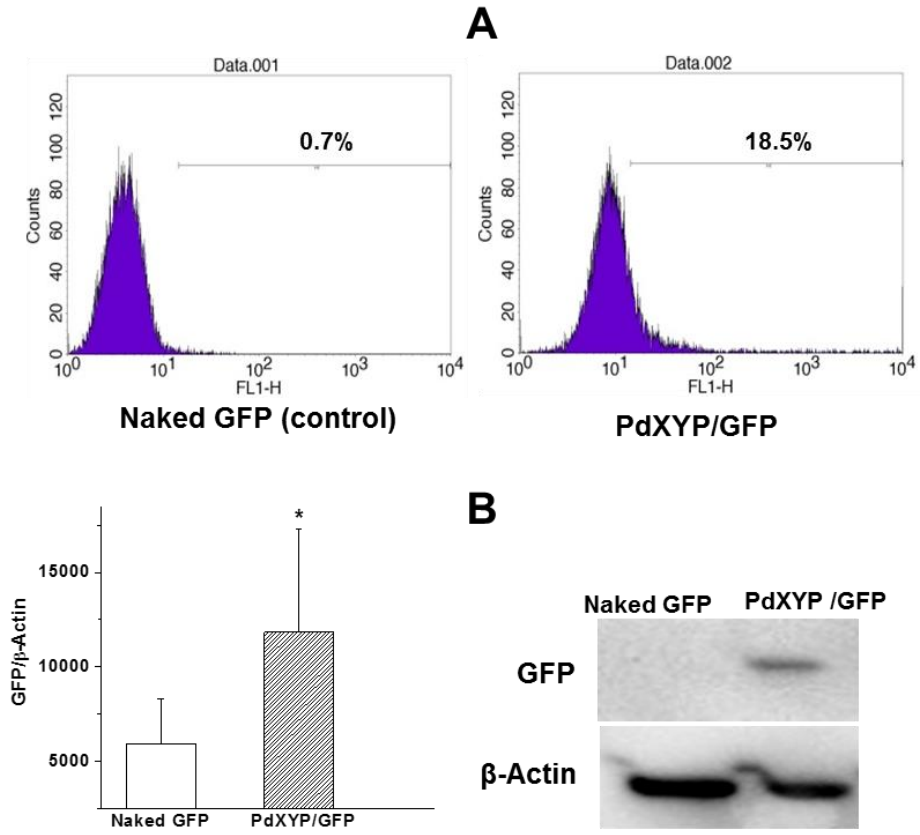

Fig. 3.12 Transfection efficiency of PdXYP/tGFP in astrocytes after crossing the BBB. (A) FACS analysis (B) Western blot analysis of GFP protein from the lysate of the transfected astrocytes after 48 h, showing a significant increase in GFP protein expression in cells treated with PdXYP/GFP complexes in contrast to the control. Data are shown as the mean ± SD of three independent experiments (*$p < 0.05$, one-way ANOVA).

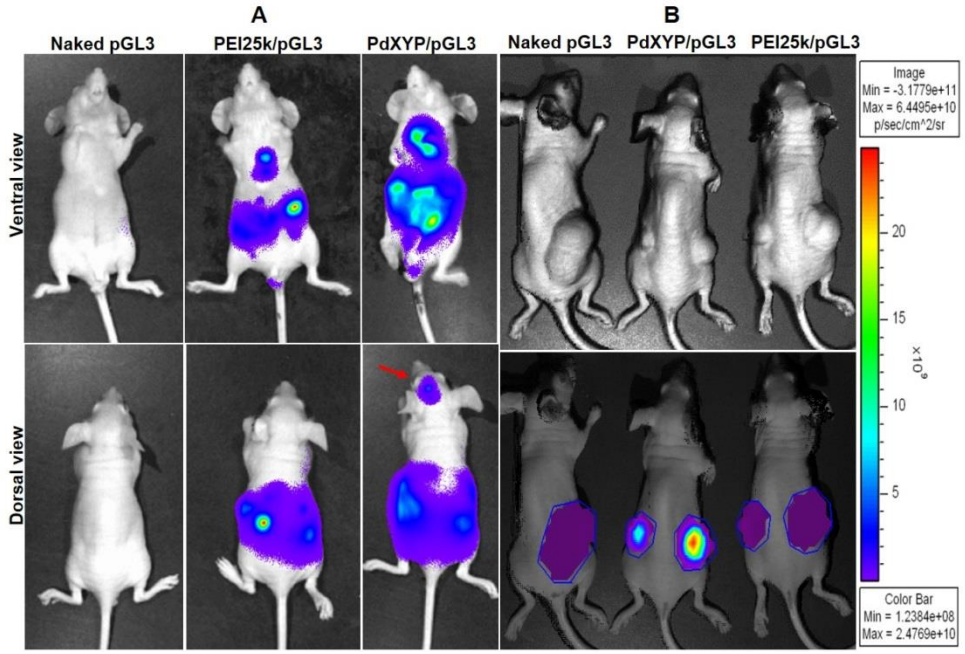

Fig. 3.13 *In vivo* bioimaging showing luciferase expression in nude Balb/c mice (n = 4). (A) *In vivo* biodistribution after 5 days of intravenous injection of PdXYP/pGL3, PEI25k/pGL3 and naked pGL3. Red arrow representing luciferase expression in brain (B) After 7 days of local injection of PdXYP/pGL3, PEI25k/pGL3 and naked pGL3 in xenograft mice showed penetration capability of PdXYP in deeper tumor locations.

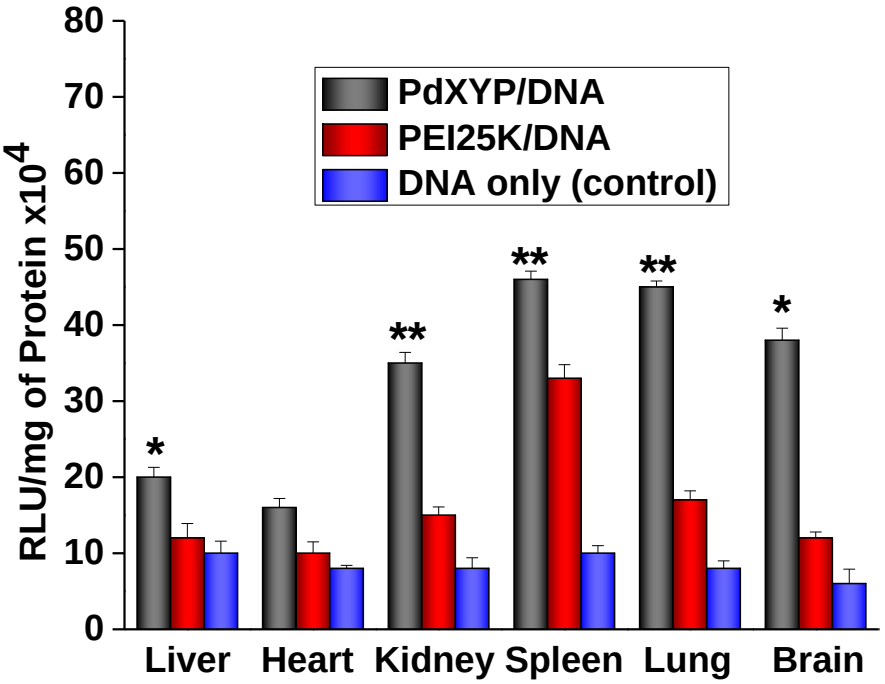

Fig. 3.14 *In vivo* biodistribution of PdXYP/DNA polyplexes in Balb/c mice (n=4) after 5 days of intravenous injection was analyzed as luciferase expression in various organs (error bar represents SD) (*p < 0.05, **p < 0.01, one-way ANOVA).

Table 3.1 Osmolarity of aqueous solutions of pure mannitol, sorbitol, dixylitol and their corresponding diacrylates at various concentrations measured as mOsm, calculated from the depression in freezing point of solutions.

Conc.	Pure Sorbitol	Pure Mannitol	Pure Dixylitol	Sorbitol-diacrylate	Mannitol-diacrylate	Dixylitol diacrylate	PdXYP/DNA polyplexes
2%	149	144	204	81	61	135	177
3%	259	267	314	118	104	282	319
5%	385	391	462	163	142	445	523
10%	803	788	1021	334	299	876	899

Similar to the BBB, the compact tumor mass is also impermeable to most therapeutics due to compactness of the tissue and stromal cells. We designed an *in vivo* experiment to assess the transfection ability of PdXYP into a grown tumor of xenograft mouse. One week after the localized injection of PdXYP/pGL3 polyplexes in tumor, a very high luciferase expression was observed compared to that obtained with naked DNA and PEI25k (Fig. 3.13B). The results show the permeability of PdXYP to uniformly transfect in to the deeper locations in compact tumor tissues.

The incorporation of osmolytes in their diacrylate forms (mannitol diacrylate, sorbitol diacrylate) into the vector backbone quenches their osmotic activity compared to their pure forms (mannitol, sorbitol) (Table 3.1). However, due to the presence of eight –OH groups in xylitol dimer, PdXYP backbone retains its osmolarity equivalent to that of clinically applied pure mannitol (Table 3.1) required for loosening of BBB. Moreover, this hyperosmotic PdXYP backbone delivers osmotic shocks to the cells, thereby assisting polyplexes not only to penetrate through the biological barriers but also enhance their uptake in astrocytes across BBB (Fig. 3.12) or deeper cells in compact tumor mass (Fig. 3.13B). Further investigations revealed that the extracellular

hyperosmotic environment led to the upregulation of caveolin-1 expression (Fig. 3.15B) present in the membrane lipid rafts. The upregulation of caveolin-1 leads to the cellular uptake by caveolae-mediated endocytosis (Fig. 3.16A) and therefore higher expression of transgene product was observed in transfected cells. The confocal microscopic images clearly elucidated the co-localization (yellow) of PdXYP/DNA^{F} polyplexes (green) with the caveolin rich membrane lipid rafts (orange) (Fig. 3.15A) to suggest enhanced cellular uptake by hyperosmotically induced caveolae-mediated endocytosis. In addition, inhibition of endosomal H^{+}-ATPases by bafilomycin A1 showed a 1000-fold decrease in PdXYP transfection, suggesting the ability of PdXYP to escape endosomal degradation (Fig. 3.16B).

3.4 Conclusion

PdXYP presents a hybrid polymer that possesses hyperosmotic property of dixylitol as an integral part of the vector capable of traversing the compact biological barriers (BBB or dense tumor tissue), thereby significantly enhancing the transfection efficiency *in vivo*. No cytotoxicity or damage to BBB was observed as indicated by unaltered TEER values after 3 h of transfection, suggesting its innocuous profile for *in vivo* application. The polydixylitol backbone through its hydroxyl

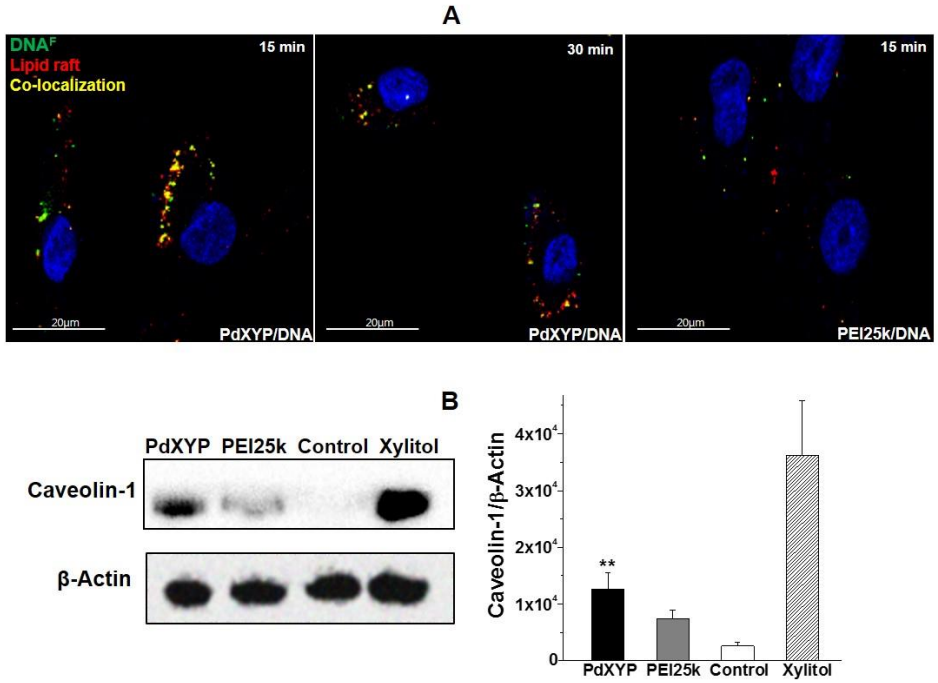

Fig. 3.15 Mechanistic investigations for caveolae mediated endocytosis of PdXYP/DNA polyplexes in A549 cells. (A) Co-localization (yellow) of PdXYP/DNA polyplexes (green) with caveolin rich lipid rafts (orange) after 15 and 30 min of transfection suggests its caveolae-mediated endocytosis (scale bar: 20μm). (B) Western blot analysis of caveolin-1 protein from the lysate of transfected A549 cells after 30 min showing a significant increase in caveolin-1 protein expression in cells treated with PdXYP/DNA polyplexes in contrast to PEI25k/DNA. Data are shown as the mean±SD (**P < 0.01, one-way ANOVA).

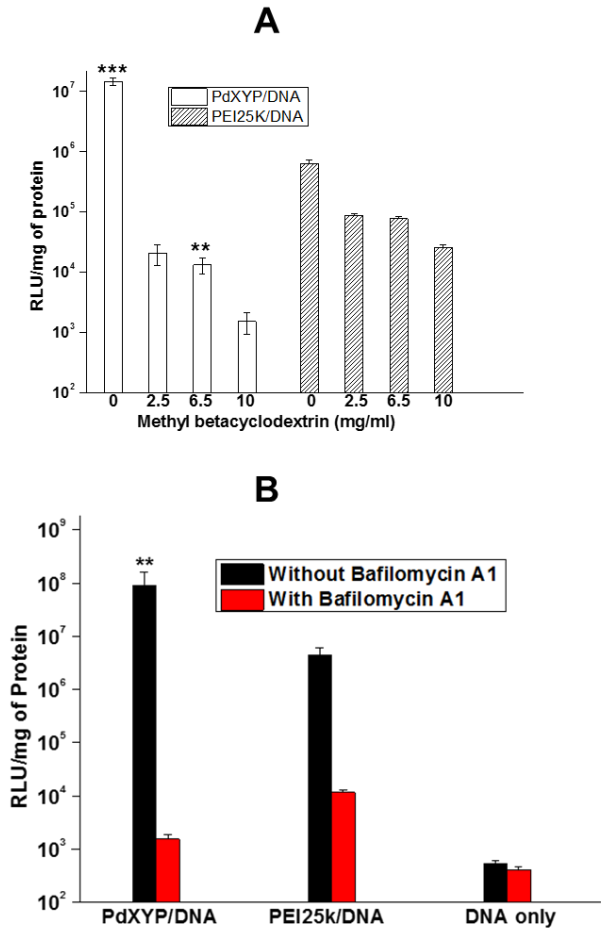

Fig. 3.16 Endocytosis inhibition study. (A) B-methyl cyclodextrin inhibition at various concentration shows decreased luciferase expression suggesting caveolae mediated endocytosis of PdXYP/DNA polyplexes. (B) Vacuolar type H^+ ATPase inhibition by Bafilomycin A1 (200nM in DMSO) shows endosomal escape of PdXYP/DNA polyplexes, (error bar represents SD) (**$p < 0.01$, ***$p < 0.001$, one-way ANOVA).

groups corresponds to better DNA complexation and polyplex stability by forming hydrogen bonds resulting in ~ 100 nm particle sizes appropriate for cellular delivery. Mechanistic studies revealed that PdXYP generates a strong hyperosmotic extracellular environment. This hyperosmotic stimulus selectively induces caveolin-1 expression resulting in enhanced cellular uptake by caveolae-mediated endocytosis and therefore PdXYP polyplexes were found co-localized with caveolin rich lipid rafts in cell membrane. This study illustrates increased cellular uptake and thus higher transfection efficiency in astrocyte across the BBB by transiently opening the barrier due to the hyperosmotic effect of PdXYP. With further success in xenograft mice model, we offer an efficient gene delivery vector to hyperosmotically transmigrate the biological barriers and increase the overall transfection efficiency of numerous brain-specific and cancer drugs non-invasively.

CHAPTER 4

Synergistically Enhanced Gene Delivery by Non-Viral Vector on Nanopatterned Matrix for Enhanced Osteogenesis of MSCs

4.1 Introduction

Gene delivery has been proposed as a potential therapy to treat various diseases through the insertion of the targeted genes into cells, yielding one of important keys in future medicine [144-146]. Currently, non-viral gene vectors are commonly suggested as a suitable gene delivery system toward clinical applications due to safety concerns compared to viral gene vectors which may induce unwanted immune responses or aberrant gene expressions [70, 146, 147]. To facilitate entry of the targeted genes to cells using non-viral vectors, positively charged materials, such as polyethylenimine (PEI), chitosan, and cationic liposome, condense negatively charged DNA to form nanoplexes. And then, the nanoplexes can usually be delivered into host cells through endocytosis [70, 148]. Although the non-viral gene delivery

systems hold great potentials, the low efficiency of gene transfection still remains a major limitation.

To overcome this considerable challenge on the use of non-viral gene vectors, the current efforts are mainly focused on the design and manipulation of new materials (e.g., synthetics of novel non-viral gene vectors) [70, 148]. On the other hand, the recent studies suggest that gene transfection efficiency is also regulated by extracellular environments including stiffness [149, 150], cell adhesion domains [151, 152], and topography [153, 154] of cell culture substrates. For example, Leong's group reported that microscale pitted substrate topographies could enhance the Lipofectamine-based gene transfection in fibroblasts probably by modulating cell-substrate interactions [153], providing an important insight into the new strategies to improve efficiency of gene transfection with non-viral gene vectors. Although these studies have provided important insights into surface topographies as an enabling tool for enhanced gene transfection, further progress is required for harnessing their potential application in gene delivery and regenerative medicine.

Bone defects are still highly common pathological problems in the world, requiring approximately 2.2 million orthopaedic procedures worldwide every year [155]. In spite of the availability of surgical treatments using alloplastic materials or autologous and allogeneic tissues, the regeneration of large bone defects remains one of the most critical orthopaedic diseases [156, 157]. It has recently been reported that the osteogenesis of human MSCs (hMSCs) was greatly enhanced by introduction of BMP-2 genes responsible for mineralization of MSCs in to bone cells [158, 159]. Therefore, an important strategy in the field of tissue engineering and regenerative medicine strategy is to develop an effective platform to improve stem cell functions by synergistic effect of efficient gene transfer and surface nanotopographies. Designing an effective material-based platform is an important part of regenerative medicine because such platforms can control or improve cellular functions, as well as construct artificial tissues for tissue regeneration. Stem cell-based bone tissue engineering provides a strategy for creating new functional bone constructs by combining stem cells with delivery of specific osteogenesis promoting genes [156]. Here, we propose a rational design for

engineering platforms for stem cell-based bone tissue engineering using the combination of tissue-mimetic nanotopography and gene delivery using BMP plasmid. We hypothesized that the bone tissue-like matrix nanotopography and enhanced BMP delivery would regulate the structure and functions of stem cells for osteogenic differentiation. To address this challenge, we prepared precisely defined bone-mimetic nanotopography using ultraviolet (UV)-assisted capillary force lithography (CFL) [160] and used for investigated how this platform synergistically influenced the function of hMSCs and enhanced Gene delivery with the goal of promoting a more osteogenic phenotype.

4.2 Materials and Methods

Fabrication of nanopatterned matrix

The nanopatterned matrix was fabricated using UV-assisted capillary force lithography. Regularly spaced polyurethane acrylate (PUA) nanogrooves with the width of 550 were replicated from the pre-prepared silicon masters over a large area of 25 × 25 mm^2. The silicon masters had been prepared by standard photolithography and dry etching. In the replication step, a UV-curable PUA precursor (Minuta

Tech., South Korea) was drop-dispensed onto the master and brought into contact with a 100 μm-thick polyethylene terephthalate (PET) film (SKC Inc., South Korea) as a backing plane. After subsequent irradiation of UV for few tens of seconds, a negative PUA replica was formed on the PET film. Then the same replication process was performed onto a cleaned cover slip using the replicated PUA pattern as a mold. The flat and patterned surfaces were generated on the same cover slip in order to maintain the same experimental conditions. The fabricated samples were coated with gold and imaged by a FESEM (JEOL, JSM-5410LV, Japan) at an accelerating voltage of 2 kV.

Preparation of non-viral vectors

Lipofectamine and branched polyethylenimine (bPEI) (1.2 or 25 k) were purchased from Sigma (St. Louis, MO, USA). PMGT was synthesized in a two-step reaction in which mannitol was first esterified with methacryloyl chloride to form mannitol dimethacrylate (MDM) monomer, and then copolymerized with bPEI (1.2 kDa) by a Michael addition reaction to obtain PMGT. Mannitol dimethacrylate (MDM) monomer was synthesized by reaction of mannitol with 2 equivalents of methacryloyl chloride. An emulsion was prepared by dissolving mannitol (1 g) in DMF (20 mL) and pyridine (10 mL) followed by drop

wise addition of methacryloyl chloride solution (1.2 mL dissolved in 5mL DMF) at 4℃ with constant stirring overnight. After reaction completion, HCl.pyridine salts were filtered and filtrate was dropped to diethylether. The product was precipitated in a syrupy liquid form and dried over vacuum. PMGT was prepared by Michael addition reaction between LMW bPEI and MDM. Briefly, the synthesized MDM (0.38 g) dissolved in DMSO (5 mL) was added drop wise to 1 equivalent of bPEI (1.2 kDa, dissolved in 10 mL DMSO) and reacted at 60℃ with constant stirring for 24 h. After reaction completion, mixture was dialyzed using a Spectra/Por membrane (MWCO: 3500Da; Spectrum Medical Industries, Inc., Los Angeles, CA, USA) for 36 h at 4℃ against distilled water. Finally, the synthesized polymer was lyophilized and stored at -70℃.

Cell culture

Human mesenchymal stem cells (MSCs) were obtained from the Ajou University School of Medicine (Suwon, Korea). NIH3T3 fibroblasts, human lung cancer A549 cells, and MSCs were cultured Dulbecco's modified Eagle medium (DMEM, Gibco-BRL, Grand Island, NY, USA) supplemented with 10% fetal bovine serum (FBS, Gibco, Milan, Italy) and 1% penicillin-streptomycin (Gibco, Milan, Italy) at 37℃ in a 5%

CO_2 atmosphere. A high density of cells during plating (10×10^4 cells/cm^2) was used for all experiments.

MTS assay

Cells were grown on the substrates. The MTS (Promega, Madison, WI, USA) solution was added to each well. After a 4 h incubation at 37°C in the dark, the absorbance was measured at 490 nm using a Power Wave X Microplate ELISA Reader (Bio-TeK Instruments, Winoski, VT, USA). All experiments were repeated 3 times.

Alizarin staining

ABMSCs were cultured for 21 days on the substrata in osteogenic differentiation media. The degree of mineralization was measured by Alizarin Red S (Sigma–Aldrich) staining of ABMSCs cultured on the substrata, and this measurement was used for quantification of the osteogenic differentiation of hMSCs. The cells stained with Alizarin Red S were destained with cetylpyridinium chloride (Sigma–Aldrich), and then the extracted stains were measured using an ELISA reader (VERSAMAX reader, Molecular Devices, Sunnyvale) at 540 nm. The immunofluorescent staining of osteocalcin (OCN; osteogenesis marker) of cells was also used to show the osteogenesis of ABMSCs on

substrata.

Transfection study

Cells (10×10^4 cells/cm^2) were cultured on the flat and nanopatterned matrix. At 80% cell confluency, Lipofectamine, PEI, and PMGT were treated with pGL3 (1 μg) to form nanoplexes in serum free medium, which was exchanged with fresh medium containing serum (10% FBS) after 3 h. The PEI (N/P 10) and PMGT (N/P 20) were used, which showed best performance on gene transfection in the preliminary study. After 24 h of standard incubation conditions, luciferase assay was performed according to the manufacturer's protocol. A chemiluminometer (Autolumat, LB953; EG&G Berthold, Germany) was used to measure relative light units (RLUs) normalized with protein concentration in the cell extract estimated using a BCA protein assay kit (Pierce Biotechnology, Rockford, IL, USA). Transfection activity was measured in triplicate as RLUs/mg protein. To observe the gene transfection efficiency in cells on the nanopatterned matrix, the green fluorescent protein (GFP) plasmid was obtained from Clontech (Palo Alto, CA, USA). NIH3T3 fibroblasts were cultured with PMGT/tGFP (1 μg) polyplexes and the transfected cells were observed using confocal microscopy.

4.3 Results and Discussion

In conjunction with current efforts, here, we propose a rational design for non-viral gene delivery platforms using the combination of appropriate non-viral gene vectors and nanopatterned matrix, which can synergistically enhance the efficiency of gene delivery. We hypothesized that (i) the nanoplexes would be more exposed to the cells by the nanotopography-controlled cell adhesion and (ii) the efficiency of gene delivery into the cells on nanopatterned matrix could be influenced according to the different types of non-viral gene vectors (Fig. 4.1a).

To address this challenge, we prepared a highly aligned nanopatterned matrix and a flat substrate as a control using ultraviolet-assisted capillary force lithography with polyurethane acrylate for cell culture [154, 161-163]. As shown in Fig. 4.1b, the 550 nm-wide nanogrooves (600 nm-deep) with inter-groove distances of 550 nm and the flat patterned substrate were fabricated onto glass coverslips. It was shown that the structures were well-defined with high physical integrity and uniformity over an area of 2.5×2.5 cm^2.

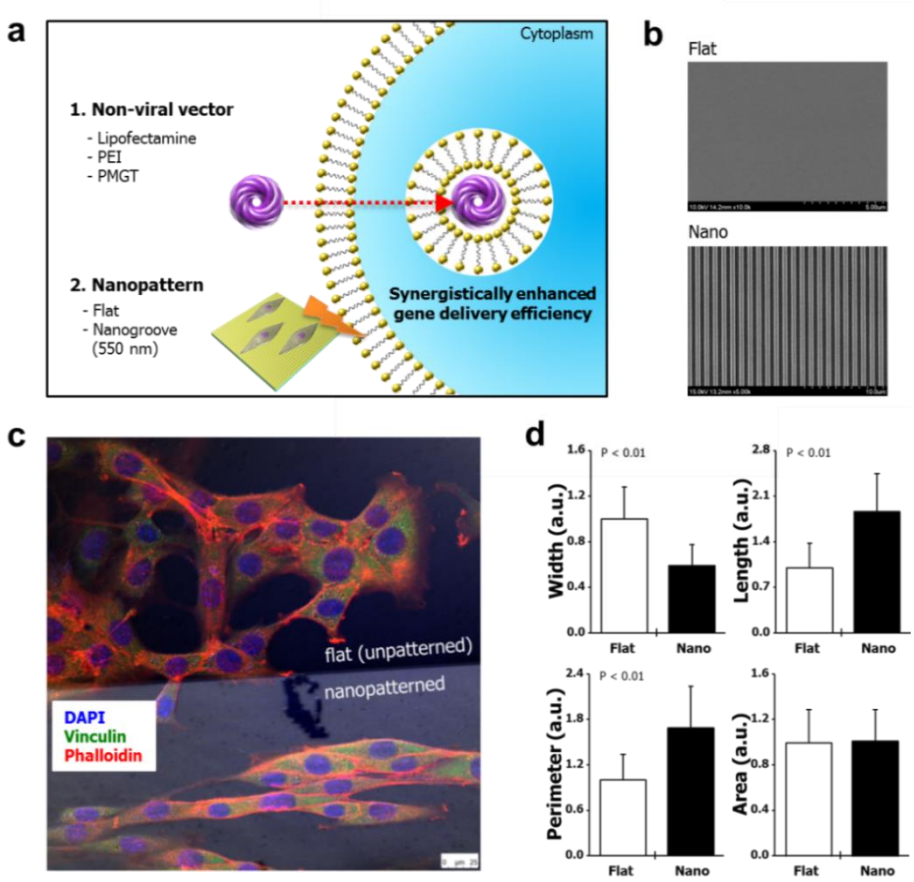

Fig. 4.1 (a) Rational design for gene delivery platforms using non-viral gene vectors and nanopatterned matrix. (b) SEM images of flat and highly aligned nanopatterned matrix. (c) Representative merged picture of immunofluorescent images (F-actin (red); vinculin (green); DAPI (blue) and phase-contrast images of NIH3T3 fibroblasts cultured on flat or nanopatterned surfaces on one substrate. (d) Quantification of cell body. The 100 cells were used for quantification. Error bars represent the SD about the means.

To investigate the effects of highly aligned nanotopography in terms of cell adhesion and shape, we cultured NIH3T3 fibroblasts on the substrates for 12 h. The immunofluorescence staining analysis clearly showed that the cell adhesion was greatly influenced as supported by the aligned cell shape (i.e., both cytoskeletal and nucleus structure) in response to the nanotopography (Fig. 4.1c). To investigate the controlled cell shape on the nanopatterned matrix in further detail, the quantitative analysis was performed (Fig. 4.1d). Interestingly, it was found that the perimeter of cell body was much larger on the nanopatterned matrix than that on the flat substrate, whereas the nanotopography cues did not much influence the cell area. Therefore, we conjectured that the enhanced cell perimeter on the nanopatterned matrix could have an important influence on sensitivity to the gene transfection efficiency. Namely, it was expected that the nanotopography-induced cell shape could allow for effective exposure to the non-viral gene vectors.

The interaction between nanopatterned matrix and non-viral gene vectors on the gene transfection efficiency in NIH3T3 fibroblasts was investigated using three types of non-viral vectors as follows:

Lipofectamine, PEI, and polymannitol based gene transporter (PMGT). It is noted that Lipofectamine and PEI are known as one of representative non-viral gene vectors which can form DNA complexes with cationic lipid (i.e., lipoplex) and positively charged polymer (i.e., polyplex), respectively. PMGT is a modified PEI-based non-viral gene vector (Fig. 4.2) that can use the hyperosmoticity contributed by polymannitol backbone leading to accelerated cellular uptake and enhanced gene transfection compared to the PEI [64].

To verify the hypothesis that the bone tissue-like nanopatterned matrix and BMP gene together can enhance the osteogenesis of ABMSCs, we first analyzed ABMSCs osteogenesis by mineralization. We cultured ABMSCs on the anisotropically nanopatterned and flat substrata in osteogenic induction media and transfected with PMGT/pBMP polyplexes. After 3 weeks the Alizarin Red S staining shown in figure 4.3 demonstrated that the calcium expression levels were higher on the nanopatterned substrata than on the flat substratum and cells transfected with BMP gene showed even higher osteogenic differentiation (Fig. 4.4).

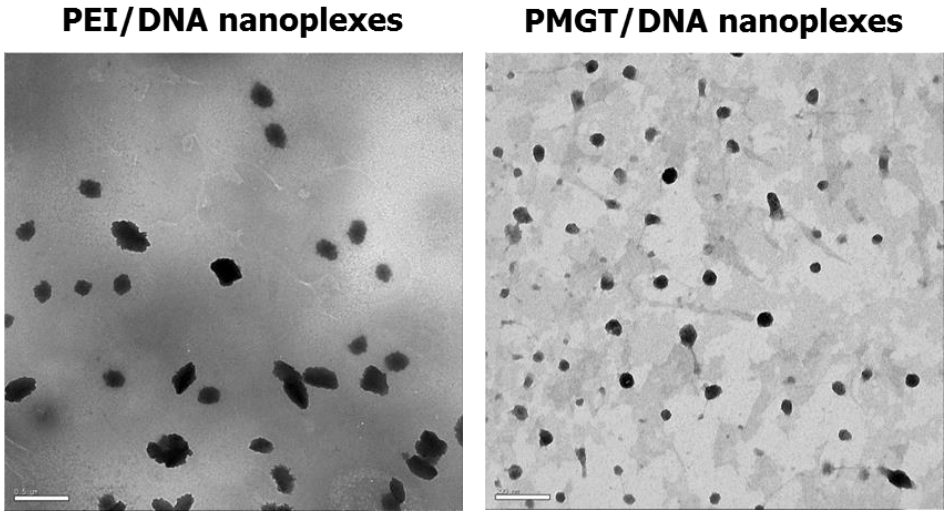

Fig. 4.2 TEM images of PEI/pGL3 and PMGT/pGL3 complexes.

Fig. 4.3 Alizarin staining of ABMSC's cultured on flat and nanopatterned surfaces showing osteogenic differentiation after 3 weeks. Images showing highest alizarin staining in cells grown on nanopatterned matrix combined with PMGT/pBMP transfection.

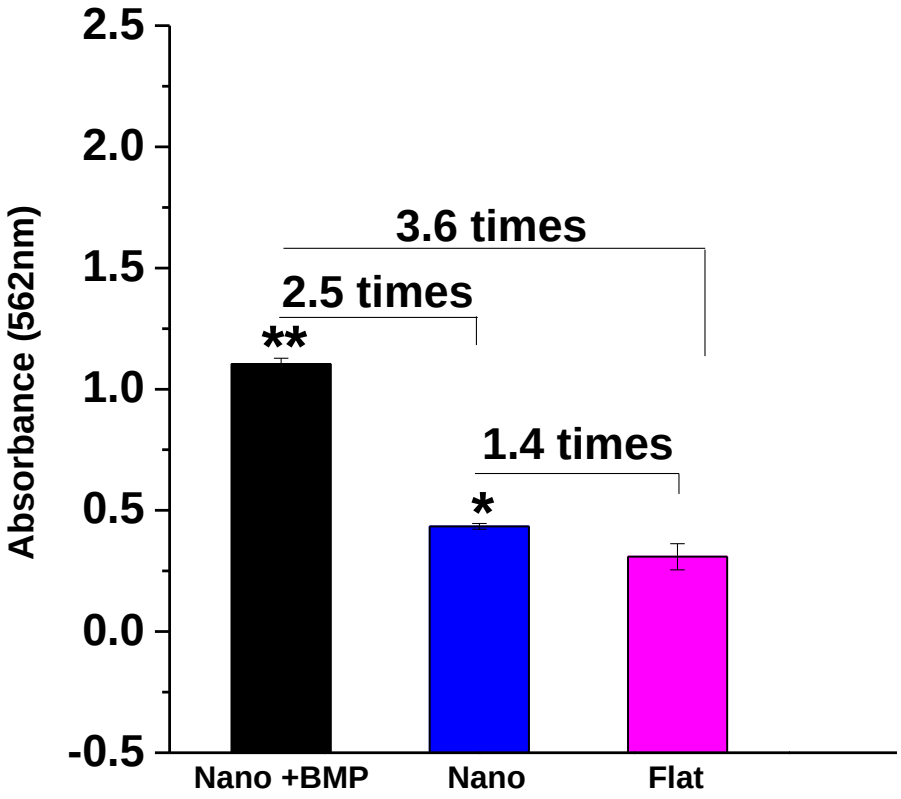

Fig. 4.4 Quantification of the degree of mineralization as measured by Alizarin staining. Error bars represent the SD about the mean (n = 3 for each group).

The cell viability on the systems was checked before investigating the gene transfection efficiency. We cultured NIH3T3 fibroblasts on the substrates for 12 h, and then the cells were exposed to the non-viral gene vectors for 3 h. As shown in Fig 4.5a, the nanotopographical property of substrates did not much influence the cell viability, whereas PMGT in both nanopatterned matrix and flat substrate showed the lowest cytotoxic effects compared to other materials. This indicates that the property of non-viral gene vectors is very important in reducing the cytotoxicity.

Next, the gene transfection efficiency was investigated. NIH3T3 fibroblasts were cultured primarily on the substrates for 12 h. The vectors were complexed with DNA (pGL3), and then they were added into the cells on the substrates. After 24 h of additional cell culture, the gene transfection was checked using luciferase assay. Two notable findings were derived from this experiment. First, regardless of any vector types used, the gene transfection efficiency was much higher on the nanopatterned matrix than that on the flat substrate (Fig. 4.5b). In particular, when the PMGT was used, the luciferase activity of cells on the nanopatterned matrix was approximately 4.5-times higher than that on the flat substrate (Fig. 4.6).

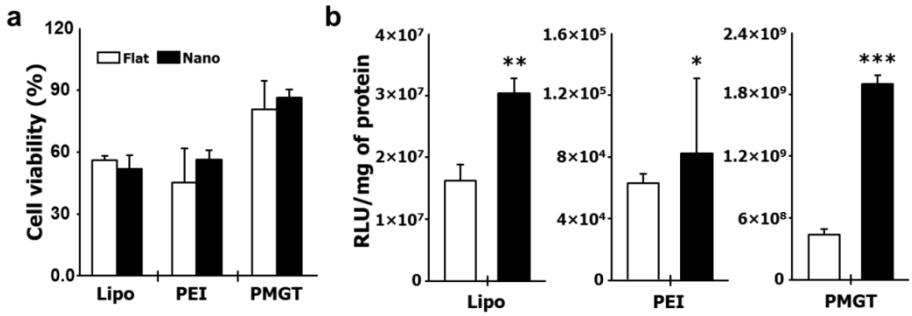

Fig. 4.5 (a) Quantification of cell viability after cell culture on the substrates (flat and nanopattern) with Lipofectamine, PEI, and PMGT (n=3 for each group). The viability was normalized with the cell viability on tissue culture polystyrene (TCPS). (b) Gene transfection of vector/DNA complexes in NIH3T3 fibroblasts cultured on substrates (n=3 for each group).

Second, the property of vectors greatly influenced the gene transfection efficiency, especially in the nanopatterned matrix than the flat substrate (Fig. 4.5b). For example, when the flat substrate was used, the luciferase activity of cells transfected with PMGT was approximately 60-times higher than that with PEI. On the other hand, the nanopatterned matrix induced approximately 270-times of an increase when PMGT was used instead of PEI. Namely, we can synergistically improve the gene transfection efficiency by the use of suitable non-viral gene vectors and nanotopography-based substrates. To verify this observation again, we cultured NIH3T3 fibroblasts with PMGT/tGFP polyplexes. As shown in Fig. 4.7, the highly increased green fluorescence was observed on the nanopatterned matrix than that on the flat substrate, indicating the enhanced gene transfection efficiency due to nanotopography-induced cell adhesion.

It has been widely discussed that the specialized gene delivery could be an essential strategy for cancer therapy or stem cell-based therapy [70, 71, 164, 165]. In this regard, designing efficient gene delivery platforms for cancer and stem cells is also one of the major challenges. Thus, we expanded our strategy

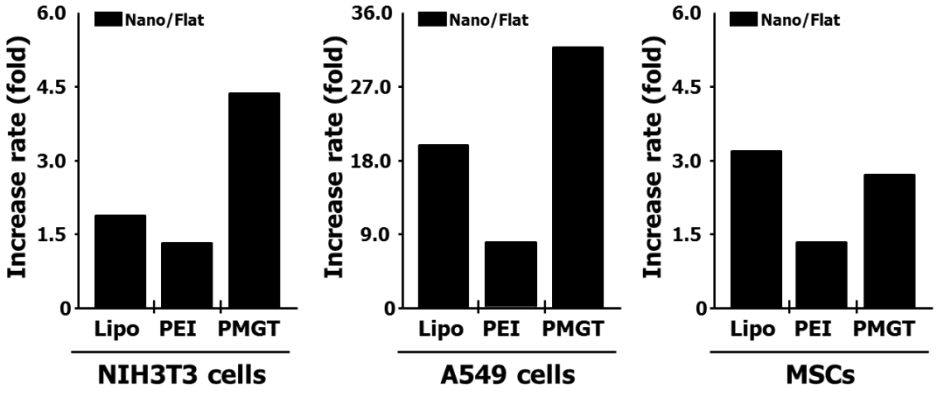

Fig. 4.6 Quantitative analysis of the data on gene transfection of vector/pGL3 complexes in various cells (Figs. 4.5 and 4.8). The values indicate the increased rate of gene transfection in flat vs. nanopatterned substrates.

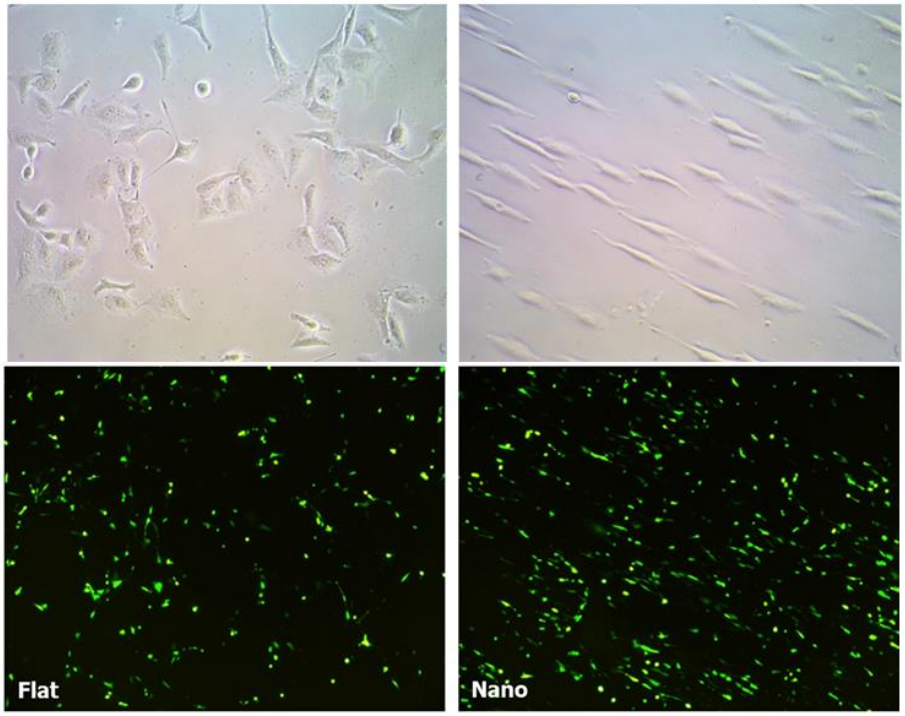

Fig. 4.7 Representative fluorescent images of cultured NIH3T3 fibroblasts on substrates transfected with PMGT/tGFP complexes shows enhanced transfection on the nanopatterned matrix.

proposed in this study by using cancer and stem cells. To this end, we cultured human lung cancer A549 cells and human mesenchymal stem cells (MSCs) on the flat substrate and the nanopatterned matrix for 12 h, respectively. Then, the nanoplexes (i.e., pGL3 with Lipofectamine, PEI, and PMGT) were added into the cells on the substrates to investigate the effects of nanotopography and gene vectors on gene transfection efficiency in cancer and stem cells. After 24 h of culture more, we performed the luciferase assay, which clearly showed that the gene transfection efficiency was greatly enhanced on the nanopatterned matrix in both the A549 cells and MSCs, regardless of the vector types used (Fig, 4.8). In particular, we learned that the gene transfection efficiency in both cells was the highest when PMGT was used with the nanopatterned matrix (Figs. 4.8 and 4.6), suggesting the importance of using suitable non-viral vectors in combination with nanotopography for improving gene transfection efficiency in cancer and stem cell.

Taken together, our results indicate that the nanopatterned matrix may have great potentials to enhance the gene transfection efficiency via non-viral vectors in various cell types including

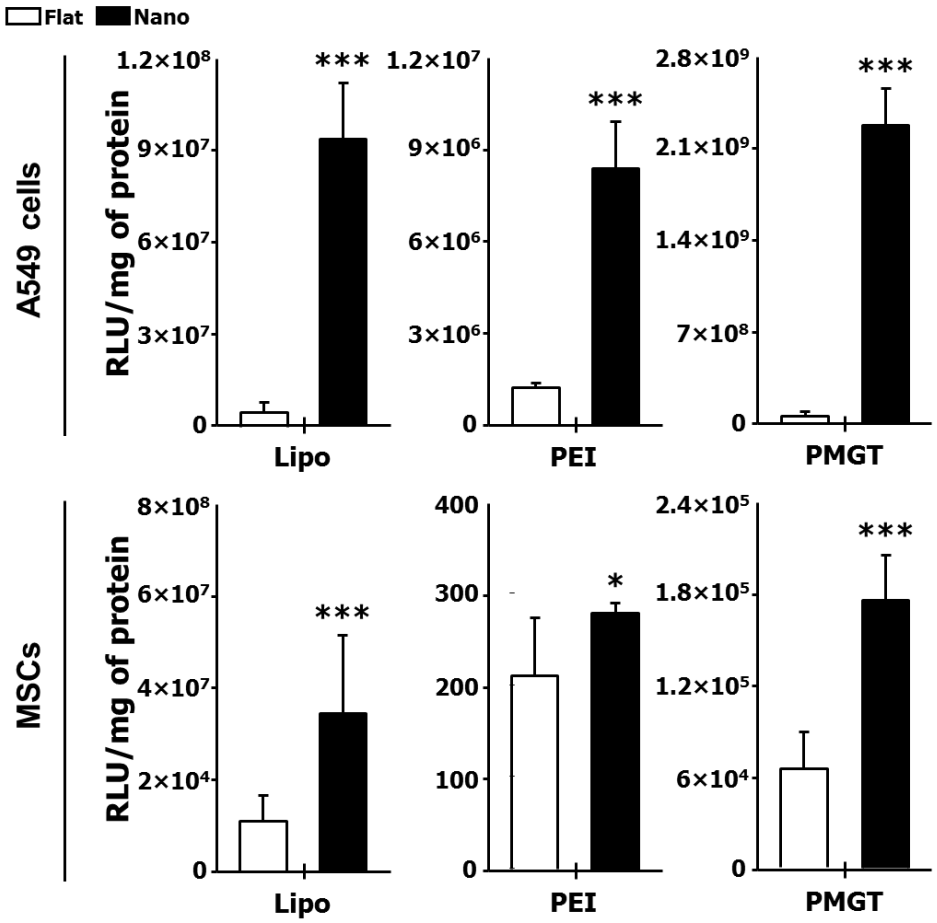

Fig. 4.8 Gene transfection of various vector/DNA complexes in A549 cancer cells and MSCs cultured on substrates (n=3 for each group). The vector/pGL3 complexes were used.

normal, cancer, and stem cells. Based on our experimental observations in this study, we report two notable findings (Figs, 4.5 and 4.8): (i) although the nanopatterned matrix could enhance the gene transfection efficiency in all types of cells compared to the flat substrate, regardless of the vector types, it could be further enhanced by the suitable combination of nanotopography and non-viral vector (i.e., nanopatterned matrix and PMGT in this study) and (ii) the nanopatterned matrix in particular promotes the transfection efficiency in cancer cells compared to that in normal or stem cells (i.e., A549 cells > NIH3T3 fibroblasts > MSCs in this study).

We discuss the following key question here: how does the nanopatterned matrix enhance the gene transfection efficiency via non-viral vectors? Although a detailed study should be performed, we propose two considerable major factors and their roles: nanotopography-mediated (1) cellular shape and (2) uptake (Fig. 4.9). (1) Basically, we speculated that the nanotopography-induced cellular shape would be an essential factor for the efficiency of gene delivery via non-viral gene vectors. Kong's group recently reported that the cell area of NIH3T3 fibroblasts

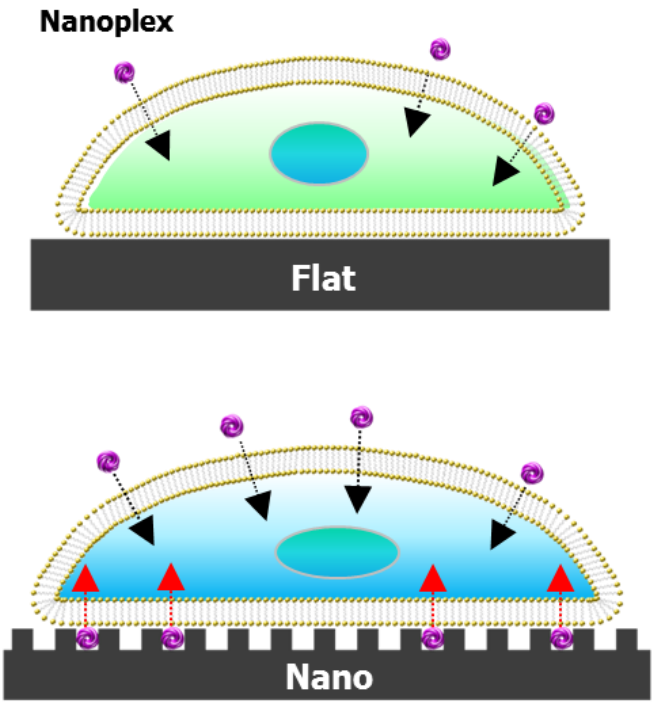

Fig. 4.9 A hypothetical model showing enhanced gene transfection via non-viral gene vectors on highly aligned nanopatterned matrix.

expanded with increasing substrate stiffness, which eventually enhanced the gene transfection efficiency [150]. In this study, while the aligned nanopatterned matrix did not quite influence the average of cell area, the cell perimeter was sensitively increased by the nanopatterned matrix than that on the flat substrate (Fig. 4.1d). In addition, the nanoplexes could be located between the nanopatterns, allowing meeting them into the cell adhesion area. Together, these factors collectively provided cells more opportunities to be exposed to the nanoplexes for enhancing gene delivery efficiency via non-viral gene vectors.

(2) We suggest that the highly aligned structures in both cell body and nucleus by the nanopatterned matrix (Fig. 4.1c) would influence the cellular uptake of nanoplexes for the efficiency of gene delivery. Although the exact mechanism is unclear, it has been known that the body or nuclear shapes can modulate the exogenous gene expression [150, 153, 166]. In this work, compared to Lipofectamine or PEI, PMGT dramatically enhanced the gene transfection on the nanopatterned matrix than on the flat substrate (Figs. 4.5 and 4.8). Note that PMGT can lead accelerated cellular uptake than PEI or Lipofectamine [64]. In addition, the

transfection efficiency was much higher in the cancer cells than normal or stem cells, regardless of types of gene vectors (Fig. 4.8). Therefore, the modulated cellular activity (e.g., endocytosis) by the changed cell structures on nanopatterned matrix may affect the enhanced transfection efficiency, but further detailed studies should be performed for understanding this mechanism.

We would like to re-emphasize our findings that the highly aligned nanopatterned matrix and non-viral vectors can synergistically enhance the efficiency of gene delivery. This, therefore, suggests that there will be a further opportunity to improve gene transfection efficiency by designing efficient nanotopography-based substrates and non-viral vectors as well as in combination with microfluidic-based platforms. We also believe that our simple strategy may represent a significant progression for the design and manipulation of platforms in the various research fields. For example, this strategy could be used for enhancing stem cell functions (e.g., efficient delivery of small molecules to control stem cell differentiation) or for scaffold fabrication toward tissue regeneration.

4.4 Conclusion

In conclusion, we have proposed a conceptual design of platform that nanopatterned matrix and non-viral vectors could promote the gene transfection efficiency by their synergistic cues. The nanotopography-induced cell adhesion can provide unique opportunity to enhance the gene transfection via non-viral vectors, which would suggest that the nanotopography definition of substrate and non-viral vectors should be considered in the design and manipulation of gene delivery systems for gene medicine as well as for stem cell and regenerative medicine.

CHAPTER 5

Silencing of JNK2 by Polymannitol-Based Transporter via COX-2 Mediated Endocytosis

5.1 Introduction

Potential of nucleic acid as drugs in treating genetically aberrant conditions using either DNA- or RNA-based therapeutics has given momentum to the development of various gene delivery methods that not only carry multiple therapeutic payloads but also facilitate delivery into specific sites across compact tissues and tumor masses [28, 167]. For an effective gene therapy in cancer therapeutics, a deeper understanding of cancer cell behavior and its intracellular signaling is required to strategically tailor a delivering vector. An insight to the tumor cell behavior may help the vector to target the major cause responsible for abnormal growth and thereby assist in cessation of tumor cell proliferation.

No doubt that tumor formation is a complex process and most of which are due to proto-oncogenic transformation that leads to the abnormal overexpression of oncogenes. Studies have shown that the proto-

oncogene c-Jun is normally required for cell cycle progression from G1 to S phase by regulating the transcriptional level of cyclin D1, but under diseased condition it is associated with uncontrolled proliferation and angiogenesis [168], and also inhibits apoptosis by downregulating p53 and p21 [169, 170]. This oncogenic transformation of transcription factor c-Jun requires N terminal phosphorylation of its transactivation domain at serine 63 and 73 by c-Jun N-terminal kinases (JNKs) [171, 172]. JNKs are a family of stress related kinases. Hence, JNK mediated activation of c-jun are responsive to stress stimuli to protect the cells against stress induced apoptosis [169]. Therefore, suppressing the N-terminal phosphorylation of c-Jun by delivering JNK siRNA is expected to inhibit tumor growth and proliferation via inducing apoptosis.

However, JNKs (JNK1, JNK2, and JNK3) tend to have contradictory cellular responses, to induce apoptosis on one side and enhancing cell survival and proliferation on the other side. Their opposing behavior can be attributed to the activation of large number of different substrates based on specific stimulus, cell type, and temporal aspects [173]. One of the major substrates of JNK mediated phosphorylation is c-Jun which is a component of AP-1 transcription factor.

Phosphorylation of c-Jun by JNKs directly increases the transcriptional activity of AP-1, which is involved in neoplastic transformation to promote tumor progression and metastasis [174]. Many tumors have been reported to constitutively express JNKs as JNKs activation and c-Jun phosphorylation are required for initial oncogenic transformation [173]. It has been reported that amongst three, JNK2 is the primary positive regulator of c-Jun expression and proliferation [175]. Therefore, inhibition of JNK2 activation caused growth arrest and apoptosis in some of the tumors [176] supporting that JNK2 is the main active JNK present in tumor cells as a potential oncokinase whose suppression may retard tumor growth.

Though the selection of an appropriate siRNA is the most important part of gene silencing technology, the need of an efficient vector that can protect siRNAs in the biological milieu where they are vulnerable for degradation by endogenous nucleases is equally important as well [127]. We recently developed polymannitol based gene transporter (PMGT) synthesized from mannitol dimethacrylate and low molecular weight branched polyethylenimine (1.2 kDa). PMGT enjoys osmotic activity of mannitol in combination with high buffering capacity of bPEI. Owing to hyperosmoticity and hydrophobicity as its inherent

properties, PMGT has accelerated the cellular uptake process to many folds [177]. Its hyperosmotic behavior has shown to modulate the cellular uptake mechanism by regulating cyclooxygenase-2 (COX-2) enzyme which induces caveolae mediated endocytosis thereby overcoming cell membrane barrier. Therefore, it was hypothesized that due to its hyperosmotic property it may also approach the compactly situated cells in a tumor mass to deliver therapeutic molecules. It may elevate blood plasma osmolality, resulting in enhanced out flow of water from tissues, thereby loosening the cell mass and facilitating the transporter to reach deep seated cells. A further higher transfection efficiency of PMGT is also contributed by its hydrophobic methyl groups which interact with phospholipid bilayer of plasma membrane facilitating smooth polyplex internalization inside the cell [105]. Moreover, hydroxyl groups in a polymer may serve different functions and alter polymer properties depending upon their number, ratio and stereochemistry [140]. In accordance, it was reported that hydroxyl groups of polymannitol backbone served for better complexation, polyplex stability, non-aggregation, lower polydispersity and higher transfection efficiency even in the presence of serum [177].

In this paper, we introduce a nanotechnology-based, potential approach for gene silencing-mediated cancer therapy. We demonstrate that PMGT electrostatically complexed with JNK2 siRNA molecules can be used to knockdown the overexpression of JNK2 which is responsible for progression and metastasis of cancer to arrest tumor growth both *in vitro* and *in vivo*. Since the route of endocytosis plays a pivotal role in determining intracellular fate of polyplexes, the various components of PMGT vector modulating these routes is expected to underscore the efficiency of siRNA transportation. The mechanism of tumor retardation by PMGT mediated JNK2 siRNA delivery was well studied to show the involvement of caspase-9 in inducing apoptosis mediated by COX-2 signaling. Therefore, based on the current study, inference was drawn that the hyperosmoticity generated by PMGT stimulates COX-2 expression that firstly induces polyplex internalization by initiating caveolae formation and later induces apoptosis by stimulating caspase-9 in tumor cells. In addition, PMGT efficiently delivered siRNA that helped in silencing JNK2 expression and hence tumor arrest. The triple action performed by PMGT intrigued to investigate the exact mechanism of cellular entry of polyplex and exhibiting gene silencing.

5.2 Materials and Methods

Materials

Branched PEI (Mn: 1.2 kDa and 25 kDa), dimethyl sulfoxide (DMSO), methacryloyl chloride (MAC), D-mannitol, genistein, wortmannin, chlorpromazine, methyl-β-cyclodextrin, and 3-(4, 5-dimethyl thioazol-2-yl)-2, 5-diphenyl tetrazolium bromide (MTT) reagent were purchased from Sigma (St. Louis, Mo, USA). Tetramethylrhodamine isothiocyanate (TRITC) fluorescent dye was purchased from Molecular Probes, Invitrogen, Oregon, USA. Nonspecific scrambled siRNA (siScr), GFP siRNA (siGFP), luciferase siRNA (siLuc) (Table 5.1) were purchased from Genolution Pharmaceuticals, Inc. (Seoul, South Korea). JNK2 siRNA (siJNK2), JNK2 antibody, COX-2 antibody, caspase-9 antibody were purchased from Santa Cruz biotechnology, Inc (CA, USA) and caveolin-1 antibody was purchased from Abcam. All other chemicals used in this study were of analytical reagent grade.

Synthesis and characterization of PMGT & PMGT/siRNA complexes

Mannitol dimethacrylate (MDM) monomer was obtained by reacting mannitol with 2 equivalents of methacryloyl chloride in DMF at 4℃. Thereafter, via a Michael addition reaction [107] bPEI (1.2 kDa) was copolymerized with MDM in anhydrous DMSO at 60℃ to synthesize

Table 5.1 siRNA sequences

siRNA	**Sense (5'→3')**	**Anti-sense (5'→3')**
siRNA	CGUACGCGGAAUACUU	UCGAAGUAUUCCGCG
scrambled	CGAUU	UACGUU
siRNA	GUUCAGCGUGUCCGGC	CUCGCCGGACACGCUG
GFP	GAGUU	AACUU
siRNA	CUUACGCUGAGUACUU	UCGAAGUACUCAGCGU
Luciferase	CGAUU	AAGUU

polymannitol based gene transporter (PMGT) [177] as shown in Fig. 2.1. The cationic PMGT polymer at N/P 20 and PEI25k at N/P 10 were then electrostatically bound with siRNA (100 pM) in ultra-pure molecular grade water (WelGENE, S. Korea) (30 min incubation at RT) to form PMGT/siRNA and PEI25k/siRNA polyplexes. Polyplexes were characterized using a transmission electron microscope (EF-TEM) (LIBRA 120, Carl Zeiss, Germany) and a dynamic light scattering spectrophotometer (DLS 8000, Otsuka Electronics, Osaka, Japan). The specimens for TEM were prepared by drop-coating the PMGT/siRNA (N/P 20) and PEI25k/siRNA (N/P 10) polyplexes dispersion onto a carbon grid and then dried for 2 h, after which they were stained with 1% uranyl acetate (10 s) and observed for their morphology. DLS samples were prepared at various N/P ratios (5, 10, 20, and 30) of PMGT/siRNA and PEI25k/siRNA polyplexes with 40 µg/mL siRNA and then measured for their hydrodynamic size and zeta potential with 90° and 20° scattering angles at 25℃.

Electrophoretic mobility shift assay

For siRNA retardation assay, PMGT was complexed with siRNA (1 µg) for 30 min at RT at various N/P ratios (0.5, 1, 2, 3, and 5). The complexed samples and equivalent amounts of free siRNA with 1X

loading dye (Biosesang, Korea) were added in individual wells in a 2% agarose gel (with 0.1 µg/mL EtBr) casted in 1X TAE buffer. The samples were resolved for 40 min in 0.5X TAE running buffer at 100 V, and images were captured under ultraviolet illumination. For RNAse protection assay, PMGT/siRNA (N/P 20) polyplexes and free siRNA were incubated with RNase (1 µg/µL) at 37℃. After 30 min, RNase was inactivated by adding 5 µL EDTA (100 mM) at 70℃ for 10 min and incubated for another 30 min at RT. Finally, the protected siRNA was released from the complexes with the addition of 5 µL 1% sodium dodecyl sulfate (SDS) for 2 h and resolved on a 2% agarose gel (with 0.1 µg/mL EtBr) in 0.5X TAE running buffer at 100 V for 40 min.

Osmolarity of PMGT/siRNA complexes

Osmolarity of aqueous solution of mannitol, PMGT and PMGT/siRNA complexes at various concentrations (2%, 3%, 5%, and 10%) were measured as mOsm using cryoscopic osmometer 030, Ganatec and calculated from the depression in freezing point of solutions.

Confocal microscopy

TRITC (Molecular Probes, Invitrogen, Oregon, USA) (25 µL, 1 mg/100 µL in DMF) was added to PMGT (1 mL, 10 mg/mL in H2O) to

block ~1% of its total amines, and the mixture was then stirred overnight ($PMGT^T$). Unreacted TRITC was removed by washing with ethyl acetate (3 x 2 mL), which was then lyophilized and resuspended in water. A549 cells were seeded at a density of 3 x 10^5 cells/well in a cover glass bottom dish (SPL Lifesciences, Korea) and incubated for 24 h in humidified chamber. Cells were transfected with $PMGT^T$/siRNA complexes and further incubated for 3 h, 2 d, 3 d, 5 d, and 7 d to study the degradation profile of PMGT polyplexes. The transfected A549 cells with fluorescently labeled complexes were washed 3 times with 1X PBS and then fixed with 4% paraformaldehyde for 10 min at 4℃. DAPI was used to counter-stain the nuclear DNA of fixed cells, and images were procured using a Leica SP8 X STED super-resolution laser scanning confocal microscope to monitor fluorescently labeled $PMGT^T$/siRNA complexes inside the treated A549 cells.

Cell culture and animals

Low passage adenocarcinoma human alveolar basal epithelial (A549) cells were cultured in T-75 culture flasks (Nunc, Thermo Scientific) in 15 mL complete medium containing Roswell Park Memorial Institute (RPMI)-1640 (HyClone Laboratories, USA) supplemented with 10% heat-inactivated fetal bovine serum (FBS, HyClone Laboratories, USA)

and 1% antibiotic cocktail of streptomycin and penicillin. Cells were maintained under standard culture conditions of 37℃ and 5% CO2 for 4 or 5 days, with the culture duration selected to maintain cells under exponential growth and reach ~80% confluency. Cells were then trypsinized, centrifuged at 1200 RPM for 5 min to pellet cells and counted using hemocytometer to seed the cells for experimental assays.

For animal study four weeks old nude Balb/c mice were obtained from Orient Bio Inc. (Republic of Korea) and kept in a laboratory animal facility maintained at 23 ± 2℃ and 50 ± 20% relative humidity under a 12 h light/dark cycle. All experimental protocols were reviewed and approved by the Animal Care and Use Committee at Seoul National University (SNU-120409-3).

Cell viability assay

Cytotoxicity of PMGT/siRNA (N/P 20) and PEI25k/siRNA (N/P 10) polyplexes at various siRNA concentrations (0, 50, 100, 150 pM) and after different incubation times (3 h, 2 d, 5 d, 7d) were measured by the reduction of a tetrazolium component (3-(4,5-dimethylthiazol-2-yl)-2,5-diphenyltetrazolium bromide, or MTT) (Sigma, St. Louis, Mo, USA) into insoluble purple colored formazan crystals by the

mitochondria of the viable cells. Polyplex transfected A549 cells that had been incubated in a 24-well plate (10 x 10^4 initial cell density/well) for 48 h were then incubated with MTT reagent (0.5 mg/mL in 1X PBS) for 3 h, followed by the addition of DMSO (500 µL) to solubilize the colored crystals, and absorbance was measured at 540 nm using a Sunrise^{TM} TECAN ELISA reader (Grödig, Austria).

In vitro GFP silencing efficiency of PMGT

A549 cells at 70% confluency (3 x 10^5 initial cell density/well) in a 6-well plate were transfected with Lipofectamine/tGFP (1 µg) complex in serum-free medium according to the manufacturer's protocol (Invitrogen, Oregon, USA). After 3 hours, the medium was replaced with fresh serum-free RPMI-1640 medium with the PMGT/siGFP complex (N/P 20) containing 100 pM of siRNA. The silencing efficiency was then compared with that of PEI25k/siGFP (N/P 10) mediated silencing. After 3 hours of incubation, the medium was again replaced with 10% serum-containing medium. After an additional 48 h, the silencing efficiency was measured using flow cytometry (BD Biosciences, San Jose, CA, USA). The percentage of GFP silencing in the cells treated with PMGT/siGFP complexes was calculated after normalizing the results with respective mock-treated cells and then

compared to the silencing of the PMGT/siScr-treated group. Nonspecific scrambled siRNA (siScr) and GFP siRNA (siGFP) were purchased from Genolution Pharmaceuticals, Inc. (Seoul, South Korea).

Transfection for RNAi silencing of JNK2

A549 cells were cultured according to standard techniques as described above. Cells were seeded at a density of 3 x 105 cells/well in a 6-well plate; and after 24 h (70% confluent) were transfected with PMGT/siJNK2 complexes. The JNK2 siRNA (siJNK2) (Santa Cruz biotechnology, Inc, CA, USA) was reconstituted in ultra-pure water (DNase/RNase free) and mixed with PMGT at an N/P ratio of 20 to a final concentration of 100 pM of JNK2 siRNA. After 30 min of incubation, A549 cells were transfected for 3 h in serum-free medium. PEI25k (N/P 10) was used as positive control, whereas naked siJNK2 and scrambled sequence (siScr) negative controls were used in all experiments. For assessment of JNK2 knockdown, 48 h post-transfection total RNA was isolated from cells using Absolutely RNA Miniprep kit (Agilent Tech., CA, USA), and real-time quantitative PCR (Q-PCR) was performed for JNK2. Extracted RNA was reverse transcribed to cDNA using the Omniscript RT kit (Qiagen, Germany) with omniscript reverse transcriptase (Qiagen) and a random primer

(Invitrogen, MA, USA). The relative abundance of each mRNA species was quantified by qPCR using the hJNK2 5'-GAAATGGTCCTCCATAA-3' (forward) and 5'-ACTGCTGCATCTGAAGGC-3' (reverse) and hGAPDH 5'-GCCCAATACGACCAAATCC-3' (forward) and 5'-AGTCAGCCGCATCTTCTT-3' (reverse) specific primers from Cosmogenetech, Seoul, Korea. PCR mixtures were prepared with 2X Prime Q-Mastermix containing 2X SYBR® Green I (Genet Bio, Nonsan, Korea) according to the manufacturer's protocol. Q-PCR was performed in quadruplicate for each group, with GAPDH as reference gene, using an iCycler Optical Module (BioRad, CA, USA) starting with 10 min of pre-incubation at 95℃ followed by 45 amplification cycles with an annealing temperature at 60℃.

Western blot analysis

At 48 h post-transfection, cells were harvested and lysed with 1X RIPA lysis buffer (Millipore, MA, USA). A BCA protein assay kit (Thermo scientific, MA, USA) was used to measure the protein concentrations. Equal amounts of the protein (25 μg) from each sample were separated by a Novex NuPAGE 4-12% SDS-PAGE gel (Life technologies, CA, USA), transferred to nitrocellulose membrane using iBlot (Invitrogen,

USA) and then non-specific binding sites were pre-blocked with 5% skim milk for 1 h at RT. The membrane was washed and probed with anti-JNK2 (Santa Cruz Biotechnology Inc., CA, USA) and anti-β-actin (Abfrontier, Seoul, Korea) antibodies (1:500 dilution) overnight at 4℃. Then, the membrane was incubated with secondary antibody (1:1000 dilution) conjugated with HRP (Invitrogen, Carlsbad, CA, USA). Bands were captured using a ChemiDoc^{TM} XRS^{+} (Biorad, CA, USA) imaging system. The band intensities were analyzed quantitatively using ImageJ software (NIH, USA) and plotted as the mean pixel value.

Immunocytochemistry (ICC)

A549 cells were seeded in an 8-well chamber slide (Lab Tek, Sigma, USA) at 5 x 10^4 initial cell density/well and transfected with the PMGT/siJNK2 complexes together with the positive controls. After 48 h, cells were rinsed in 1X PBS and fixed with 4% paraformaldehyde at 37℃ for 10 min. After fixation, cells were washed twice with ice cold PBS and then permeabilized with ice-cold 0.2% Tween 20 in PBS for 10 min. Non-specific binding was blocked using 10% BSA in 1X PBS for 5 min at RT and then at 4℃ for 1 h because cooling prevents endocytosis of antibodies. Cells were incubated with JNK2 antibody (Santa Cruz Biotechnology Inc., CA, USA) diluted in 3% BSA (1:50

dilution) at 4℃ overnight. After washing several times with PBS, cells were incubated with fluorophore-conjugated secondary antibodies diluted in 3% BSA (1:100 dilution) for 2 h at RT away from light. Nuclei were stained with DAPI (0.1 μg/mL) for 10 min and mounted with Aqua poly/mount (Polysciences, PA, USA). The images were procured from Nikon eclipse Ti inverted fluorescence microscope system (Tokyo, Japan).

In vitro and in vivo TUNEL assay

The transfected A549 cells in the 8-well chamber slide and the *in vivo* treated tumor sections were analyzed for apoptotic death using a DeadEnd colorimetric TUNEL (TdT mediated dUTP nick end labeling) system from Promega, USA, which end-labels the fragmented DNA of apoptotic cells. The paraffin embedded tissue sections were deparaffinized using xylene and rehydrated by sequentially immersing the slides into 100%, 95%, 85%, 70%, and 50% ethanol. The tissue sections and the cultured cells were fixed with 4% paraformaldehyde for 25 min at RT and washed twice with PBS. The tissue cells and cultured cells were then permeabilized using proteinase K (20 μg/mL) and 0.2% Triton X-100 respectively, for 10 min at RT and rinsed twice with PBS. Biotinylated nucleotides were incorporated at the 3'-OH

DNA ends using a recombinant terminal deoxynucleotidyl transferase, (rTdT) enzyme. Horseradish peroxidase-conjugated streptavidin was then bound to biotinylated nucleotides, which were detected with hydrogen peroxide and diaminobenzimide (DAB). The images were captured using a light microscope. Cells treated with DNase I to induce DNA strand breaks were used as a positive control.

Tumor implantation and in vivo JNK2 suppression

Five weeks old nude Balb/c mice (male, 4 mice/group) were subcutaneously injected with 100 µL of a single cell suspension containing 3 x 10^6 A549 cells. The treatment of tumors with siJNK2 was started after 1 month when the tumor size reached 800-1000 mm^3 as measured by Vernier caliper. Tumor volume was calculated by using its mean diameter and applying the formula $m = 0.5 \times a \times b^2$, where a and b are the smallest and largest diameters, respectively. 100 µL of PMGT/siJNK2 (30 µg) complexes (N/P 20) in normal saline was injected directly into the tumor at an interval of 48 h, which continued for one month. PEI25k/siJNK2 (N/P 10) complexes prepared under identical conditions were used as vector controls, and normal saline was used as a negative control. After treatment over one month, the tumors were dissected, chopped, and homogenized, and the protein

concentrations of the lysates were measured. Equal amounts of protein (25 μg) were separated by SDS-PAGE and transferred onto a nitrocellulose membrane for immunoblot analysis.

Immunohistochemistry (IHC)

The dissected tumors were fixed in 10% neutral buffered formalin and embedded in paraffin wax. Tissue sections (4-12 μm thick) were prepared using a microtome and placed on positively charged slides and dried in an oven at 60℃. The slides were then deparaffinized, rehydrated and processed for antigen retrieval using 10 mM sodium citrate buffer, pH 6.0 at 95-100℃. Immunostaining with JNK2 antibody (1:50 dilution) was performed using a mouse specific HRP/DAB detection IHC kit (Abcam, Cambridge, UK). Harris hematoxylin solution (Sigma) was used to stain the nuclei, and images were taken using a light microscope.

COX-2 ELISA assay

A549 cells were seeded in 8.8 cm^2 culture dishes (40 x 10^4 initial cell density/dish) and treated with PMGT/siJNK2 (N/P 20) and PEI25k/siJNK2 (N/P 10) complexes. Cells were harvested at different time intervals (1h, 3h and 6h) to obtain cell lysate containing expressed

proteins. COX-2 ELISA (Pathscan, cell signaling technology, USA) was performed according to manufacturer's protocol and absorbance was measured at 450 nm.

Co-localization of COX-2 and caveolin-1

After 120 min of transfection with naked siJNK2, PMGT/siJNK2 (N/P 20) and PEI25k/siJNK2 (N/P 10) complexes, A549 cells were washed with PBS and fixed with 4% paraformaldehyde for 15 min at RT. After washing with PBS cells were permeabilized with ice cold 0.2% Tween 20 for 10 min at RT. The cells were then washed and blocked with 10% BSA for 1 h at RT. Rabbit COX-2 and mouse Cav-1 IgG antibodies (1:50 dilution in 10% BSA) were added and incubated at 4℃ overnight. The cells were washed 5 times with PBS and incubated with anti-rabbit FITC and anti-mouse RITC antibodies (Invitrogen, Oregon, USA) respectively for 1 h at RT. Then washed with PBS 5 times and incubated with DAPI for 10 min. After washing it once with PBS antifade aqua mount (Polysciences, PA, USA) was added and images were captured under confocal microscope.

Expression of COX-2, caveolin-1and caspase-9

A549 cells transfected with PMGT/siJNK2 (N/P 20) and PEI25k/siJNK2 (N/P 10) complexes were lysed after 3 h and protein concentration was measured. Equal amounts of protein (25 µg) were separated on SDS-PAGE and transferred on nitrocellulose membrane to analyze the immunoblot for the expression of COX-2, caveolin-1 and caspase-9 proteins using their respective antibodies at 1:500 dilutions.

Statistical analysis

Data are expressed as mean ± SD of 3 independent experiments unless stated otherwise. Statistical analysis was performed by one-way ANOVA (OriginPro 9.0 software) in conjunction with Bonferroni's test for the comparison of means of different groups. A value of $P < 0.05$ was considered statistically significant.

5.3 Results

siRNA transport efficiency of PMGT

Electrophoretic mobility shift assay demonstrated a high complexation ability of PMGT with siRNA by completely retarding its migration in the agarose gel at a lower N/P ratio of 3 (Fig. 5.1A). Ability of PMGT to also protect the complexed siRNA was further demonstrated by

RNAse protection & release assay as visible in lane 2 of figure 5.1B to suggest its protection against intracellular RNase degradation contrary to the complete degradation of free siRNA (lane 4). Electrostatic condensation of siRNA with PMGT resulted in nanosized cationic particles suitable for cellular uptake, as confirmed by DLS and EF-TEM. PMGT/siRNA nanoplex sizes decreased from 180 to 110 nm with increasing N/P ratios (Fig. 5.1D) due to stronger complexation. On the other hand, initial decrease and then stability in zeta potential at around +17 to +21 mV with increasing N/P ratios (Fig. 5.1E) suggest the role of polymannitol hydroxyl groups in shielding the surface charge of complexes by the formation of hydrogen bonds leading to stable zeta potential contrary to PEI25k/siRNA complexes. An optimum charge density on PMGT polyplex ensures interaction with anionic membrane proteins to initiate their internalization and also reduces its cytotoxicity caused due to high charge density that leads to cell membrane rupture [178]. This stable behavior of polyplexes can be attributed to the hydroxyl groups of polymannitol backbone which shields the polyplex by making intermolecular hydrogen bonds with DNA [179]. Therefore polyplex maintain uniform size distribution throughout its voyage to the nucleus which is also apparent from the

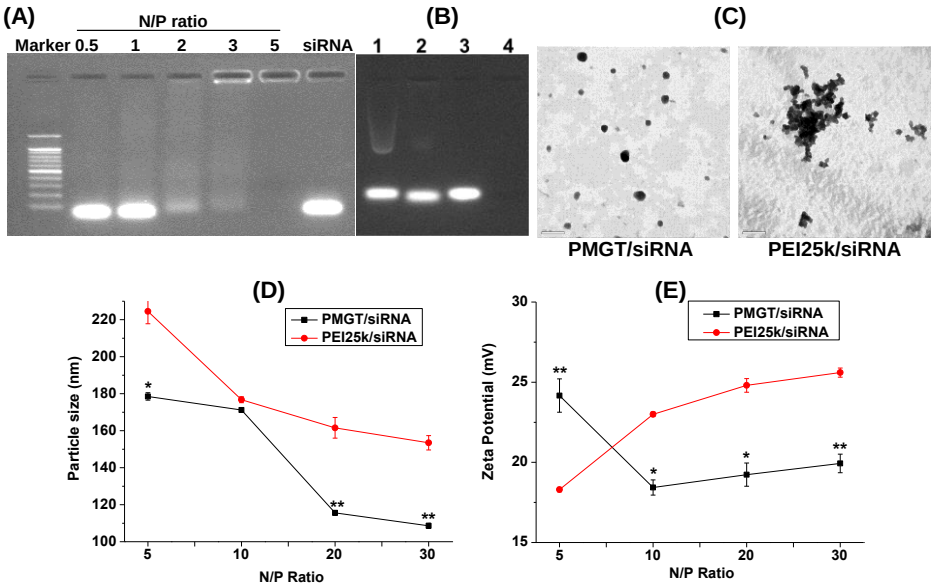

Fig. 5.1 Physicochemical characterization of PMGT/siRNA complexes. (A) Electrophoretic mobility shift assay of PMGT/siRNA (0.1 µg) complexes at various N/P ratios (0.5, 1, 2, 3, and 5) shows complete siRNA retardation at an N/P ratio of 3. (B) RNase protection and release assay. Complexed siRNA with PMGT (N/P 20) was released using 1% SDS: (Lane 1) PMGT/siRNA complexes without RNase; (Lane 2) PMGT/siRNA complexes with RNase (1 µg/µL) demonstrates the protection of the siRNA; (Lane 3) free siRNA without RNase; (Lane 4) free siRNA with RNase (1 µg/µL) shows its complete degradation. (C) EF-TEM image of PMGT/siRNA (N/P 20) and PEI25k/siRNA complexes shows PMGT particle size ~110 nm (scale bar: 200 nm). (D) Particle size and (E) zeta potential of PMGT/siRNA

complexes at various N/P ratios (5, 10, 20, and 30) shows its size ~150 nm and zeta potential + 18 mV (n = 3, error bar represents SD) (*P < 0.05, **P < 0.01; one-way ANOVA).

polydispersity index (PDI) of < 0.2 and EF-TEM images (Fig. 5.1C). A well-defined spherical morphologies and no aggregation, in comparison to PEI25k/siRNA was observed under electron microscope to demonstrate their robustness.

The osmolarity of PMGT/siRNA complexes though less than pure PMGT, tend to increase with the increase in its concentration (Table 2.1) reflecting its tendency to induce hyperosmotic stress on the cells.

The lower surface charge and non-aggregation of the PMGT complexes with siRNA does not intend to disrupt the integrity of the cell membrane surface [180, 181] which results in higher cell viability of PMGT/siRNA complexes (> 95%) in comparison to PEI25k/siRNA (~70%) complexes (Fig. 5.2C) in A549 cells. In addition, the presence of degradable ester linkages in PMGT backbone (Fig. 2.1) ensured a gradual disappearance of PMGT after 3 h, 2, 3, 5, and 7 days of transfection (Fig. 5.2A) by hydrolyzing into smaller degradation products that can be exocytosed [177]. Therefore, the occurrence of vesicles was observed to increase with time (maximum on day 5). This further increases the cell viability of PMGT complexes (Fig. 5.2B) and makes it innocuous for cellular uptake. The gene silencing efficiency of vectors was analyzed by suppressing transgenic GFP expression in

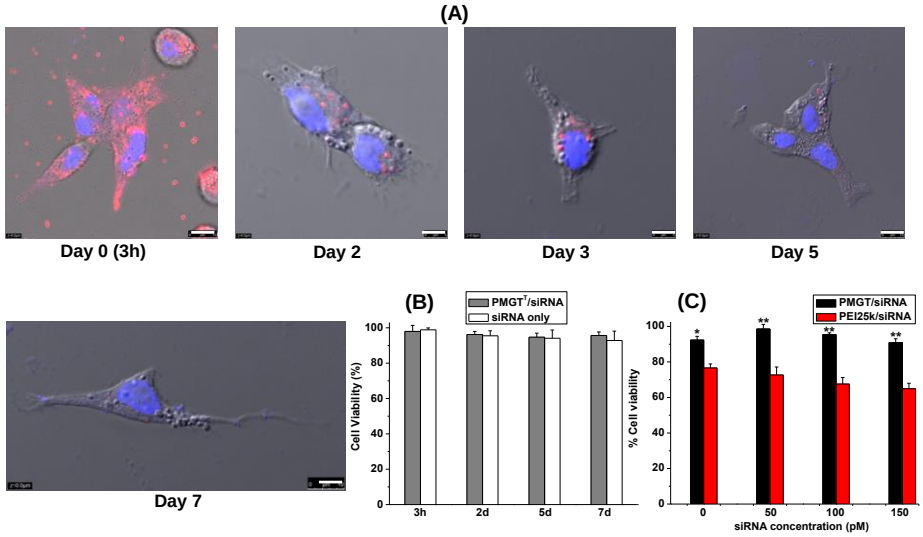

Fig. 5.2 Degradation and cell viability study. (A) Study of $PMGT^T$/siRNA nanoplex uptake and degradation in A549 cells. Confocal microscopic images of A549 cells with DAPI nuclear staining (blue), observed up to 7 days following transfection with TRITC-labeled $PMGT^T$ (red). $PMGT^T$ after cellular uptake (3 h) is gradually degraded up to day 7 (scale bar: 10 μm), and the occurrence of vesicular structures represents the increased exocytosis of fragmented $PMGT^T$. (B) Cytotoxicity measurements of $PMGT^T$/siRNA (N/P 20) complexes by MTT assay after 3 h, 2d, 5d, and 7d of transfection in A549 cells show no cytotoxic effects. (C) Cytotoxicity of PMGT/siRNA complexes at various siRNA concentrations (0, 50, 100, 150 pM) show no cytotoxicity. ($n = 3$, error bar represents SD) (*$P < 0.05$; **$P < 0.01$, one-way ANOVA).

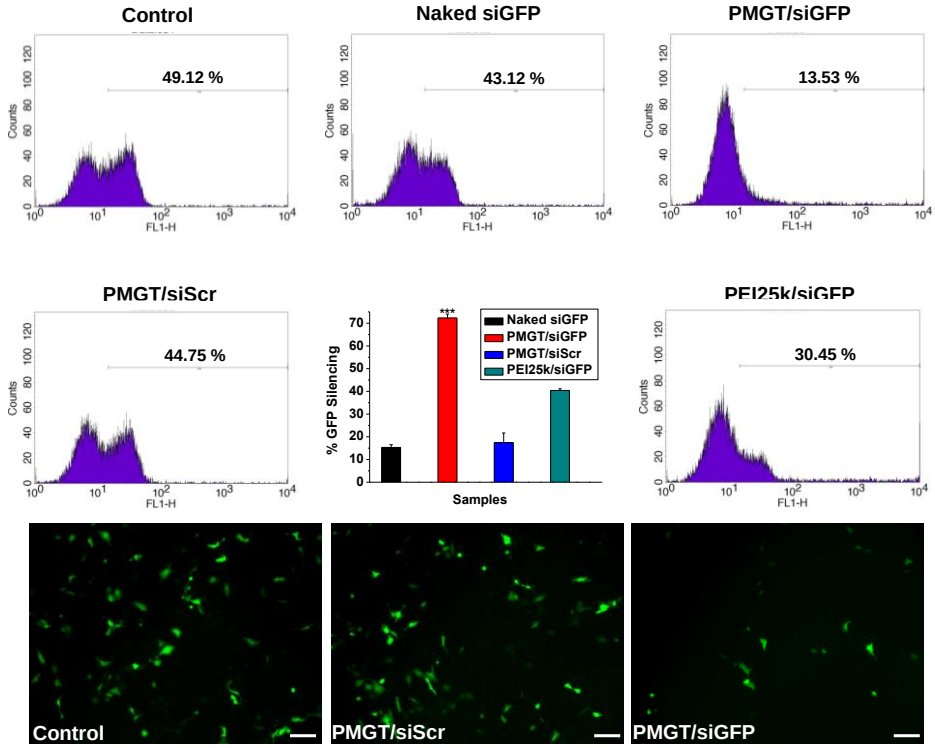

Fig. 5.3 GFP silencing efficiency of PMGT/siRNA complexes in A549 cells. The pre-transfected GFP gene was silenced using siGFP (100 pM) complexed with PMGT (N/P 20), and transgene expression was measured using FACS. The percentage GFP silencing was calculated in reference to the control cells without siGFP treatment, and the maximum silencing was found to be mediated by PMGT (70%). (n = 3, error bar represents SD) (***$P < 0.001$, one-way ANOVA). Corresponding transfection images were taken with a Nikon fluorescence microscope (scale bar: 500 μm) to show maximum GFP suppression by PMGT mediated siGFP delivery.

A549 cells. PMGT/siGFP exhibited 72% GFP silencing in comparison to 40% by PEI25k/siGFP and negligible by naked siGFP and complexes with non-specific scrambled siRNA (siScr) (Fig. 5.3).

PMGT efficiently delivers siRNA to silence JNK2 expression

JNK2 suppression by PMGT/siJNK2 was observed in A549 cells up to 48 h post-transfection using quantitative real time (Q)-PCR which showed a remarkable suppression of JNK2 (~90%) in comparison to PEI25k/siJNK2 (57%) (Fig. 5.4B), indicating an enhanced gene silencing efficiency. Further, western blot showed that PMGT mediated delivery of siJNK2 resulted in ~45% knockdown of JNK2 protein expression, which was higher than that obtained by PEI25k/siJNK2 (~23%) polyplexes in reference to the control after 48 h (Fig. 5.4A). Immunocytochemical analysis also showed the suppressed gene expression of JNK2 by PMGT/siJNK2 treatment (Fig. 5.4C). The crucial result is the increased gene silencing efficiency of PMGT over PEI25k, which is indicative of the involvement of hyperosmoticity in internalization of the polyplex.

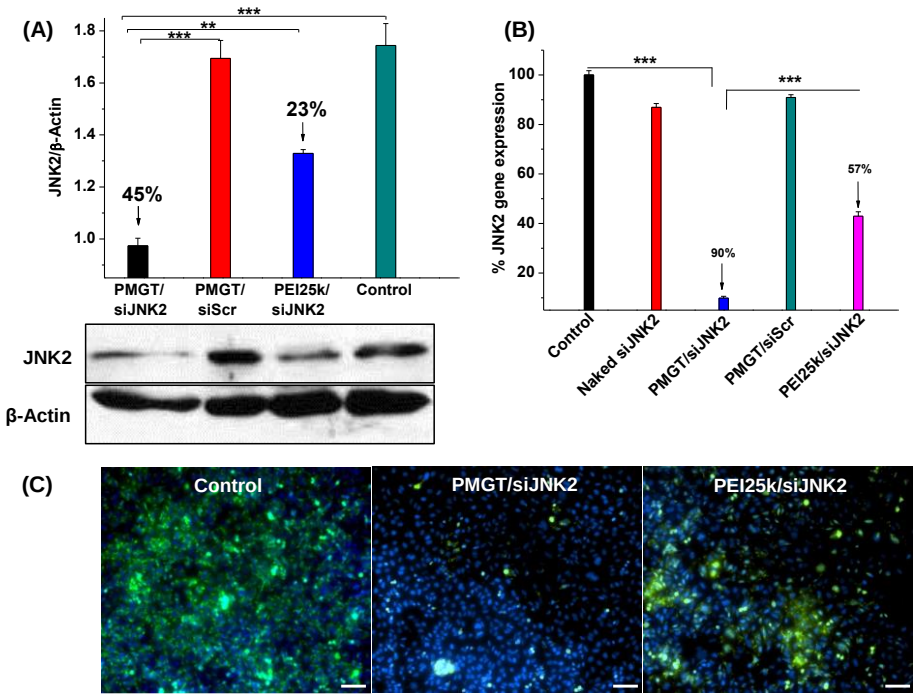

Fig. 5.4 JNK2 gene silencing efficiency of PMGT/siJNK2 complexes. (A) Western blot analysis of JNK2 protein from the lysate of transfected A549 cells after 48 h showing no change in β-actin protein expression and a significant decrease in JNK2 protein expression in cells treated with PMGT/siJNK2 complexes in contrast to other treated controls. Densitometric analysis of the JNK2 protein band in reference to the untreated control cells (100% JNK2 expression) shows a 45% decrease in JNK2 expression in PMGT/siJNK2 treated cells. Data are shown as the mean ± SD of 3 independent experiments (**P < 0.01; ***P < 0.001, one-way ANOVA). (B) JNK2 gene expression monitored

at 48 h post-transfection in A549 cells using quantitative real-time PCR (Q-PCR). Maximum JNK2 suppression (~90%) was observed by PMGT/siJNK2 complexes. Data are expressed as the mean ± SEM of 3 experiments. Statistical significance was determined using one-way ANOVA (***P < 0.001). (C) Immunocytochemical analysis shows least JNK2 expression (red) in PMGT-treated A549 cells in comparison to PEI25k-treated and control cells after 48 h of transfection (scale bar: 500 μm).

Knockdown of JNK2 expression resulted in increased apoptotic events

To determine the cause of the decline in growth of PMGT/siJNK2-treated cell populations, we first examined the effect on cell DNA synthesis. We observed no differences in ethynyl deoxyuridine (EdU) incorporation relative to the number of viable cells among any of the treatment groups (data not shown); therefore, the reduction in growth of PMGT/siJNK2-treated cells could not be explained by an inhibition of DNA replication.

Cells treated with PMGT/siJNK2 revealed features consistent with apoptosis, including cell rounding, membrane blebbing, and detachment from the tissue culture dish. Loss of nuclear disintegration is the characteristic feature of apoptotic cells [182, 183].Therefore, enumeration of apoptosis in the treated cancer cells was done using colorimetric TUNEL assay, where the ends of the apoptosis-induced DNA strand breaks were labeled and detected as dark brown stained nuclei. The results showed higher DNA fragmentation (dark brown) in PMGT/siJNK2 treated cells than the cells treated with PEI25k/siJNK2 and the controls (Fig. 5.5).

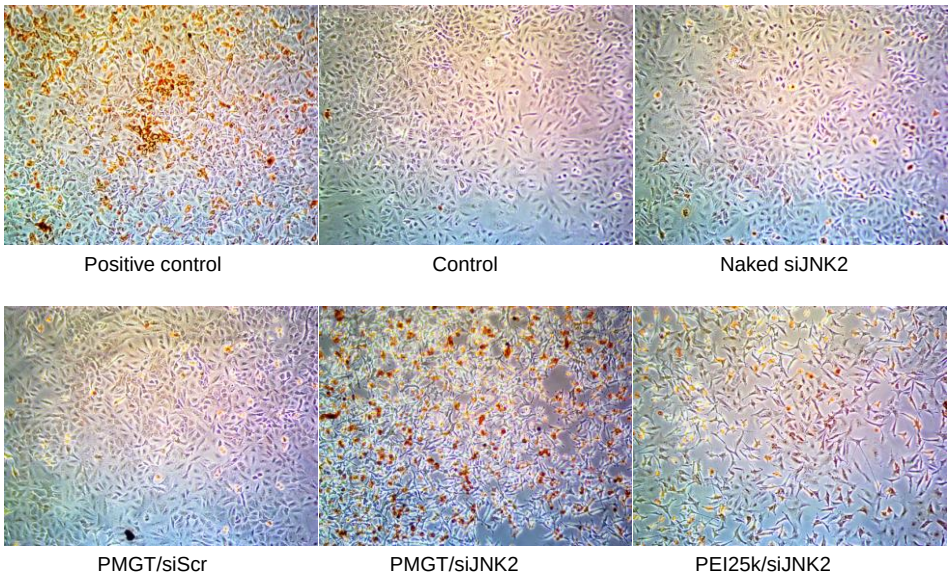

Fig. 5.5 Effect of JNK2 knockdown on the behavior of A549 cells. TUNEL assay in A549 cells for the comparison of apoptotic events in the various treatment groups shows the maximum apoptosis induction in the PMGT-mediated siJNK2 delivery; apoptosis is represented by brown stained nuclei (scale bar: 500 μm).

Induction of caspase-9

Overexpression of caspase-9 and its activation is known to induce apoptosis [184]. The PMGT/siJNK2 transfected A549 cells showed enhanced expression of apoptosis-related caspase-9 in comparison to the other control cells (Fig. 5.6) to suggest its contribution towards apoptotic cells death.

COX-2 stimulation

COX-2 ELISA reports that PMGT instigated increased COX-2 expression compared to PEI25k due to hyperosmotic effect of hydroxyl groups (Fig. 5.7A). PEI's toxicity to the cell membrane might have induced a weak COX-2 expression as an inflammatory response after 1 h of transfection but later remained constant. However, PMGT complexes constantly induced the increased expression of COX-2 with time. The western blot of COX-2 after 3 h of transfection also shows increased COX-2 expression in PMGT/siJNK2 treated cells (Fig. 5.7B). These results suggest accelerated internalization to be encouraged by release of osmoprotectant COX-2.

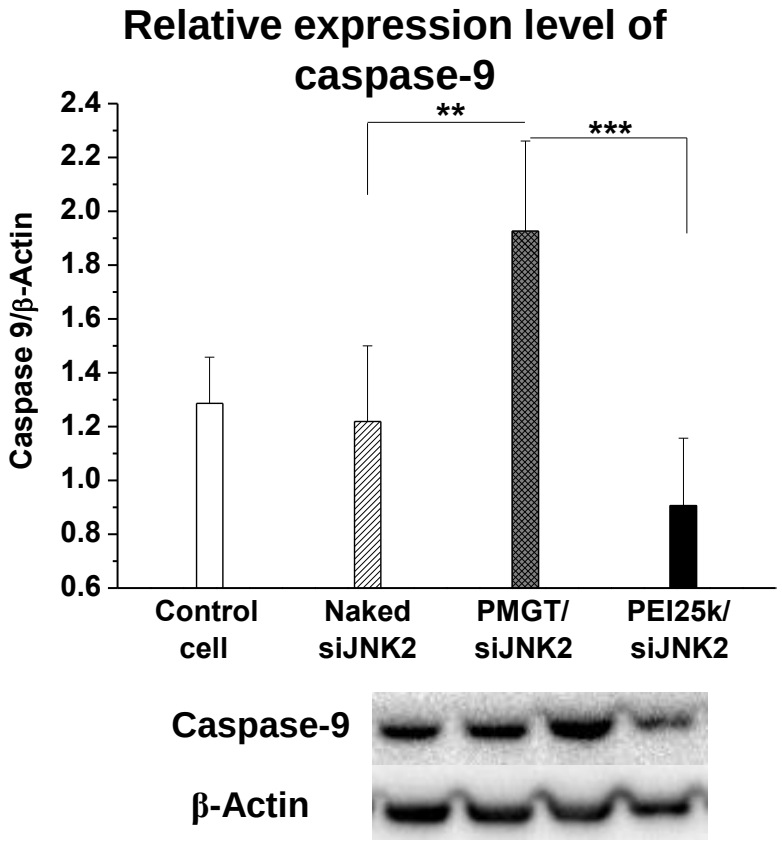

Fig. 5.6 Western blot analysis of caspase-9 protein from the lysate of transfected A549 cells after 3 h showing no change in β-actin protein expression and a significant increase in caspase-9 protein expression in cells treated with PMGT/siJNK2 complexes in contrast to other treated controls. Data are shown as the mean ± SD of 3 independent experiments (**P < 0.01; ***P < 0.001, one-way ANOVA).

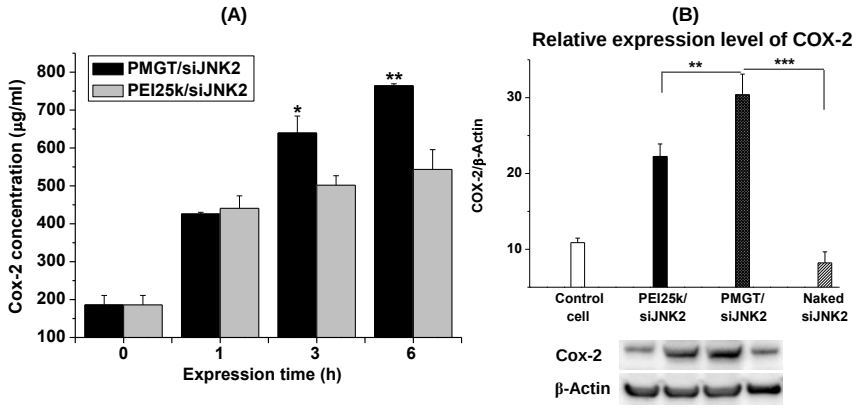

Fig. 5.7 Mechanistic investigations for enhanced transfection of PMGT. (A) COX-2 ELISA assay estimating protein expression at different time intervals (1 h, 3 h, 6 h) induced by PMGT (N/P 20) and PEI25k (N/P 10) polyplexes. (B) Western blot analysis of COX-2 protein from the lysate of transfected A549 cells after 3 h showing no change in β-actin protein expression and a significant increase in COX-2 protein expression in cells treated with PMGT/siJNK2 complexes in contrast to other treated controls. Data are shown as the mean ± SD of 3 independent experiments (error bar represents SD) (**$p < 0.01$; ***$p < 0.001$, one-way ANOVA).

Induction of caveolin-1

The western blot results of protein lysates after 3 h of transfection revealed that the extracellular hyperosmotic environment induced by PMGT/siJNK2 complexes led to the upregulation of caveolin-1 expression (Fig. 5.8). The upregulation of caveolin-1 leads to the cellular uptake by caveolae-mediated endocytosis and therefore higher suppression of JNK2 was observed in transfected cells.

Colocalization of COX-2 and caveolin-1

The up-regulation of caveolin-1 suggests internalization of PMGT/siJNK2 complexes primarily through caveolae-mediated endocytosis. In addition, elegant early findings reveal that under hypertonic conditions, osmotic equilibrium is regained by an intracellular accumulation of organic osmolytes via COX-2 induction [113]. Therefore, the confocal images show colocalization of COX-2 (green) with caveolin-1 (red) after 120 min of transfection with PMGT/siJNK2 complexes (Fig. 5.9), suggesting the role of osmotic effect of polymannitol in PMGT in increasing the rate of caveolae-mediated endocytosis by COX-2 induction for intracellular accumulation of PMGT complexes to restore osmotic equilibrium.

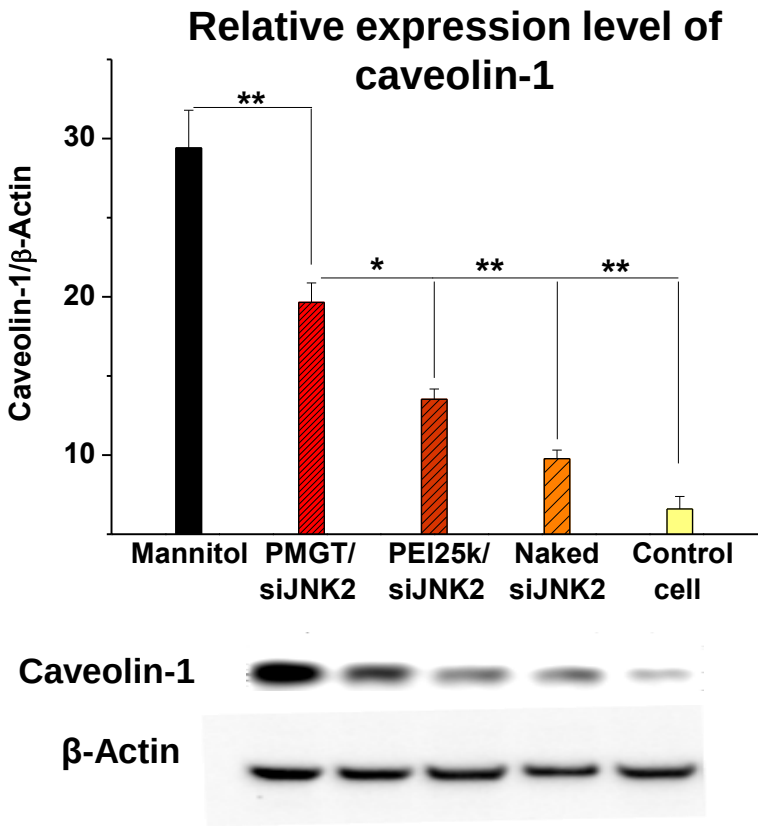

Fig. 5.8 Western blot analysis of caveolin-1 protein from the lysate of transfected A549 cells after 3 h showing no change in β-actin protein expression and a significant increase in caveolin-1 protein expression in cells treated with PMGT/siJNK2 complexes in contrast to other treated controls. Data are shown as the mean ± SD of 3 independent experiments (error bar represents SD) (*$p < 0.05$, **$p < 0.01$; one-way ANOVA).

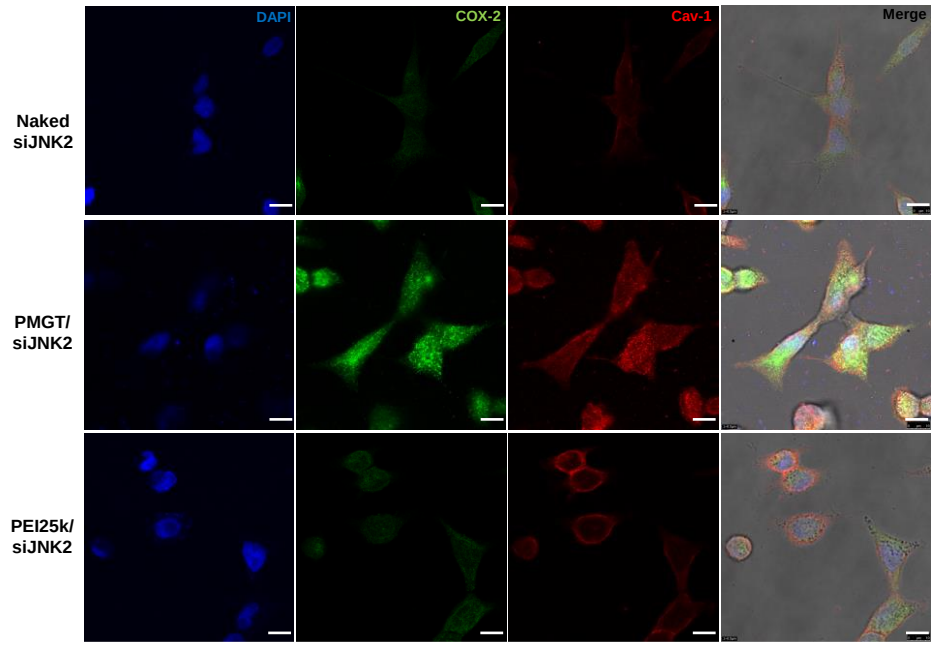

Fig. 5.9 Co-localization study of caveolin-1 (Cav-1) (red) with COX-2 (green) in post-transfected A549 cells, showed maximum co-localization with PMGT/siJNK2 treated cells in contrast to the control suggesting COX-2 stimulation and induction of caveolae-mediated endocytosis upon hyperosmotic stress by PMGT (scale bar: 10 μm).

In contrast, naked siJNK2 and PEI25k/siJNK2 complexes not only showed less colocalized proteins, but also resulted in lower induction of COX-2 and caveolin-1 proteins (less intense fluorescence).

PMGT-mediated knockdown of JNK2 retarded tumor growth in xenograft mice

Instead of systemic, local administration of siRNA avoids the obstacles of low bioavailability, systemic toxicity, rapid excretion and inefficient targeting [185].

Therefore, the subcutaneous tumor (~1000 mm^3) bearing xenograft mice were treated with the local administration of PMGT/siJNK2 after every 48 h until 1 month. A decrease in JNK2 expression in PMGT treated group (56%) (Fig. 5.10) demonstrated tumor growth inhibition, in contrast to the PEI25k (20% decrease) treated cells where they failed to suppress JNK2 expression, certainly due to their lower gene transport efficiency. Immunohistochemical analysis also showed decreased brown staining of the JNK2 protein throughout the tumor section of PMGT/siJNK2-treated group (Fig. 5.11). The effect of JNK2 suppression in PMGT/siJNK2-treated tumor is also seen as the presence of apoptotic cells in tumor section (Fig. 5.12) which suggests

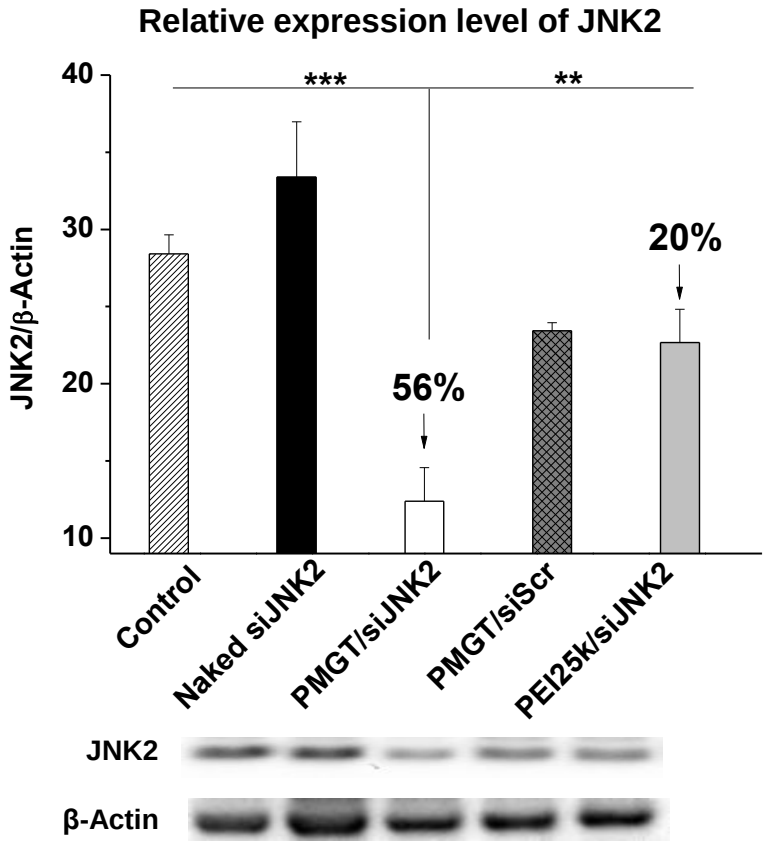

Fig. 5.10 Effect of JNK2 silencing on tumor growth and proliferation in xenograft mice (n = 4). Western blot analysis of the tumor mass after 1 month of treatment shows suppressed JNK2 expression in PMGT-mediated treated tumor. Data are shown as the mean ± SD of 3 independent experiments (**P < 0.01; ***P < 0.001, one-way ANOVA).

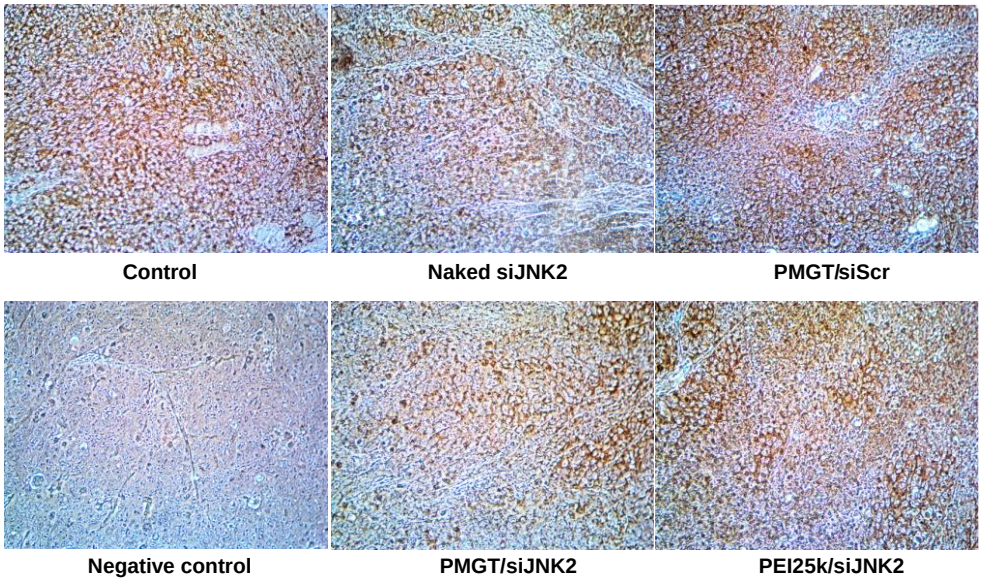

Fig. 5.11 Immunohistochemistry of the formalin fixed tumor sections (scale bar: 500 μm) show decreased staining in PMGT treated tumor section, suggesting suppression of JNk2 gene expression.

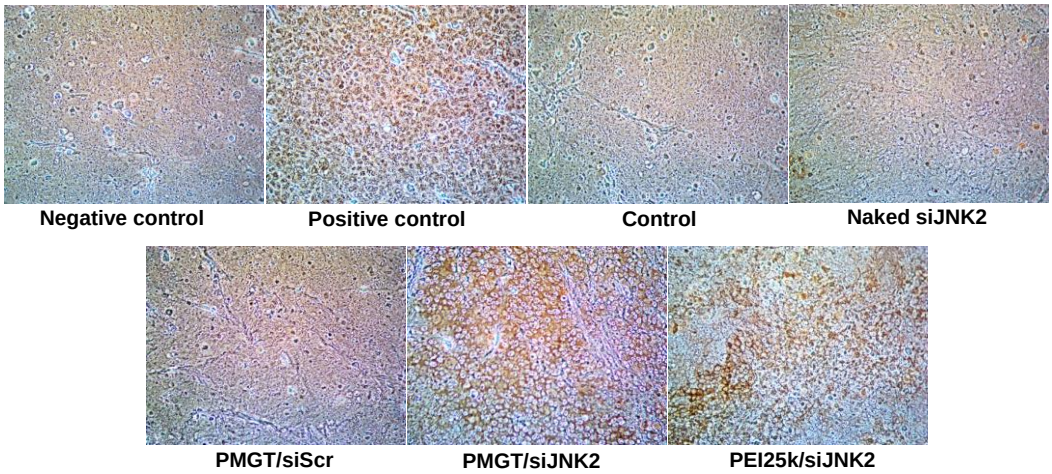

Fig. 5.12 *In vivo* TUNEL assay of formalin fixed tumor sections show a high level of apoptotic events occurring in PMGT/siJNK2 treated tumors in xenograft mice (n = 4) (scale bar: 500 μm).

the significance of JNK2 inactivation in treating cancer and applicability of hyperosmotic vector in enhancing siJNK2 delivery.

5.4 Discussion

Our findings show that, the inherent hyperosmotic property of gene transporter can modify and accelerate the cellular uptake process by initiating cell signaling events resulting in enhancement of transfection efficiency in cancer cells. This mechanism was thereafter utilized to achieve JNK2 silencing as a potential therapeutic measure for treatment of cancer. Using polymannitol, modified into a polymer, PMGT, we sought that polymannitol could trail the gene transporter to osmotic stress induced intracellular route. PMGT complexes with siRNA form particles with size <200 nm which predominantly contribute to the trouble free cellular uptake [186]. The polymannitol backbone in PMGT played a crucial role in maintaining a stable zeta potential with increasing N/P ratios due to the formation of inter-molecular hydrogen bonds. Despite the lower surface charge, the high transfection and silencing activity of PMGT is its most striking feature.

JNKs are group of kinase proteins that are involved in the activation of c-Jun transcription factors which is required in the cell cycle from the

G1 to S phase [168, 171, 172]. On oncogenic transformation, c-Jun remains constantly activated primarily by JNK2 leading to tumorigenesis [175]. Therefore, therapeutic manipulation of JNK2 raised exciting opportunities as well as challenges in the path of cancer gene therapy. Inhibition of c-Jun activation due to JNK2 knockdown by enhanced delivery of JNK2 siRNA via PMGT is anticipated to retard tumor growth. A pictorial representation of the PMGT mediated JNK2 silencing, illustrated in Fig. 5.13, articulates the cellular machinery involved in inhibiting tumor growth and progression.

The JNK2 silencing consequently results in apoptotic cancer cell death (Fig. 5.5). The obtained *in vivo* results illustrate that the inactivation of JNK2 in situ can bring about substantial decrease in JNK2 expression of the cancer cells. We may infer that antagonizing JNK2 function radically inhibits tumor growth and that this effect is enhanced by delivery with hyperosmotic PMGT compared to other non-hyperosmotic vectors.

The mechanism of PMGT mediated JNK2 silencing was demonstrated to occur via COX-2 induced caveolae-mediated endocytosis. The cumulative results of COX-2 ELISA, caveoin-1 induction and colocalization of COX-2 and caveolin-1 suggest the pivotal role of

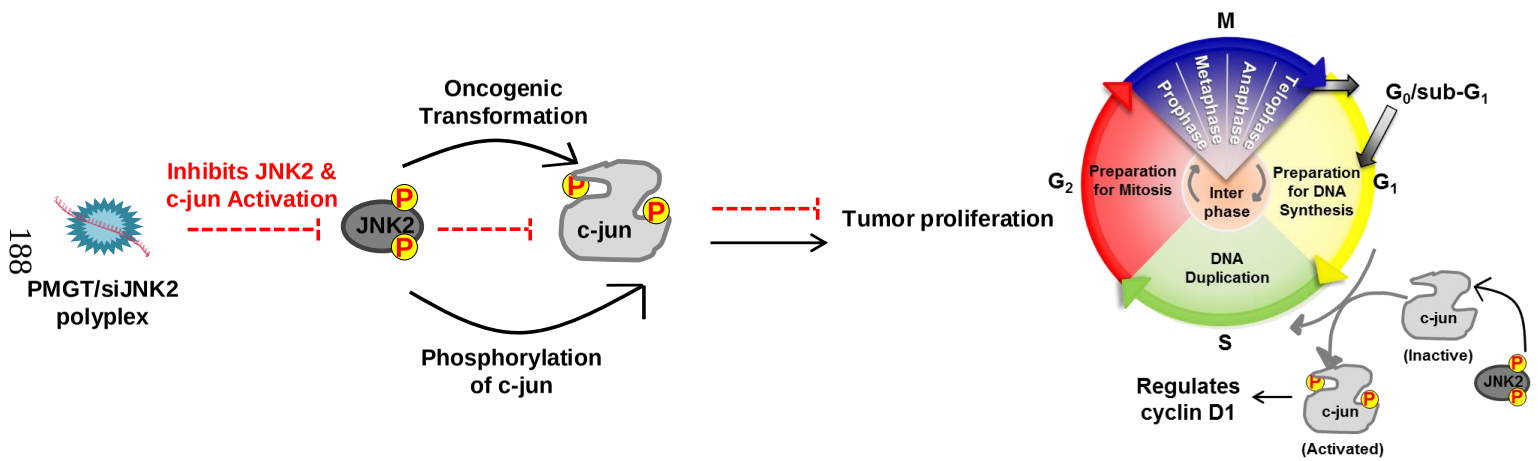

Fig. 5.13 Diagrammatic representation of the proposed mechanism of PMGT mediated JNK2

PMGT induced hyperosmotic stress in selectively increasing the cellular uptake of complexes by triggering caveolae endocytic route in order to restore homeostasis. Caveolae are cholesterol rich pits involved in endocytosis, transcytosis, and numerous signal transduction pathways. Caveolae is formed by the oligomerization and association of caveolin proteins with cholesterol rich lipid raft domains. Transmission of signal from extracellular to intracellular compartment has been proposed to be the primary function of caveolae [187]. Therefore, the extracellular hyperosmotic environment created by PMGT induces caveolae formation for cellular uptake mediated by the co-localized COX-2. COX–2 expression is induced as an inflammatory response to regain equilibrium across the cell membrane which leads to fast cellular uptake of hyperosmotic polymer via caveolae mediated endocytosis resulting in enhanced silencing efficiency.

5.5 Conclusion

In conclusion, polymannitol based gene transporter avails the hyperosmotic properties of mannitol as an integral part of the vector for enhanced and fast nucleic acid delivery. The polymannitol backbone in PMGT via its hydroxyl groups corresponds to better DNA complexation ability and polyplex stability with particle size of 150 nm

desirable for cellular uptake. The ester linkage between PEI and MDM corresponds to degradability of PMGT and hence lower cytotoxicity in comparison to 25kD bPEI. Accelerated uptake of polyplexes due to the hyperosmotic property of polymannitol leading to increased transfection efficiency was demonstrated by confocal studies. Moreover, mechanistic investigation showed COX-2 driven accelerated uptake of polyplexes via caveolae mediated endocytosis as a response to extracellular osmotic changes. Co-localization of COX-2 in the caveolar pits gave a plausible explanation for association of COX-2 and caveolae in rapid internalization of polyplexes. Silencing JNK2 function in cancer cells *in vitro* and in xenograft mice showed detrimental effect on tumor growth with subsequent onset of apoptosis. These results demonstrated and envision the potential application of PMGT in developing a profound gene and drug delivery system.

CHAPTER 6

Summary

The effectivity of competent gene delivery vectors can only be evaluated if in addition to modulating its cellular uptake, it is equally capable of penetrating through the compact tissues (biological barriers) to reach the target cells. The greatest impediment in gene therapy is to target the vector to the exact site of action for which it needs to cross various extracellular and intracellular barriers. Nanotherapeutics promises to provide a common platform for combining various therapeutic characteristics into a single vector. In this research study, the hyperosmotic behavior due to the insertion of alcohol groups in vector backbone was utilized to enhance the transfection activity of the vector. It was also observed that increasing the number of monomeric –OH groups elevate the hyperosmotic tendency of the polymeric gene transporter to several folds and subsequently enhance transfection capability. Polymannitol- (PMGT) and polydixylitol-based (PdXYP) vectors were thoroughly studied for their capability in crossing the blood-brain-barrier (BBB) using *in vitro* BBB model and compact mass of tumor cells in xenograft mice. The four free –OH groups of

monomeric mannitol dimethacrylate (MDM) in PMGT backbone is responsible for its hyperosmoticity. And, the six free –OH groups of dixylitol diacrylate (dXdA) monomer in PdXYP polymer backbone elevates its hyperosmotic activity even further in comparison to that of PMGT. MDM and dXdA monomers were reacted with non-toxic LMW bPEI (1.2 kDa) by Michael addition reaction to synthesize their respective polymers (PMGT and PdXYP) with inherent hyperosmotic properties. The backbone of the hyperosmotic polymeric vectors through their hydroxyl groups corresponds to better complexation with therapeutic nucleic acids (of ~100 nm size) and polyplex stability by forming inter-molecular hydrogen bonds. This inter-molecular hydrogen bonding shields the polyplex surface from non-specific interactions with the blood serum proteins which facilitates its quick penetration through compact tissues into the target cells. The endosomal escape of the polyplexes is ensured by their high buffering tendency via proton sponge effect. Moreover, the polymers do not threat cytotoxicity due the presence of degradable ester linkages between the LMW bPEI (1.2 kDa) and monomers.

The tight junctions of BBB or compact tumor mass are impermeable to most of the competent therapeutic drugs and preclude pharmacotherapy.

However, the hyperosmotic vectors facilitate in crossing these barriers due to the increased blood plasma osmolality resulting in an enhanced flow of water from tissues and loosening the tissue compactness.

The probable mechanism for osmolality induced uptake of vectors was also investigated and the up-regulation of an osmoprotectant, cyclooxygenase-2 (COX-2) was found to be the key regulator to enforce the caveolae-mediated vector entry into the cells. The polyplexes generate an extracellular hyperosmotic environment. In order to restore the osmotic equilibrium across the cell membrane, the osmoprotectant molecule COX-2 is induced. COX-2 further stimulates caveolin-1 proteins which associate with the membrane lipid rafts to endocytose the polyplexes. This is how the hyperosmotic polyplexes gain safe entry into the cells and consequently transgene expression is enhanced.

This study demonstrates that the use of hyperosmotic vectors owing to flexibility in their synthesis and capabilities promises their varied potential applications in treating brain related disorders by penetrating through the BBB, or in cancer gene therapy, or in the field of regenerative medicine.

LIST OF PUBLICATIONS

1. Hyperosmotic polydixylitol for crossing blood brain barrier and efficient nucleic acid delivery. P. Garg*, S. Pandey*, Seonwoo Hoon, Seungmin Yeom, Choung Yun-Hoon, Cho Chong-Su, Choung Pill-Hoon and Chung Jong Hoon. Chem Comm 2015.

2. Nucleotide biosynthesis arrest by silencing SHMT1 function via vitamin B6-coupled vector and effects on tumor growth inhibition. S Pandey*, P Garg*, Somin Lee, Yun-Hoon Choung, Pill-Hoon Choung, and Jong Hoon Chung. Biomaterials vol. 35, 9332-9342, 2014.

3. Highly efficient gene transfection by hyperosmotic polymannitol based gene tranporter through regulation of caveolae and COX-2 induced endocytosis. P Garg, S Pandey, B Kang, J Kim, K T Lim, M H Cho, T-E Park, Y J Choi, P H Choung, C S Cho and J H Chung, J. Mater. Chem. B, **2**, 2666-2679 2014.

4. The efficiency of membrane transport of vitamin B_6 coupled to Poly(ester amine) gene transporter and transfection in cancer cells. S Pandey*, P Garg*, KT Lim, J Kim, YH Choung, YJ Choi, PH

Choung, CS Cho and JH Chung. Biomaterials. Vol. 34, pp. 3746-3728. 2013.

5. Synergistic Effects of Nanotopography and Co-Culture with Endothelial Cells on Osteogenesis of Mesenchymal Stem Cells. J Kim, HN Kim, KT Lim, Y Kim, S Pandey, P Garg, YH Choung, PH Choung, KY Suh and JH Chung. Biomaterials. Vol. 34, pp. 7257-7268, 2013.

6. Triphenylamine coupled chitosan with high buffering capacity and low viscosity for enhanced transfection in mammalian cells *in vitro* and *in vivo*. P Garg*, S Kumar*, S Pandey, H Seonwoo, PH Choung, J Koh and JH Chung. J. Mater. Chem. B., Vol. 1, 6053-6065, 2013.

7. Molecular responses in osteogenic differentiation of mesenchymal stem cells induced by physical stimulation. A togloom, K T Lim, J H Kim, H Seonwoo, P Garg, P H Choung, C S Cho, Y H Choung and J H Chung. Tissue eng. and reg. Medicine, Vol. 8, No. 3, pp 271-281, 2011.

NOTE: *equal contributions

REFERENCES

[1] Yin H, Kanasty RL, Eltoukhy AA, Vegas AJ, Dorkin JR, Anderson DG. Non-viral vectors for gene-based therapy. Nat Rev Genet. 2014;15:541-55.

[2] Kay MA. State-of-the-art gene-based therapies: the road ahead. Nat Rev Genet. 2011;12:316-28.

[3] Mingozzi F, High KA. Therapeutic in vivo gene transfer for genetic disease using AAV: progress and challenges. Nat Rev Genet. 2011;12:341-55.

[4] Dr. Christopher Baum OK, Ute Modlich, Zhixiong Li, and Boris Fehse. Mutagenesis and oncogenesis by chromosomal insertion of gene transfer vectors. Human Gene Therapy. 2006;17:253-63.

[5] Bessis N, GarciaCozar FJ, Boissier MC. Immune responses to gene therapy vectors: influence on vector function and effector mechanisms. Gene Ther. 0000;11:S10-S7.

[6] Waehler R, Russell SJ, Curiel DT. Engineering targeted viral vectors for gene therapy. Nat Rev Genet. 2007;8:573-87.

[7] Thomas CE, Ehrhardt A, Kay MA. Progress and problems with the use of viral vectors for gene therapy. Nat Rev Genet. 2003;4:346-58.

[8] Marshall E. Gene therapy death prompts review of adenovirus vector. Science. 1999;286:2244-5.

[9] Kohn DB, Sadelain M, Glorioso JC. Occurrence of leukaemia following gene therapy of X-linked SCID. Nat Rev Cancer. 2003;3:477-88.

[10] Alexis F, Pridgen E, Molnar LK, Farokhzad OC. Factors affecting the clearance and biodistribution of polymeric nanoparticles. Molecular Pharmaceutics. 2008;5:505-15.

[11] Kim SW. Polylysine copolymers for gene delivery. Cold Spring Harbor Protocols. 2012;2012:pdb.ip068619.

[12] Bazile D, Prud'homme C, Bassoullet M-T, Marlard M, Spenlehauer G, Veillard M. Stealth Me.PEG-PLA nanoparticles avoid uptake by the mononuclear phagocytes system. Journal of Pharmaceutical Sciences. 1995;84:493-8.

[13] Boussif O, Lezoualc'h F, Zanta MA, Mergny MD, Scherman D, Demeneix B, et al. A versatile vector for gene and oligonucleotide

transfer into cells in culture and in vivo: polyethylenimine. Proceedings of the National Academy of Sciences. 1995;92:7297-301.

[14] Lungwitz U, Breunig M, Blunk T, Göpferich A. Polyethylenimine-based non-viral gene delivery systems. European Journal of Pharmaceutics and Biopharmaceutics. 2005;60:247-66.

[15] Wightman L, Kircheis R, Rössler V, Carotta S, Ruzicka R, Kursa M, et al. Different behavior of branched and linear polyethylenimine for gene delivery in vitro and in vivo. The Journal of Gene Medicine. 2001;3:362-72.

[16] Lv H, Zhang S, Wang B, Cui S, Yan J. Toxicity of cationic lipids and cationic polymers in gene delivery. Journal of Controlled Release. 2006;114:100-9.

[17] Petersen H, Fechner PM, Martin AL, Kunath K, Stolnik S, Roberts CJ, et al. Polyethylenimine-graft-poly(ethylene glycol) copolymers: Influence of copolymer block structure on DNA complexation and biological activities as gene delivery system. Bioconjugate Chemistry. 2002;13:845-54.

[18] Breunig M, Lungwitz U, Liebl R, Goepferich A. Breaking up the correlation between efficacy and toxicity for nonviral gene delivery. Proceedings of the National Academy of Sciences. 2007;104:14454-9.

[19] Thomas M, Klibanov AM. Enhancing polyethylenimine's delivery of plasmid DNA into mammalian cells. Proceedings of the National Academy of Sciences. 2002;99:14640-5.

[20] Wasungu L, Hoekstra D. Cationic lipids, lipoplexes and intracellular delivery of genes. Journal of Controlled Release. 2006;116:255-64.

[21] Funhoff AM, van Nostrum CF, Lok MC, Kruijtzer JAW, Crommelin DJA, Hennink WE. Cationic polymethacrylates with covalently linked membrane destabilizing peptides as gene delivery vectors. Journal of Controlled Release. 2005;101:233-46.

[22] Pouton CW, Lucas P, Thomas BJ, Uduehi AN, Milroy DA, Moss SH. Polycation-DNA complexes for gene delivery: a comparison of the biopharmaceutical properties of cationic polypeptides and cationic lipids. Journal of Controlled Release. 1998;53:289-99.

[23] Fayazpour F, Lucas B, Alvarez-Lorenzo C, Sanders NN, Demeester J, De Smedt SC. Physicochemical and transfection properties of cationic hydroxyethylcellulose/DNA nanoparticles. Biomacromolecules. 2006;7:2856-62.

[24] Garg P, Kumar S, Pandey S, Seonwoo H, Choung P-H, Koh J, et al. Triphenylamine coupled chitosan with high buffering capacity and low viscosity for enhanced transfection in mammalian cells, in vitro and in vivo. Journal of Materials Chemistry B. 2013;1:6053-65.

[25] Carrillo C, Suñé JM, Pérez-Lozano P, García-Montoya E, Sarrate R, Fàbregas A, et al. Chitosan nanoparticles as non-viral gene delivery systems: Determination of loading efficiency. Biomedicine & Pharmacotherapy. 2014;68:775-83.

[26] Martirosyan A, Olesen MJ, Howard KA. Chapter eleven - Chitosan-based nanoparticles for mucosal delivery of RNAi therapeutics. In: Leaf Huang DL, Ernst W, editors. Advances in Genetics: Academic Press; 2014. p. 325-52.

[27] Choi JS, Nam K, Park J-y, Kim J-B, Lee J-K, Park J-s. Enhanced transfection efficiency of PAMAM dendrimer by surface modification with l-arginine. Journal of Controlled Release. 2004;99:445-56.

[28] Pack DW, Hoffman AS, Pun S, Stayton PS. Design and development of polymers for gene delivery. Nat Rev Drug Discov. 2005;4:581-93.

[29] Park TG, Jeong JH, Kim SW. Current status of polymeric gene delivery systems. Advanced Drug Delivery Reviews. 2006;58:467-86.

[30] Mastrobattista E, Hennink WE. Polymers for gene delivery: Charged for success. Nat Mater. 2012;11:10-2.

[31] Pannier AK, Shea LD. Controlled release systems for DNA delivery. Mol Ther. 2004;10:19-26.

[32] Jones CH, Chen C-K, Ravikrishnan A, Rane S, Pfeifer BA. Overcoming nonviral gene delivery barriers: Perspective and future. Molecular Pharmaceutics. 2013;10:4082-98.

[33] Allen MH, Green MD, Getaneh HK, Miller KM, Long TE. Tailoring charge density and hydrogen bonding of imidazolium copolymers for efficient gene delivery. Biomacromolecules. 2011;12:2243-50.

[34] Al-Dosari M, Gao X. Nonviral gene delivery: Principle, limitations, and recent progress. AAPS J. 2009;11:671-81.

[35] Zhang Y, Satterlee A, Huang L. In vivo gene delivery by nonviral vectors: Overcoming hurdles. Mol Ther. 2012;20:1298-304.

[36] Rehman Zu, Zuhorn IS, Hoekstra D. How cationic lipids transfer nucleic acids into cells and across cellular membranes: Recent advances. Journal of Controlled Release. 2013;166:46-56.

[37] F Sakurai TN, H Saito, T Baba, A Okuda, O Matsumoto, T Taga, F Yamashita, Y Takakura and M Hashida. Interaction between DNA-cationic liposome complexes and erythrocytes is an important factor in systemic gene transfer via the intravenous route in mice: the role of the neutral helper lipid. Gene Therapy. 2001;8:677-86.

[38] McCray PB, Wang G, Kline JN, Zabner J, Chada S, Jolly DJ, et al. Alveolar macrophages inhibit retrovirus-mediated gene transfer to airway epithelia. Human Gene Therapy. 1997;8:1087-93.

[39] Yasuda K, Ogawa Y, Yamane I, Nishikawa M, Takakura Y. Macrophage activation by a DNA/cationic liposome complex requires endosomal acidification and TLR9-dependent and -independent pathways. Journal of Leukocyte Biology. 2005;77:71-9.

[40] Wolff JA, Rozema DB. Breaking the bonds: Non-viral vectors become chemically dynamic. Mol Ther. 2007;16:8-15.

[41] Paul B. McCray J, Guoshun Wang, Joel N. Kline, Joseph Zabner, Sunil Chada, Doug J. Jolly, Steven M. W. Chang, and Beverly L. Davidson. Alveolar macrophages inhibit retrovirus-mediated gene transfer to airway epithelia. Human Gene Therapy. 1997;8:1087-93.

[42] de Boer AG, PJ G. Drug targeting to the brain. Annual Review of Pharmacology and Toxicology. 2007;47:323-55.

[43] Shimamura M S, N MR. Experimental and clinical application of plasmid DNA in the field of central nervous diseases. Current Gene Therapy. 2011;11:491-500.

[44] Felgner PL, Tsai YJ, Sukhu L, Wheeler CJ, Manthorpe M, Marshall J, et al. Improved cationic lipid formulations for in vivo gene therapy. Annals of the New York Academy of Sciences. 1995;772:126-39.

[45] Matsui H, Johnson LG, Randell SH, Boucher RC. Loss of binding and entry of liposome-DNA complexes decreases transfection

efficiency in differentiated airway epithelial cells. Journal of Biological Chemistry. 1997;272:1117-26.

[46] Zuhorn IS, Kalicharan R, Hoekstra D. Lipoplex-mediated transfection of mammalian cells occurs through the cholesterol-dependent clathrin-mediated pathway of endocytosis. Journal of Biological Chemistry. 2002;277:18021-8.

[47] El-Sayed A, Harashima H. Endocytosis of gene delivery vectors: From clathrin-dependent to lipid raft-mediated endocytosis. Mol Ther. 2013;21:1118-30.

[48] Hillaireau H, Couvreur P. Nanocarriers' entry into the cell: relevance to drug delivery. Cell Mol Life Sci. 2009;66:2873-96.

[49] Gilleron J, Querbes W, Zeigerer A, Borodovsky A, Marsico G, Schubert U, et al. Image-based analysis of lipid nanoparticle-mediated siRNA delivery, intracellular trafficking and endosomal escape. Nat Biotech. 2013;31:638-46.

[50] Poteryaev D, Datta S, Ackema K, Zerial M, Spang A. Identification of the switch in early-to-late endosome transition. Cell. 2010;141:497-508.

[51] Akinc A, Thomas M, Klibanov AM, Langer R. Exploring polyethylenimine-mediated DNA transfection and the proton sponge hypothesis. The Journal of Gene Medicine. 2005;7:657-63.

[52] Dominska M, Dykxhoorn DM. Breaking down the barriers: siRNA delivery and endosome escape. Journal of Cell Science. 2010;123:1183-9.

[53] Funhoff AM, van Nostrum CF, Koning GA, Schuurmans-Nieuwenbroek NME, Crommelin DJA, Hennink WE. Endosomal escape of polymeric gene delivery complexes is not always enhanced by polymers buffering at low pH. Biomacromolecules. 2003;5:32-9.

[54] Rehman Zu, Hoekstra D, Zuhorn IS. Mechanism of polyplex- and lipoplex-mediated delivery of nucleic acids: Real-time visualization of transient membrane destabilization without endosomal lysis. ACS Nano. 2013;7:3767-77.

[55] Graessmann M, Menne J, Liebler M, Graeber I, Graessmann A. Helper activity for gene expression, a novel function of the SV40 enhancer. Nucleic Acids Research. 1989;17:6603-12.

[56] Capecchi MR. High efficiency transformation by direct microinjection of DNA into cultured mammalian cells. Cell. 1980;22:479-88.

[57] Pollard H, Remy J-S, Loussouarn G, Demolombe S, Behr J-P, Escande D. Polyethylenimine but not cationic lipids promotes transgene delivery to the nucleus in mammalian cells. Journal of Biological Chemistry. 1998;273:7507-11.

[58] A Fasbender JZ, B G Zeiher and M J Welsh. A low rate of cell proliferation and reduced DNA uptake limit cationic lipid-mediated gene transfer to primary cultures of ciliated human airway epithelia. Gene Therapy. 1997;4:1173-80.

[59] Dominic J. Glover LG, Hans J. Lipps, David A. Jans. Overcoming barriers to achieve safe, sustained and efficient non-viral gene therapy. Advances in Gene, Molecular and Cell Therapy. 2007;1:126-40.

[60] Polderman KH, van de Kraats G, Dixon JM, Vandertop WP, Girbes ARJ. Increases in spinal fluid osmolarity induced by mannitol. Critical Care Medicine.2003;31:584-9010.1097/01.CCM.0000050287.68977.84.

[61] Doran SE, Ren XD, Betz AL, Pagel MA, Neuwelt EA, Roessler BJ, et al. Gene expression from recombinant viral vectors in the central nervous system after blood-brain barrier disruption. Neurosurgery. 1995;36:965-70.

[62] Ibrahim BM, Park S, Han B, Yeo Y. A strategy to deliver genes to cystic fibrosis lungs: A battle with environment. Journal of Controlled Release. 2011;155:289-95.

[63] Islam MA, Yun C-H, Choi Y-J, Shin J-Y, Arote R, Jiang H-L, et al. Accelerated gene transfer through a polysorbitol-based transporter mechanism. Biomaterials. 2011;32:9908-24.

[64] Garg P, Pandey S, Kang B, Lim K-T, Kim J, Cho M-H, et al. Highly efficient gene transfection by a hyperosmotic polymannitol based gene tranporter through regulation of caveolae and COX-2 induced endocytosis. Journal of Materials Chemistry B. 2014.

[65] Lee W-S, Kim Y-K, Zhang Q, Park T-E, Kang S-K, Kim D-W, et al. Polyxylitol-based gene carrier improves the efficiency of gene transfer through enhanced endosomal osmolysis. Nanomedicine: Nanotechnology, Biology and Medicine. 2014;10:525-34.

[66] Moffatt S, Wiehle S, Cristiano RJ. A multifunctional PEI-based cationic polyplex for enhanced systemic p53-mediated gene therapy. Gene Ther. 2006;13:1512-23.

[67] Lee H, Jeong JH, Park TG. PEG grafted polylysine with fusogenic peptide for gene delivery: high transfection efficiency with low cytotoxicity. Journal of Controlled Release. 2002;79:283-91.

[68] Ogris M, Walker G, Blessing T, Kircheis R, Wolschek M, Wagner E. Tumor-targeted gene therapy: strategies for the preparation of ligand–polyethylene glycol–polyethylenimine/DNA complexes. Journal of Controlled Release. 2003;91:173-81.

[69] Kakudo T, Chaki S, Futaki S, Nakase I, Akaji K, Kawakami T, et al. Transferrin-modified liposomes equipped with a pH-sensitive fusogenic peptide: An artificial viral-like delivery system. Biochemistry. 2004;43:5618-28.

[70] Pandey S, Garg P, Lim KT, Kim J, Choung Y-H, Choi Y-J, et al. The efficiency of membrane transport of vitamin B6 coupled to poly(ester amine) gene transporter and transfection in cancer cells. Biomaterials. 2013;34:3716-28.

[71] Pandey S, Garg P, Lee S, Choung H-W, Choung Y-H, Choung P-H, et al. Nucleotide biosynthesis arrest by silencing SHMT1 function via vitamin B6-coupled vector and effects on tumor growth inhibition. Biomaterials. 2014;35:9332-42.

[72] Maitani YHaY. Folate-linked lipid-based nanoparticle for targeted gene delivery. Current Drug Delivery. 2005;2:243-52.

[73] Caplan M, Rosca E. Targeting drugs to combinations of receptors: A modeling analysis of potential specificity. Ann Biomed Eng. 2005;33:1113-24.

[74] Zhang Y, Zhang Y-f, Bryant J, Charles A, Boado RJ, Pardridge WM. Intravenous RNA interference gene therapy targeting the human epidermal growth factor receptor prolongs survival in intracranial brain cancer. Clinical Cancer Research. 2004;10:3667-77.

[75] Pinyon JL, Tadros SF, Froud KE, Y. Wong AC, Tompson IT, Crawford EN, et al. Close-field electroporation gene delivery using the cochlear implant electrode array enhances the bionic ear. Science Translational Medicine. 2014;6:233ra54.

[76] Gehl J. Electroporation: theory and methods, perspectives for drug delivery, gene therapy and research. Acta Physiologica Scandinavica. 2003;177:437-47.

[77] MacQueen LA, Buschmann MD, Wertheimer MR. Gene delivery by electroporation after dielectrophoretic positioning of cells in a non-uniform electric field. Bioelectrochemistry. 2008;72:141-8.

[78] Hernot S, Klibanov AL. Microbubbles in ultrasound-triggered drug and gene delivery. Advanced Drug Delivery Reviews. 2008;60:1153-66.

[79] Mayer CR, Geis NA, Katus HA, Bekeredjian R. Ultrasound targeted microbubble destruction for drug and gene delivery. Expert Opinion on Drug Delivery. 2008;5:1121-38.

[80] Nishiyama N, Iriyama A, Jang W-D, Miyata K, Itaka K, Inoue Y, et al. Light-induced gene transfer from packaged DNA enveloped in a dendrimeric photosensitizer. Nat Mater. 2005;4:934-41.

[81] Sonawane ND, Szoka FC, Verkman AS. Chloride accumulation and swelling in endosomes enhances DNA transfer by polyamine-DNA polyplexes. Journal of Biological Chemistry. 2003;278:44826-31.

[82] Ziady A-G, Ferkol T, Dawson DV, Perlmutter DH, Davis PB. Chain length of the polylysine in receptor-targeted gene transfer complexes affects duration of reporter gene expression both in vitro and in vivo. Journal of Biological Chemistry. 1999;274:4908-16.

[83] Roth CM, Sundaram S. Engineering synthetic vectors for improved DNA delivery: Insights from intracellular pathways. Annual Review of Biomedical Engineering. 2004;6:397-426.

[84] Ward CM, Read ML, Seymour LW. Systemic circulation of poly(l-lysine)/DNA vectors is influenced by polycation molecular weight and type of DNA: differential circulation in mice and rats and the implications for human gene therapy2001.

[85] Sebestyen MG, Ludtke JJ, Bassik MC, Zhang G, Budker V, Lukhtanov EA, et al. DNA vector chemistry: The covalent attachment of signal peptides to plasmid DNA. Nat Biotech. 1998;16:80-5.

[86] Choi Y, Jeon Y-H, Kang J-H, Chung J-K, Schmidt M, Kim, et al. MIDGE/hNIS vaccination generates antigen-associated CD8+IFN-γ+ T cells and enhances protective antitumor immunity. International Journal of Cancer. 2007;120:1942-50.

[87] Carriere M, Escriou V, Savarin A, Scherman D. Coupling of importin beta binding peptide on plasmid DNA: transfection efficiency is increased by modification of lipoplex's physico-chemical properties. BMC Biotechnology. 2003;3:14.

[88] Ferrari M. Cancer nanotechnology: opportunities and challenges. Nat Rev Cancer. 2005;5:161-71.

[89] Ruge CA, Kirch J, Lehr C-M. Pulmonary drug delivery: from generating aerosols to overcoming biological barriers—therapeutic possibilities and technological challenges. The Lancet Respiratory Medicine. 2013;1:402-13.

[90] Xu L, Anchordoquy T. Drug delivery trends in clinical trials and translational medicine: Challenges and opportunities in the delivery of nucleic acid-based therapeutics. Journal of Pharmaceutical Sciences. 2011;100:38-52.

[91] Vasir JK, Reddy MK, Labhasetwar VD. Nanosystems in drug targeting: Opportunities and challenges. Current Nanoscience. 2005;1:47-64.

[92] Pouton CW, Seymour LW. Key issues in non-viral gene delivery. Advanced Drug Delivery Reviews. 2001;46:187-203.

[93] Wong SY, Pelet JM, Putnam D. Polymer systems for gene delivery—Past, present, and future. Progress in Polymer Science. 2007;32:799-837.

[94] Pardridge WM. Blood–brain barrier delivery of protein and non-viral gene therapeutics with molecular trojan horses. Journal of Controlled Release. 2007;122:345-8.

[95] Langer R, Tirrell DA. Designing materials for biology and medicine. Nature. 2004;428:487-92.

[96] Morille M, Passirani C, Vonarbourg A, Clavreul A, Benoit J-P. Progress in developing cationic vectors for non-viral systemic gene therapy against cancer. Biomaterials. 2008;29:3477-96.

[97] Merdan T, Kopeček J, Kissel T. Prospects for cationic polymers in gene and oligonucleotide therapy against cancer. Advanced Drug Delivery Reviews. 2002;54:715-58.

[98] Ruponen M, Honkakoski P, Rönkkö S, Pelkonen J, Tammi M, Urtti A. Extracellular and intracellular barriers in non-viral gene delivery. Journal of Controlled Release. 2003;93:213-7.

[99] Kogure K, Akita H, Yamada Y, Harashima H. Multifunctional envelope-type nano device (MEND) as a non-viral gene delivery system. Advanced Drug Delivery Reviews. 2008;60:559-71.

[100] Koren E, Torchilin VP. Cell-penetrating peptides: breaking through to the other side. Trends in Molecular Medicine. 2012;18:385-93.

[101] Margus H, Padari K, Pooga M. Cell-penetrating peptides as versatile vehicles for oligonucleotide delivery. Mol Ther. 2012;20:525-33.

[102] Bae YH, Park K. Targeted drug delivery to tumors: Myths, reality and possibility. Journal of Controlled Release. 2011;153:198-205.

[103] Park T-E, Kang B, Kim Y-K, Zhang Q, Lee W-S, Islam MA, et al. Selective stimulation of caveolae-mediated endocytosis by an osmotic polymannitol-based gene transporter. Biomaterials. 2012;33:7272-81.

[104] Luu Q-P, Shin J-Y, Kim Y-K, Islam MA, Kang S-K, Cho M-H, et al. High gene transfer by the osmotic polysorbitol-mediated transporter through the selective caveolae endocytic pathway. Molecular Pharmaceutics. 2012;9:2206-18.

[105] Gurtovenko AA, Anwar J. Modulating the structure and properties of cell membranes: The molecular mechanism of action of dimethyl sulfoxide. The Journal of Physical Chemistry B. 2007;111:10453-60.

[106] Teo PY, Yang C, Hedrick JL, Engler AC, Coady DJ, Ghaem-Maghami S, et al. Hydrophobic modification of low molecular weight polyethylenimine for improved gene transfection. Biomaterials. 2013;34:7971-9.

[107] Mather BD, Viswanathan K, Miller KM, Long TE. Michael addition reactions in macromolecular design for emerging technologies. Progress in Polymer Science. 2006;31:487-531.

[108] Escriou V, Ciolina C, Lacroix F, Byk G, Scherman D, Wils P. Cationic lipid-mediated gene transfer: effect of serum on cellular uptake and intracellular fate of lipopolyamine/DNA complexes.

Biochimica et Biophysica Acta (BBA)-Biomembranes. 1998;1368:276-88.

[109] Rudolph C, Schillinger U, Ortiz A, Plank C, Golas MM, Sander B, et al. Aerosolized nanogram quantities of plasmid DNA mediate highly efficient gene delivery to mouse airway epithelium. Mol Ther. 2005;12:493-501.

[110] Begley DJ. Delivery of therapeutic agents to the central nervous system: the problems and the possibilities. Pharmacology & Therapeutics. 2004;104:29-45.

[111] Mastakov MY, Baer K, Xu R, Fitzsimons H, During MJ. Combined injection of rAAV with mannitol enhances gene expression in the rat brain. Mol Ther. 2001;3:225-32.

[112] Arote RB, Lee E-S, Jiang H-L, Kim Y-K, Choi Y-J, Cho M-H, et al. Efficient gene delivery with osmotically active and hyperbranched poly(ester amine)s. Bioconjugate Chemistry. 2009;20:2231-41.

[113] Moeckel GW, Zhang L, Fogo AB, Hao C-M, Pozzi A, Breyer MD. COX2 activity promotes organic osmolyte accumulation and adaptation

of renal medullary interstitial cells to hypertonic stress. Journal of Biological Chemistry. 2003;278:19352-7.

[114] Apodaca G. Modulation of membrane traffic by mechanical stimuli. American Journal of Physiology - Renal Physiology. 2002;282:F179-F90.

[115] Pelkmans L, Fava E, Grabner H, Hannus M, Habermann B, Krausz E, et al. Genome-wide analysis of human kinases in clathrin- and caveolae/raft-mediated endocytosis. Nature. 2005;436:78-86.

[116] Rejman J, Bragonzi A, Conese M. Role of clathrin- and caveolae-mediated endocytosis in gene transfer mediated by lipo- and polyplexes. Mol Ther. 2005;12:468-74.

[117] Aa MAEM, Huth US, Häfele SY, Schubert R, Oosting RS, Mastrobattista E, et al. Cellular uptake of cationic polymer-DNA complexes via caveolae plays a pivotal role in gene transfection in COS-7 cells. Pharmaceutical Research. 2007;24:1590-8.

[118] Liou J-Y, Deng W-G, Gilroy DW, Shyue S-K, Wu KK. Colocalization and interaction of cyclooxygenase-2 with caveolin-1 in

human fibroblasts. Journal of Biological Chemistry. 2001;276:34975-82.

[119] Lim W, Jung J, Surh Y, Inoue H, Lee Y. Hypertonic sodium choloride and mannitol induces COX-2 via different signaling pathways in mouse cortical collecting duct M-1 cells. Life Sciences. 2007;80:2085-92.

[120] Gupta RA, DuBois RN. Colorectal cancer prevention and treatment by inhibition of cyclooxygenase-2. Nat Rev Cancer. 2001;1:11-21.

[121] Yang T, Huang Y, Heasley LE, Berl T, Schnermann JB, Briggs JP. MAPK mediation of hypertonicity-stimulated cyclooxygenase-2 expression in renal medullary collecting duct cells. Journal of Biological Chemistry. 2000;275:23281-6.

[122] Zhao H, Tian W, Tai C, Cohen DM. Hypertonic induction of COX-2 expression in renal medullary epithelial cells requires transactivation of the EGFR. American Journal of Physiology - Renal Physiology. 2003;285:F281-F8.

[123] Favale NO, Casali CI, Lepera LG, Pescio LG, Fernández-Tome MC. Hypertonic induction of COX2 expression requires TonEBP/NFAT5 in renal epithelial cells. Biochemical and Biophysical Research Communications. 2009;381:301-5.

[124] Hao C-M, Redha R, Morrow J, Breyer MD. Peroxisome proliferator-activated receptor δ activation promotes cell survival following hypertonic stress. Journal of Biological Chemistry. 2002;277:21341-5.

[125] Chen J, Zhao M, Rao R, Inoue H, Hao C-M. C/EBPβ and its binding element are required for NFκB-induced COX2 expression following hypertonic stress. Journal of Biological Chemistry. 2005;280:16354-9.

[126] Deli M, Á brahám C, Kataoka Y, Niwa M. Permeability studies on In vitro blood–brain barrier models: Physiology, pathology, and pharmacology. Cell Mol Neurobiol. 2005;25:59-127.

[127] Bonoiu AC, Mahajan SD, Ding H, Roy I, Yong K-T, Kumar R, et al. Nanotechnology approach for drug addiction therapy: Gene silencing using delivery of gold nanorod-siRNA nanoplex in

dopaminergic neurons. Proceedings of the National Academy of Sciences. 2009.

[128] Mossop B, Barr R, Henshaw J, Zaharoff D, Yuan F. Electric fields in tumors exposed to external voltage sources: Implication for electric field-mediated drug and gene delivery. Ann Biomed Eng. 2006;34:1564-72.

[129] Henshaw J, Mossop B, F. Y. Enhancement of electric field-mediated gene delivery through pretreatment of tumors with a hyperosmotic mannitol solution. Cancer Gene Therapy.2011:26-33.

[130] Liang B, He M-L, Chan C-y, Chen Y-c, Li X-P, Li Y, et al. The use of folate-PEG-grafted-hybranched-PEI nonviral vector for the inhibition of glioma growth in the rat. Biomaterials. 2009;30:4014-20.

[131] NSC MJA. Nanostructured biomaterials for overcoming biological barriers. 2012.

[132] Louboutin J-P, Chekmasova AA, Marusich E, Chowdhury JR, Strayer DS. Efficient CNS gene delivery by intravenous injection. Nat Meth. 2010/11//print;7.

[133] Zhang X, Lili Zhao JW, Hong Dong FX, Gong G, Hu Y. Current advances in vehicles for brain gene delivery. Current Gene Therapy. 2012;12: 423-36 (14).

[134] Pérez-Martínez F, Guerra J, Posadas I, Ceña V. Barriers to non-viral vector-mediated gene delivery in the nervous system. Pharm Res. 2011;28:1843-58.

[135] Burger C, Gorbatyuk OS, Velardo MJ, Peden CS, Williams P, Zolotukhin S, et al. Recombinant AAV viral vectors pseudotyped with viral capsids from serotypes 1, 2, and 5 display differential efficiency and cell tropism after delivery to different regions of the central nervous system. Mol Ther. 2004/08//print;10:302-17.

[136] MJ A, P C. Chapter 1 Historical view of the design and development of nanocarriers for overcoming biological barriers. nanostructured biomaterials for overcoming biological barriers: The Royal Society of Chemistry. 2012;3-36.

[137] Carty N, Lee D, Dickey C, Ceballos-Diaz C, Jansen-West K, Golde TE, et al. Convection-enhanced delivery and systemic mannitol increase gene product distribution of AAV vectors 5, 8, and 9 and

increase gene product in the adult mouse brain. Journal of Neuroscience Methods. 2010;194:144-53.

[138] Mastakov MY, Baer K, Xu R, Fitzsimons H, During MJ. Combined injection of rAAV with mannitol enhances gene expression in the rat brain. Mol Ther. 2001/02/print;3.

[139] Ikeda M, Nagashima T, Bhattacharjee AK, Kondoh T, Kohmura E, Tamaki N. Quantitative analysis of hyperosmotic and hypothermic blood-brain barrier opening. In: Kuroiwa T, Baethmann A, Czernicki Z, Hoff JT, Ito U, Katayama Y, et al., editors. Brain Edema XII: Springer Vienna; 2003. p. 559-63.

[140] Liu Y, Reineke TM. Hydroxyl stereochemistry and amine number within poly(glycoamidoamine)s affect intracellular DNA delivery. Journal of the American Chemical Society. 2005;127:3004-15.

[141] Hann RM, Ness AT, Hudson CS. Diacetone xylitol (2,3,4,5-Di-isopropylidene-D,L-xylitol). Journal of the American Chemical Society. 1944;66:73-6.

[142] Sólyom S, Szilágyi K, Toldy L. Neue synthese der corticosteron-seitenkette. Liebigs Annalen der Chemie. 1987;1987:153-60.

[143] Akiyama H, Tanaka A, Hiramatsu H, Nagasawa Ji, Tamaoki N. Reflection colour changes in cholesteric liquid crystals after the addition and photochemical isomerization of mesogenic azobenzenes tethered to sugar alcohols. Journal of Materials Chemistry. 2009;19:5956-63.

[144] Luo D, Saltzman WM. Synthetic DNA delivery systems. Nat Biotech. 2000;18:33-7.

[145] Glover DJ, Lipps HJ, Jans DA. Towards safe, non-viral therapeutic gene expression in humans. Nat Rev Genet. 2005;6:299-310.

[146] Kim J, Hwang I, Britain D, Chung TD, Sun Y, Kim D-H. Microfluidic approaches for gene delivery and gene therapy. Lab on a Chip. 2011;11:3941-8.

[147] Kim T-H, Jiang H-L, Jere D, Park I-K, Cho M-H, Nah J-W, et al. Chemical modification of chitosan as a gene carrier in vitro and in vivo. Progress in Polymer Science. 2007;32:726-53.

[148] O'Rorke S, Keeney M, Pandit A. Non-viral polyplexes: Scaffold mediated delivery for gene therapy. Progress in Polymer Science. 2010;35:441-58.

[149] Kong HJ, Liu J, Riddle K, Matsumoto T, Leach K, Mooney DJ. Non-viral gene delivery regulated by stiffness of cell adhesion substrates. Nat Mater. 2005;4:460-4.

[150] Chu C, Kong H. Interplay of cell adhesion matrix stiffness and cell type for non-viral gene delivery. Acta Biomaterialia. 2012;8:2612-9.

[151] Kong HJ, Hsiong S, Mooney DJ. Nanoscale cell adhesion ligand presentation regulates nonviral gene delivery and expression. Nano Letters. 2006;7:161-6.

[152] Dhaliwal A, Maldonado M, Han Z, Segura T. Differential uptake of DNA–poly(ethylenimine) polyplexes in cells cultured on collagen and fibronectin surfaces. Acta Biomaterialia. 2010;6:3436-47.

[153] Adler AF, Speidel AT, Christoforou N, Kolind K, Foss M, Leong KW. High-throughput screening of microscale pitted substrate topographies for enhanced nonviral transfection efficiency in primary human fibroblasts. Biomaterials. 2011;32:3611-9.

[154] Teo BKK, Goh S-H, Kustandi TS, Loh WW, Low HY, Yim EKF. The effect of micro and nanotopography on endocytosis in drug and gene delivery systems. Biomaterials. 2011;32:9866-75.

[155] Giannoudis PV, Dinopoulos H, Tsiridis E. Bone substitutes: An update. Injury. 2005;36:S20-S7.

[156] Kim HN, Jiao A, Hwang NS, Kim MS, Kang DH, Kim D-H, et al. Nanotopography-guided tissue engineering and regenerative medicine. Advanced Drug Delivery Reviews. 2013;65:536-58.

[157] McMahon RE, Wang L, Skoracki R, Mathur AB. Development of nanomaterials for bone repair and regeneration. Journal of Biomedical Materials Research Part B: Applied Biomaterials. 2013;101B:387-97.

[158] Ma J, van den Beucken JJJP, Yang F, Both SK, Cui F-Z, Pan J, et al. Coculture of osteoblasts and endothelial cells: Optimization of culture medium and cell ratio. Tissue Engineering Part C: Methods. 2010;17:349-57.

[159] Xue Y, Xing Z, Hellem S, Arvidson K, Mustafa K. Endothelial cells influence the osteogenic potential of bone marrow stromal cells. BioMedical Engineering OnLine. 2009;8:34.

[160] Suh K-Y, Park MC, Kim P. Capillary force lithography: A versatile tool for structured biomaterials interface towards cell and tissue engineering. Advanced Functional Materials. 2009;19:2699-712.

[161] Kim D-H, Seo C-H, Han K, Kwon KW, Levchenko A, Suh K-Y. Cell migration: guided cell migration on microtextured substrates with variable local density and anisotropy. Advanced Functional Materials. 2009;19:n/a-n/a.

[162] Kim J, Kim HN, Lim K-T, Kim Y, Seonwoo H, Park SH, et al. Designing nanotopographical density of extracellular matrix for controlled morphology and function of human mesenchymal stem cells. Sci Rep. 2013;3.

[163] Kim J, Kim HN, Lim K-T, Kim Y, Pandey S, Garg P, et al. Synergistic effects of nanotopography and co-culture with endothelial cells on osteogenesis of mesenchymal stem cells. Biomaterials. 2013;34:7257-68.

[164] Solanki A, Shah S, Yin PT, Lee K-B. Nanotopography-mediated reverse uptake for siRNA delivery into neural stem cells to enhance neuronal differentiation. Sci Rep. 2013;3.

[165] Shah S, Solanki A, Sasmal PK, Lee K-B. Single vehicular delivery of siRNA and small molecules to control stem cell differentiation. Journal of the American Chemical Society. 2013;135:15682-5.

[166] Masters TA, Pontes B, Viasnoff V, Li Y, Gauthier NC. Plasma membrane tension orchestrates membrane trafficking, cytoskeletal remodeling, and biochemical signaling during phagocytosis. Proceedings of the National Academy of Sciences. 2013;110:11875-80.

[167] Farokhzad OC, Langer R. Nanomedicine: Developing smarter therapeutic and diagnostic modalities. Advanced Drug Delivery Reviews. 2006;58:1456-9.

[168] Vleugel MM, Greijer AE, Bos R, van der Wall E, van Diest PJ. c-Jun activation is associated with proliferation and angiogenesis in invasive breast cancer. Human Pathology. 2006;37:668-74.

[169] Wisdom R, Johnson RS, Moore C. c-Jun regulates cell cycle progression and apoptosis by distinct mechanisms. EMBO J. 1999;18:188-97.

[170] Schreiber M, Kolbus A, Piu F, Szabowski A, Möhle-Steinlein U, Tian J, et al. Control of cell cycle progression by c-Jun is p53 dependent. Genes & Development. 1999;13:607-19.

[171] Axel Behrens, Wolfram Jochum, Maria Sibilia, Wagner EF. Oncogenic transformation by ras and fos is mediated by c-Jun N-terminal phosphorylation. Oncogene. 2000;19:2657-63.

[172] Ip YT, Davis RJ. Signal transduction by the c-Jun N-terminal kinase (JNK) — from inflammation to development. Current Opinion in Cell Biology. 1998;10:205-19.

[173] Bode AM, Dong Z. The functional contrariety of JNK. Molecular Carcinogenesis. 2007;46:591-8.

[174] Dong Z, Birrer MJ, Watts RG, Matrisian LM, Colburn NH. Blocking of tumor promoter-induced AP-1 activity inhibits induced transformation in JB6 mouse epidermal cells. Proceedings of the National Academy of Sciences. 1994;91:609-13.

[175] Jaeschke A, Karasarides M, Ventura J-J, Ehrhardt A, Zhang C, Flavell RA, et al. JNK2 is a positive regulator of the cJun transcription factor. Molecular Cell. 2006;23:899-911.

[176] Bost F, McKay R, Bost M, Potapova O, Dean NM, Mercola D. The Jun kinase 2 isoform is preferentially required for epidermal growth factor-induced transformation of human A549 lung carcinoma cells. Molecular and Cellular Biology. 1999;19:1938-49.

[177] Garg P, Pandey S, Kang B, Lim KT, Kim J, Cho MH, et al. Highly efficient gene transfection by a Hyperosmotic polymannitol based gene tranporter through regulation of caveolae and COX-2 induced endocytosis. Journal of Materials Chemistry B. 2014;2:2666-79.

[178] Anderson DG, Akinc A, Hossain N, Langer R. Structure/property studies of polymeric gene delivery using a library of poly([beta]-amino esters). Mol Ther. 2005;11:426-34.

[179] Ma M, Li F, Yuan Z-f, Zhuo R-x. Influence of hydroxyl groups on the biological properties of cationic polymethacrylates as gene vectors. Acta Biomaterialia. 2010;6:2658-65.

[180] Lim Y-b, Kim S-m, Suh H, Park J-s. Biodegradable, endosome disruptive, and cationic network-type polymer as a highly efficient and nontoxic gene delivery carrier. Bioconjugate Chemistry. 2002;13:952-7.

[181] Arote RB, Hwang S-K, Yoo M-K, Jere D, Jiang H-L, Kim Y-K, et al. Biodegradable poly(ester amine) based on glycerol dimethacrylate and polyethylenimine as a gene carrier. The Journal of Gene Medicine. 2008;10:1223-35.

[182] Duvall E, Wyllie AH. Death and the cell. Immunology Today. 1986;7:115-9.

[183] Wyllie AH, Kerr JFR, Currie AR. Cell Death: The significance of apoptosis. In: G.H. Bourne JFD, Jeon KW, editors. International Review of Cytology: Academic Press; 1980. p. 251-306.

[184] Druškovič M, Šuput D, Milisav I. Overexpression of caspase-9 triggers its activation and apoptosis in vitro. Croatian medical journal. 2006;47:832-40.

[185] Durcan N, Murphy C, Cryan S-A. Inhalable siRNA: Potential as a therapeutic agent in the lungs. Molecular Pharmaceutics. 2008;5:559-66.

[186] Prabha S, Zhou W-Z, Panyam J, Labhasetwar V. Size-dependency of nanoparticle-mediated gene transfection: studies with fractionated nanoparticles. International Journal of Pharmaceutics. 2002;244:105-15.

[187] Parton RG, Simons K. The multiple faces of caveolae. Nat Rev Mol Cell Biol. 2007;8:185-94.